RESEARCH ALERT

VOL.34 NO.5-8, 2024

CSIR–SERC
ENGINEERING SUSTAINABLE STRUCTURES

Knowledge Resource Division
CSIR-Structural Engineering Research Centre
Taramani, Chennai 600113

TABLE OF CONTENTS

RESEARCH PAPERS FROM JOURNALS

Pages: 1-62

Advances in Structural Engineering

2024/801
Experimental study on bond performance between carbon/glass-hybrid-fiber-reinforced polymer bars and concrete
Liang, M.; et al.
Vol. 27, No. 4, Mar 2024, pp 525-541

2024/802
On the effectiveness of sparse regularization for structural damage diagnosis using dynamic strain measurements
Ren, P.; Yang, C.; Yuan, B.
Vol. 27, No. 4, Mar 2024, pp 542-564

2024/803
Mesoscale modeling of flexural fracture behavior in steel fiber reinforced concrete
Yu, Y.; et al.
Vol. 27, No. 4, Mar 2024, pp 565-584

2024/804
Nonlinear bond-slip model for fiber-reinforced polymer laminates externally bonded to thermally damaged concrete
Lv, H.; Xie, W.; Gao, W.
Vol. 27, No. 4, Mar 2024, pp 585-605

2024/805
Vertical stiffness limit of 400 km/h high-speed railway simple-supported bridge considering excitation randomness
Chen, X.; et al.
Vol. 27, No. 4, Mar 2024, pp 606-619

2024/806
Structural damage identification under ambient temperature variations based on CNN and normalized modal flexibility-autoregressive coefficients hybrid index
Gu, J.; et al.
Vol. 27, No. 4, Mar 2024, pp 620-636

2024/807
In-situ measurements of temperature and strain fields of large-diameter concrete-filled steel tube columns and the refined finite element modeling
Liu, X.; et al.
Vol. 27, No. 4, Mar 2024, pp 637-653

2024/808
Accurate rotation identification of flexural structures using long-gauge fiber optical sensors
Huang, H.; Wu, Z.; Wang, X.
Vol. 27, No. 4, Mar 2024, pp 654-674

2024/809
Static performance of precast concrete arches with carbon fiber reinforced polymer reinforcement
Zhao, X.; et al.
Vol. 27, No. 4, Mar 2024, pp 675-687

2024/810
Rock anchor hanger effect on single-tower earth-anchored suspension bridge mechanical performance: An analytical model and multi-objective golden eagle optimization
Chen, Y.; Zhang, W.
Vol. 27, No. 4, Mar 2024, pp 688-705

2024/811
Residual axial strength of reinforced concrete columns after exposure to standard and non-standard fires
Cao, V. V.; Ngo, S. T.
Vol. 27, No. 5, Apr 2024, pp 709-721

2024/812
Reliable design rules for cold-formed ferritic stainless steel closed built-up beams
Karthik, C.; Anbarasu, M.; Dar, M. A.
Vol. 27, No. 5, Apr 2024, pp 722-742

2024/813
Experimental study on axial compression properties of concrete filled steel tubular stub columns in varying ambient temperature
Wang, L.; et al.
Vol. 27, No. 5, Apr 2024, pp 743-757

2024/814
Efficient calculation of higher order time history response derivatives by sub structuring method
Li, J.; Wu, Q.; Weng, S.
Vol. 27, No. 5, Apr 2024, pp 758-774

2024/815
Flexural behavior of concrete beams hybrid-reinforced with glass fiber-reinforced polymer, carbon fiber-reinforced polymer, and steel rebars
Terzioglu, H.; et al.
Vol. 27, No. 5, Apr 2024, pp 775-795

2024/816
Cold–formed thin–walled steel walls filled with phosphogypsum subjected to lateral cyclic loading: testing and analysis
Hu, S.; Zhou, L.; Huang, Y.
Vol. 27, No. 5, Apr 2024, pp 796-818

2024/817
Bearing condition assessment of a simply elastic supported beam based on impact vibration testing
Xia, Q.; et al.
Vol. 27, No. 5, Apr 2024, pp 819-834

2024/818
A new constitutive model of shape memory alloy and its seismic mitigation capacity compared with existing models
Liu, J.; et al.
Vol. 27, No. 5, Apr 2024, pp 835-853

2024/819
Effect of strengthening by carbon fiber reinforced polymer sheets on the flexural behavior of reinforced self-compacting concrete beams under repeated loads
Abbas Al-Khafaji, A. G.; et al.
Vol. 27, No. 5, Apr 2024, pp 854-870

2024/820
Simulation and design model for reinforced concrete slabs with lacing systems
Ali Al-Tameemi, S. K.; et al.
Vol. 27, No. 5, Apr 2024, pp 871-892

2024/821
Fatigue performance analysis of precast segmental assembled concrete beams
Liang, Y.; et al.
Vol. 27, No. 6, Apr 2024, pp 895-911

2024/822
Research on the deformation and settlement characteristics of tunnel lining structures based on distributed fibre optic sensing technology
Wu, F.; et al.
Vol. 27, No. 6, Apr 2024, pp 912-939

2024/823
Improved softened truss model of prestressed concrete box girders subjected to combined bending and torsion
Zhang, H.; et al.
Vol. 27, No. 6, Apr 2024, pp 940-961

2024/824
Study on structural performance of repaired reinforced concrete beams with partially debonded longitudinal rebars
Hattori, T.; et al.
Vol. 27, No. 6, Apr 2024, pp 962-980

2024/825
Performance evaluation of cable-stayed bridge expansion joints based on Lasso dimensionality reduction and temperature-displacement-correlation model
Xiao, T.; et al.
Vol. 27, No. 6, Apr 2024, pp 981-994

2024/826
Experimental and numerical study of the three-dimensional temperature field in the arch ribs of the reinforced concrete ribbed arch bridge during construction
Tian, Z.; et al.
Vol. 27, No. 6, Apr 2024, pp 995-1015

2024/827
Experimental study on the aerodynamic characteristics of combined angle transmission tower subject to skew wind
Shen, G.; Que, L.; Wan, H.
Vol. 27, No. 6, Apr 2024, pp 1016-1030

2024/828
Seismic behavior of horizontally spliced single-side superposed shear wall using a concealed column
Xu, K.; et al.
Vol. 27, No. 6, Apr 2024, pp 1031-1054

2024/829
Full-scale aerodynamic study on the effects of tower wind shields and road-sign gantries on passing high-sided vehicles in the tower region at the Queensferry Crossing
Zhu, L.; McCrum, D.; Keenahan, J.
Vol. 27, No. 6, Apr 2024, pp 1055-1070

2024/830
Experimental study on the flexural behavior of partially encased composite beams with corrugated steel webs
Chu, L.; et al.
Vol. 27, No. 6, Apr 2024, pp 1071-1084

Applied Mechanics Reviews

2024/831
MechGPT, a Language-Based Strategy for Mechanics and Materials Modeling That Connects Knowledge Across Scales, Disciplines, and Modalities
Buehler, M. J.
Vol. 76, No. 2, Mar 2024, Article No. 21001

Canadian Journal of Civil Engineering

2024/832
An extended car-following model considering backward-looking effect: A machine learning approach
Adewale, A.; Lee, C.
Vol. 51, No. 3, Mar 2024, pp 264-280

2024/833
Nonlinear finite element investigation on shear behaviour of simply supported and continuous RC T-beams retrofitted with deep embedded CFRP/steel bars
Dutta, B.; et al.
Vol. 51, No. 3, Mar 2024, pp 281-297

2024/834
Use of axle load spectra (ALS) for estimating calibration drift in weigh-in-motion (WIM) systems
Masud, M. M.; et al.
Vol. 51, No. 3, Mar 2024, pp 298-312

2024/835
Network-level evaluation method of the overall–intralayer–interlayer interface structural states of semi-rigid asphalt pavement
Fan, J.; et al.
Vol. 51, No. 3, Mar 2024, pp 313-330

2024/836
Evaluation of WIM data consistency based on temporal axle load spectra
Masud, M. M.; et al.
Vol. 51, No. 3, Mar 2024, pp 331-344

2024/837
Characteristics of naturally formed semitruck platoons on interstate highways and their implications for truck platooning field deployment
Hu, X.; et al.
Vol. 51, No. 3, Mar 2024, pp 345-355

2024/838
An eye gaze-aided virtual tape measure for smart construction
Wang, L.; et al.
Vol. 51, No. 4, Apr 2024, pp 357-368

2024/839
Uniformity inspection of tack coats through measurement conducted on drone-collected images
Silva, A.; et al.

Vol. 51, No. 4, Apr 2024, pp 369-378

2024/840
Utilizing different artificial intelligence techniques for efficient condition assessment of building components
Ahmed, H.; Mostafa, K.; Hegazy, T.
Vol. 51, No. 4, Apr 2024, pp 379-389

2024/841
Engineering properties-based parameters used for moisture damage evaluation of asphalt mixtures: a review
Do, T. C.
Vol. 51, No. 4, Apr 2024, pp 390-398

2024/842
Evaluating the dynamic behavior of railway-bridge transition zone: numerical and field measurements
Heydari, H.
Vol. 51, No. 4, Apr 2024, pp 399-408

2024/843
Nonlinear modelling of the association between winter weather severity and maintenance expenditures
Qi, Y.; Velpur, V. R.
Vol. 51, No. 4, Apr 2024, pp 409-422

2024/844
Pavement freezing depth estimation using hybrid deep-learning models
Roh, S.; et al.
Vol. 51, No. 4, Apr 2024, pp 423-433

2024/845
Microscopic self-healing of multi-walled carbon nanotube-modified asphalt based on the dual diffusion-energy theory
Xiao, M.; et al.
Vol. 51, No. 4, Apr 2024, pp 434-448

2024/846
The cyclic performance of column base plate connections using different types of stiffeners
Al-Sharmootee, M.; et al.
Vol. 51, No. 4, Apr 2024, pp 449-460

Cement and Concrete Composites

2024/847
Rheological enhancement of fresh polymer-modified cement composites via surface-modified graphene oxide
Naseem, Z.; et al.
Vol. 147, Mar 2024, Article No. 105413

2024/848
Mesoscopic discrete modeling of compression and fracture behavior of concrete: Effects of aggregate size distribution and interface transition zone
Yang, L.; et al.
Vol. 147, Mar 2024, Article No. 105411

2024/849
Methodology to design eco-friendly fiber-reinforced concrete for 3D printing
Li, H.; et al.
Vol. 147, Mar 2024, Article No. 105415

2024/850
Design of a smart protective coating with molybdate-loaded halloysite nanotubes towards corrosion protection in reinforced concrete
Liu, Y.; Shi, J.
Vol. 147, Mar 2024, Article No. 105419

2024/851
Multi-scale experimental studies on mechanical properties of three-dimensional porous graphene cementitious composite
Ying, J.; et al.
Vol. 147, Mar 2024, Article No. 105412

2024/852
Rheology, mechanical properties, and hydration of synergistically activated coal gasification slag with three typical solid wastes
Xiang, J.; et al.
Vol. 147, Mar 2024, Article No. 105418

2024/853
Double percolation phenomenon of carbon nanotube/cement composites as piezoresistivity sensing elements with exposure to salt environment
Wang, X.; et al.
Vol. 147, Mar 2024, Article No. 105401

2024/854
Alkaline activated cements obtained from ferrous and non-ferrous slags. Electric arc furnace slag, ladle furnace slag, copper slag and silico-manganese slag
Gomez-Casero, M. A.; et al.
Vol. 147, Mar 2024, Article No. 105427

2024/855
Preparation and mechanical characterization of multi-functional high-ductility engineered magnesium oxysulfate cement-based composites
Zhu, M.; et al.
Vol. 147, Mar 2024, Article No. 105428

2024/856
Investigation of high strain rate effects on strain-hardening cementitious composites using Voronoi-cell lattice models
Park, J. W.; et al.
Vol. 147, Mar 2024, Article No. 105408

2024/857
Effect of the incorporation ratio of recycled concrete aggregate on the properties of self-compacting mortar
Li, T.; et al.
Vol. 147, Mar 2024, Article No. 105429

2024/858
Insight into ion exchange behavior of LDHs: Asynchronous chloride adsorption and intercalated ions release processes
Xu, Z.; et al.
Vol. 147, Mar 2024, Article No. 105433

2024/859
Gold-sputtered LPG fiber sensor pulse electroplated with iron-carbon for monitoring passivation and depassivation of carbon steel in concrete pore solutions
Zhou, G.; et al.
Vol. 147, Mar 2024, Article No. 105432

2024/860
Analysis of the tensile behavior of FRP textile for multi-scale fiber reinforced cementitious composite
Zhou, P.; Feng, P.; Qiu, J.
Vol. 147, Mar 2024, Article No. 105416

2024/861
Alkali thermal fusion: A prospective route to enhance the reactivity of low-grade clay and utilize as supplementary cementitious material (SCM)
Borno, I. B.; Nair, N.; Ashraf, W.
Vol. 147, Mar 2024, Article No. 105417

2024/862
High ductility cementitious composites incorporating seawater and coral sand (SCS-HDCC) for offshore engineering: Microstructure, mechanical performance and sustainability
Li-ping, G.; et al.
Vol. 147, Mar 2024, Article No. 105414

2024/863
Impact of triethanolamine on the hydration of Portland cement in the presence of high pozzolanic activity supplementary cementitious materials
Jiang, J.; et al.
Vol. 147, Mar 2024, Article No. 105435

2024/864
Toward smart and sustainable cement manufacturing process: Analysis and optimization of cement clinker quality using thermodynamic and data-informed approaches
Goncalves, J. P.; et al.
Vol. 147, Mar 2024, Article No. 105436

2024/865
Investigating the influence of fibre type and content on the toughness and ductility of geopolymer mortar with acoustic emission technology
Zhang, H.; et al.
Vol. 147, Mar 2024, Article No. 105434

2024/866
Influence of engineered self-healing systems on ASR damage development in concrete
De Souza, D. J.; Sanchez, L. F. M.; Biparva, A.
Vol. 147, Mar 2024, Article No. 105440

2024/867
Behaviour of alkali-activated fly ash-slag paste at elevated temperatures: An experimental study
Tu, W.; et al.
Vol. 147, Mar 2024, Article No. 105438

2024/868
Autolytic capsules incorporating alkali-activated slag system for self-healing cementitious composites
Xiang, J.; et al.
Vol. 147, Mar 2024, Article No. 105439

2024/869
Characterisation of a 3D-printed alkali-activated material based on waste mineral wool at room and elevated temperatures
Pavlin, M.; et al.
Vol. 147, Mar 2024, Article No. 105445

2024/870
Mitigating chloride attack in cementitious materials without compromising other properties via the use of viscosity modifying admixture
Zhao, L.; et al.
Vol. 147, Mar 2024, Article No. 105441

2024/871
Spray-based 3D concrete printing parameter design model: Actionable insight for high printing quality
Liu, X.; et al.
Vol. 147, Mar 2024, Article No. 105446

2024/872
Contradict mechanism of long-term magnesium and sodium sulfate attacks of nano silica-modified cement mortars – Experimental and thermodynamic modelling
Huang, Q.; Wang, Q.; Zhu, X.
Vol. 147, Mar 2024, Article No. 105444

2024/873
High ferrite cement clinker doped with PbO: Solidification and hydration behaviors
Zhang, Z.; et al.
Vol. 148, Apr 2024, Article No. 105451

2024/874
Rheological area division method for coupling process parameters to fabricate geopolymer foams with optimized pore structures and mechanical strength
Zhang, X.; et al.
Vol. 148, Apr 2024, Article No. 105453

2024/875
Effect of vacuum–vibration–compaction molding on the properties and performances of polymer-modified cementitious material
Wang, B.; et al.
Vol. 148, Apr 2024, Article No. 105450

2024/876
A comprehensive review of ultra-high-performance concrete (UHPC) behaviour under blast loads
Liu, J.; et al.
Vol. 148, Apr 2024, Article No. 105449

2024/877
Effect of accelerated carbonation of fully recycled aggregates on fracture behaviour of concrete
Tang, Y.; et al.
Vol. 148, Apr 2024, Article No. 105442

2024/878
Interaction between zeolite and sulfate, and its influences on cement hydration

Zheng, X.; et al.
Vol. 148, Apr 2024, Article No. 105448

2024/879
Fresh, mechanical, and microstructural properties of lithium slag concretes
Rahman, S. A.; Shaikh, F. U. A.; Sarker, P. K.
Vol. 148, Apr 2024, Article No. 105469

2024/880
The adsorption and diffusion behavior of chloride in recycled aggregate concrete incorporated with calcined LDHs
Gao, S.; et al.
Vol. 148, Apr 2024, Article No. 105452

2024/881
Recent advances in cementless ultra-high-performance concrete using alkali-activated materials and industrial byproducts: A review
Yoo, D.; et al.
Vol. 148, Apr 2024, Article No. 105470

2024/882
The performance of α'-belite calcium sulfoaluminate (C$A) cement preserved under SO2 atmosphere compared to commercial products
Kocis, J.; et al.
Vol. 148, Apr 2024, Article No. 105468

2024/883
Investigation into the changes in the splitting tensile strength of concrete subjected to long-term drying using a three-phase mesoscale RBSM
Sasano, H.; Maruyama, I.
Vol. 148, Apr 2024, Article No. 105462

2024/884
Hydration kinetics and mechanism of C3S with cellulose nanocrystals
Guo, A.; et al.
Vol. 148, Apr 2024, Article No. 105447

2024/885
Effect of chloride salt types on corrosion resistance of reinforcing steel in cement mortar mixed with DNA primer inhibitor
Yang, G.; et al.
Vol. 148, Apr 2024, Article No. 105454

2024/886
Mechanical behavior of textile reinforced concrete with newly developed mineral-impregnated carbon fabrics submitted to elevated temperatures
Silva, R. M. C.; et al.
Vol. 148, Apr 2024, Article No. 105467

2024/887
Design of self-compacting ultra-high performance concrete (SCUHPC) towards to the cementitious materials packing optimization
Wang, X.; et al.
Vol. 148, Apr 2024, Article No. 105443

2024/888
Multiscale and multiphysics discrete model of self-healing of matrix and interfacial cracks in fibre reinforced cementitious composites: Formulation, implementation and preliminary results
Cibelli, A.; Ferrara, L.; Luzio, G. D.
Vol. 148, Apr 2024, Article No. 105465

2024/889
Mechanical characterization of high-strength and ultra-high-performance engineered cementitious composites reinforced with polyvinyl alcohol and polyethylene fibers subjected to monotonic and cyclic loading
Ramezani, M.; Ozbulut, O. E.; Sherif, M. M.
Vol. 148, Apr 2024, Article No. 105472

2024/890
Recursive aggregate segmentation by erosion and reconstitution (RASER) to characterize concrete microstructure using complementarity of X-ray and neutron computed tomography
Razakamandimby, D. F. T.; et al.

Vol. 148, Apr 2024, Article No. 105437

2024/891
Development of self-sensing ultra-high-performance concrete using hybrid carbon black and carbon nanofibers
Li, W.; et al.
Vol. 148, Apr 2024, Article No. 105466

2024/892
Low-carbon, expansive engineered cementitious composites (ECC) in the context of 3D printing
Zhou, W.; et al.
Vol. 148, Apr 2024, Article No. 105473

2024/893
Synthesis of geopolymer composites using bauxite residue-based spheres as aggregate: Novel and eco-friendly strategy to produce lightweight building materials
Alves, Z.; et al.
Vol. 148, Apr 2024, Article No. 105478

2024/894
Prediction of concrete abrasion depth and computational design optimization of concrete mixtures
Liu, Q.; Andersen, L. V.; Wu, M.
Vol. 148, Apr 2024, Article No. 105431

2024/895
Understanding the setting behaviours of alkali-activated slag from the dissolution-precipitation point of view
Zhu, X.; et al.
Vol. 148, Apr 2024, Article No. 105474

2024/896
Effects of hygrothermal and natural aging on the durability of multilayer insulation systems incorporating thermal mortars with EPS and aerogel
Parracha, J. L.; et al.
Vol. 148, Apr 2024, Article No. 105483

2024/897
3D printed concrete with sewage sludge ash: Fresh and hardened properties
Ding, T.; et al.
Vol. 148, Apr 2024, Article No. 105475

2024/898
Understanding the CaCO3 phase transition of carbonated wollastonite composites caused by sodium tripolyphosphate: From amorphous to crystalline
Cheng, L.; et al.
Vol. 148, Apr 2024, Article No. 105477

2024/899
Hardened property changes due to the pumping process of self-consolidating concrete
Li, F.; et al.
Vol. 148, Apr 2024, Article No. 105481

2024/900
The secret of ancient Roman hydraulic mortar: the lesson learnt from the past for future cements
Medeghini, L.; et al.
Vol. 148, Apr 2024, Article No. 105484

2024/901
Experimental investigation into the self-carbonation mechanism of magnesium oxide carbon sequestration foamed concrete
Zhang, X.; et al.
Vol. 148, Apr 2024, Article No. 105486

2024/902
Effect of corrosion pit distribution of rebar on pore, and crack characteristics in concrete
Taheri-Shakib, J.; Al-Mayah, A.
Vol. 148, Apr 2024, Article No. 105476

2024/903
Effect of vehicle-induced vibration on the strength, nano-mechanical properties, and microstructural characteristics of ultra-high-performance concrete during hardening process
Leng, J.; et al.

Vol. 148, Apr 2024, Article No. 105487

2024/904
Durability of micro-cracked UHPC subjected to coupled freeze-thaw and chloride salt attacks
Zhong, R.; et al.
Vol. 148, Apr 2024, Article No. 105471

2024/905
A conceptual design of two-stream alkali-activated materials
Sun, Y.; et al.
Vol. 148, Apr 2024, Article No. 105485

2024/906
Transfer learning enables prediction of steel corrosion in concrete under natural environments
Ji, H.; et al.
Vol. 148, Apr 2024, Article No. 105488

2024/907
Hydration kinetics of cation exchanged clinoptilolite zeolite based cementitious materials
Islam, M. S.; Biernacki, J. J.; Mohr, B. J.
Vol. 148, Apr 2024, Article No. 105480

2024/908
Influence of hybrid steel-polyacrylonitrile fibers on the mechanical toughness and freeze-thaw resistance of sulfoaluminate cement composites
Wang, J.; et al.
Vol. 148, Apr 2024, Article No. 105489

2024/909
Optimization of printing precision and mechanical property for powder-based 3D printed magnesium phosphate cement using fly ash
Liu, X.; et al.
Vol. 148, Apr 2024, Article No. 105482

2024/910
Unveiling the synergistic effect of in-situ generated calcium carbonate by CO2 mixing on the reaction of calcined clay
Dong, Y.; et al.
Vol. 148, Apr 2024, Article No. 105490

2024/911
Factors affecting free chloride contents of hardened cement paste with a low water-to-binder ratio determined by rapid water extraction
Zhao, Y.; et al.
Vol. 148, Apr 2024, Article No. 105491

Cement and Concrete Research

2024/912
The neutralization of tricalcium aluminate hexahydrate and its spontaneous transformation into Friedel's salt, a layered double hydroxide
Kasa, E.; et al.
Vol. 177, Mar 2024, Article No. 107414

2024/913
Hydration and phase assemblage of limestone calcined clay cements (LC3) with clinker content below 50 %
Sun, J.; Zunino, F.; Scrivener, K.
Vol. 177, Mar 2024, Article No. 107417

2024/914
Modification of magnesium hydroxide for improved performance in CO2 sequestration
Du, Z.; Unluer, C.
Vol. 177, Mar 2024, Article No. 107418

2024/915
Modeling the ionic diffusion coefficient of unsaturated hardened cement paste: A micromechanical approach
Zhang, M.; et al.
Vol. 177, Mar 2024, Article No. 107415

2024/916
Retardation effect of the pozzolanic reaction of low-calcium supplementary cementitious materials on clinker hydration at later age: Effects of pore solution, foreign ions, and pH
Wang, T.; et al.
Vol. 177, Mar 2024, Article No. 107416

2024/917
Phase stabilities and thermodynamic properties of crystalline phases in CaO–SiO2–H2O above 100 °C
Hirsch, T.; Lothenbach, B.
Vol. 177, Mar 2024, Article No. 107412

2024/918
The intrinsic mechanical properties of hydromagnesite, Mg5(CO3)4(OH)2·4H2O, a key phase of reactive MgO carbonate cement
Zhang, W.; Li, J.
Vol. 177, Mar 2024, Article No. 107410

2024/919
Bayesian design of concrete with amortized Gaussian processes and multi-objective optimization
Pfeiffer, O. P.; et al.
Vol. 177, Mar 2024, Article No. 107406

2024/920
Theoretical model for the coupling effect of moisture transport on chloride penetration in concrete
Dehwah, O. H. A.; Xi, Y.
Vol. 177, Mar 2024, Article No. 107431

2024/921
Understanding the role of magnesium ions on setting of metakaolin-based geopolymer
Zhang, S. S.; Wang, S.; Chen, X.
Vol. 177, Mar 2024, Article No. 107430

2024/922
Investigation of compressive creep of calcium-silicate-hydrates (C-S-H) in hardened cement paste through micropillar testing
Guo, W.; Wei, Y.
Vol. 177, Mar 2024, Article No. 107427

2024/923
Probing the hydration behavior of tricalcium aluminate under the in situ polymerization of acrylic acid
Liu, Q.; et al.
Vol. 177, Mar 2024, Article No. 107429

2024/924
Understanding water vapor sorption hysteresis and scanning behaviors of hardened cement pastes: Experiments and modeling
Wang, Z.; Li, K.
Vol. 177, Mar 2024, Article No. 107435

2024/925
Aqueous carbonation of aged blended Portland cement pastes: Impact of the Al/Si ratio on the structure of the alumina-silica gel
Neto, F. M.; Snellings, R.; Skibsted, J.
Vol. 177, Mar 2024, Article No. 107428

2024/926
Thermodynamic study on phase composition of hardened Portland cement paste exposed to CaCl2 solution: Effects of temperature, CaCl2 concentration, and type and dosage of supplementary cementitious materials
Li, T.; et al.
Vol. 178, Apr 2024, Article No. 107437

2024/927
Multi technique characterization of the carbonation affected zone including non-destructive single sided 1H NMR
Glawe, C.; et al.
Vol. 178, Apr 2024, Article No. 107438

2024/928
Dissolution behaviors and mechanisms of metakaolin in acidic activators
Bu, M.; et al.
Vol. 178, Apr 2024, Article No. 104772

2024/929
Structural evolution of calcium sodium aluminosilicate hydrate (C-(N-)A-S-H) gels induced by water exposure: The impact of Na leaching
Liu, C.; et al.
Vol. 178, Apr 2024, Article No. 107432

2024/930
The role of water-treated municipal solid waste incineration (MSWI) bottom ash in

microstructure formation and strength development of blended cement pastes
Chen, B.; Ye, G.
Vol. 178, Apr 2024, Article No. 107440

2024/931
Macro and microstructural evolution of low-calcium fly ash-based geopolymer mortar exposed to sulphuric acid corrosion
Ariyadasa, P. W.; et al.
Vol. 178, Apr 2024, Article No. 107436

2024/932
Stabilizing mechanisms of metastable vaterite in cement systems
Zhao, D.; et al.
Vol. 178, Apr 2024, Article No. 107441

2024/933
New insights into strain evolution of concrete under different freeze-thaw conditions: Investigation based on real-time and full-field monitoring
Chen, S.; et al.
Vol. 178, Apr 2024, Article No. 107443

2024/934
Citrate sorption on cement hydrates
Guidone, R. E.; et al.
Vol. 178, Apr 2024, Article No. 107404

2024/935
The influence of Al2O3, CaO, MgO and TiO2 content on the early-age reactivity of GGBS in blended cements, alkali-activated materials and supersulfated cements
Blotevogol, S.; et al.
Vol. 178, Apr 2024, Article No. 107439

2024/936
Quantification of carbonated Mg-based cement pastes by Raman spectroscopy
Mi, T.; et al.
Vol. 178, Apr 2024, Article No. 107454

2024/937
Numerical analysis of concrete permeability measurements in laboratory and in field
Multon, S.; et al.
Vol. 178, Apr 2024, Article No. 107455

2024/938
Chemical degradation of magnesium potassium phosphate cement pastes during leaching by demineralized water: Experimental investigation and modelling
Caselles, L. D.; et al.
Vol. 178, Apr 2024, Article No. 107456

2024/939
A damage constitutive model for concrete under uniaxial compression capturing strain localization
Wang, Y.
Vol. 178, Apr 2024, Article No. 107457

2024/940
Surface properties of clinker phases and clay minerals characterized by inverse gas chromatography (IGC) and their link to reactivity
Zunino, F.; et al.
Vol. 178, Apr 2024, Article No. 107458

2024/941
Hydrothermal synthesis of sodium silicate from rice husk ash: Effect of synthesis on silicate structure and transport properties of alkali-activated concrete
Alnahhal, M. F.; et al.
Vol. 178, Apr 2024, Article No. 107461

2024/942
Magnesium silicate hydrate (M-S-H) stability under carbonation
Bernard, E.; Nguyen, H.
Vol. 178, Apr 2024, Article No. 107459

2024/943
Effect of SiO2-modified calcined layered double hydroxides on the properties of cement-based material: Crucial role of the phase-transformation induced by alkaline pore solution
Liu, J.; Gao, X.; Chen, T.
Vol. 178, Apr 2024, Article No. 107465

2024/944
Influence of calcination temperature on the physical and chemical characteristics of kaolinitic clays for use as supplementary cementitious materials
Dhar, M.; Bishnoi, S.
Vol. 178, Apr 2024, Article No. 107464

2024/945
In situ synchrotron powder diffraction study of LC3 cement activation at very early ages by C-S-H nucleation seeding
Morales-Cantero, A.; et al.
Vol. 178, Apr 2024, Article No. 107463

2024/946
Effect of gypsum on hydration properties, composition and kinetics of low carbon belite-ye'elimite-Q phase-ferrite clinker
Minwang, L. V.; et al.
Vol. 178, Apr 2024, Article No. 107466

Composites Part B: Engineering

2024/947
Towards sustainable reprocessable structural composites: Benzoxazines as biobased matrices for natural fibers
Seychal, G.; et al.
Vol. 272, Mar 2024, Article No. 111201

2024/948
Polyelectrolyte composite hydrogels based on a derivative of functional dietary fiber for long-term gastric retention and drug delivery
Yang, J.; et al.
Vol. 272, Mar 2024, Article No. 111194

2024/949
Understanding factors affecting the process efficiency, quality and carbon emission in laser drilling of CFRP composite via tailored sequence multiple-ring scanning
Zhu, M.; et al.
Vol. 272, Mar 2024, Article No. 111156

2024/950
A novel methodology to measure the transverse Poisson'sratiointheelastic and plastic regions for composite materials
Cozar, I. R.; et al.
Vol. 272, Mar 2024, Article No. 111098

2024/951
Tailoring nanostructured MXene to adjust its dispersibility in conductive hydrogel for self-powered sensors
Zhang, Y.; et al.
Vol. 272, Mar 2024, Article No. 111191

2024/952
Unleashing excellent antibacterial performance of natural rubber composites via herbal extracts
Chen, X.; et al.
Vol. 272, Mar 2024, Article No. 111171

2024/953
Incorporation of hexagonal boron nitride and multi-walled carbon nanotube for motion sensing triboelectric nanogenerators
Hyun, B. G.; et al.
Vol. 272, Mar 2024, Article No. 111193

2024/954
Selective transfer of mini-light-emitting diodes via the laser-induced switching of adhesives based on azobenzene composites
Lee, T.; et al.
Vol. 272, Mar 2024, Article No. 111175

2024/955
A deep material network approach for predicting the thermomechanical response of composites
Shin, D.; et al.
Vol. 272, Mar 2024, Article No. 111177

2024/956
3D printing of topologically optimized wing spar with continuous carbon fiber reinforced composites
Huang, Y.; et al.
Vol. 272, Mar 2024, Article No. 111166

2024/957
A wrapped and infiltrated ~20-μm-thick 3D ceramic framework composite enables fast Li+ diffusion and interfacial compatibility for lithium-metal batteries
Wei, B.; et al.
Vol. 272, Mar 2024, Article No. 111192

2024/958
A small-diameter vascular graft promotes rapid and benign remodeling of the neointima through dual release of nitric oxide and hydrogen sulfide
Liang, F.; et al.
Vol. 272, Mar 2024, Article No. 111172

2024/959
Powder sheet additive manufacturing of multi-material structures: Experimental and computational characterizations
Zhang, W.; et al.
Vol. 272, Mar 2024, Article No. 111203

2024/960
A novel thermoplastic water-soluble sizing agent for the interfacial enhancement of carbon fiber/polyether ether ketone composites
Yan, F.; et al.
Vol. 272, Mar 2024, Article No. 111205

2024/961
Investigation on moisture absorption behavior on GFRP and neat epoxy systems in hygrothermal salt fog aging
Silva, G. A. S.; et al.
Vol. 272, Mar 2024, Article No. 111214

2024/962
Porous PLGA/MBG scaffold enhanced bone regeneration through osteoimmunomodulation
Liu, Y.; et al.
Vol. 272, Mar 2024, Article No. 111202

2024/963
Co-delivery of Zn ions and resveratrol via bioactive glass-integrated injectable microspheres for postoperative regeneration of bone tumor defects
Dai, Q.; et al.
Vol. 272, Mar 2024, Article No. 111220

2024/964
Effects of hexagonal boron nitride content on forming quality and performance of laser powder bed fusion manufactured nickel-based hastelloy X composites
Sun, J.; et al.
Vol. 272, Mar 2024, Article No. 111218

2024/965
Channel engineering strategy of precisely modified MOF/nanofiber composite separator for advanced aqueous zinc ion batteries
Liu, C.; et al.
Vol. 272, Mar 2024, Article No. 111227

2024/966
Preventing partial discharge in liquid metal polymer composites under steep voltage pulses
Faruqe, O.; et al.
Vol. 272, Mar 2024, Article No. 111206

2024/967
Concurrently achieving strength-ductility combination and robust anti-wear performance in an in-situ high-entropy bulk metallic glass composite
Du, Y.; et al.
Vol. 272, Mar 2024, Article No. 111222

2024/968
A nacre-inspired thermo conductive and healable nanocomposite captures extremely enhanced stiffness and toughness
Zhang, H.; et al.
Vol. 272, Mar 2024, Article No. 111228

2024/969
Rotating gliding arc plasma: Innovative treatment for adhesion improvement

between stainless steel heating elements and thermoplastics in resistance welding of composites
Zhao, G.; et al.
Vol. 272, Mar 2024, Article No. 111210

2024/970
Engineered nanocomposites through embedding of smaller “organic inorganic” nanoparticles in thermoplastic Poly(2-Vinylpyridine) polymer matrix
Gupta, S.; Henson, A.
Vol. 272, Mar 2024, Article No. 111207

2024/971
One-dimensional deep convolutional autoencoder active infrared thermography: Enhanced visualization of internal defects in FRP composites
Zhang, Y.; et al.
Vol. 272, Mar 2024, Article No. 111216

2024/972
Laminated composite fabricated using high-performance polyamine thermoset: Ultra heat resistance and excellent mechanical property
Shen, Y.; et al.
Vol. 272, Mar 2024, Article No. 111209

2024/973
Structurally engineered 3D porous graphene-based phase change composite with highly efficient multi-energy conversion and versatile applications
Zhu, X.; et al.
Vol. 272, Mar 2024, Article No. 111233

2024/974
Research on low flow stress and quantitative DRX analysis in B4C/Al composites with interfacial amorphous B2O3 layer
Xue, W.; et al.
Vol. 272, Mar 2024, Article No. 111226

2024/975
Full-field characterizations of additively manufactured composite cellular structures
Singh, A.; Koohbor, B.; Youssef, G.
Vol. 272, Mar 2024, Article No. 111208

2024/976
In-situ constructing hybrid cross-linked networks in brominated butyl rubber via amphiphilic graphene oxide cross-linkers: Retaining excellent gas barrier and mechanical properties after fatigue
Yang, S.; et al.
Vol. 272, Mar 2024, Article No. 111224

2024/977
‘Resin welding’: A novel route to joining acrylic composite components at room temperature
Devine, M.; et al.
Vol. 272, Mar 2024, Article No. 111212

2024/978
Concerns in tension-tension fatigue testing of unidirectional composites: Specimen design and test setup
Fazlali, B.; Lomov, S. V.; Swolfs, Y.
Vol. 272, Mar 2024, Article No. 111213

2024/979
A straightforward and efficient gradient pressure method for bamboo flattening: Strain and multi-scale deformation
Wang, X.; et al.
Vol. 272, Mar 2024, Article No. 111232

2024/980
A coupled ductile damage model for metal matrix composites: Development and application
Ren, Q.; et al.
Vol. 272, Mar 2024, Article No. 111229

2024/981
Exploring the self-nucleation effect: Transforming crystalline morphology for improved mechanical performance of carbon fiber reinforced polyphenylene sulfide composites
Ren, Y.; et al.
Vol. 272, Mar 2024, Article No. 111231

2024/982
Dual microparticles programmed delivery system regulating stem cell-based cartilage regeneration by cartilage-specific matrix hydrogels
Ran, X.; et al.
Vol. 272, Mar 2024, Article No. 111221

2024/983
Highly thermally conductive and soft thermal interface materials based on vertically oriented boron nitride film
Niu, H.; et al.
Vol. 272, Mar 2024, Article No. 111219

2024/984
Multifunctional carbon fibre composites using electrochemistry
Zenkert, D.; et al.
Vol. 273, Mar 2024, Article No. 111240

2024/985
Reducing stress concentrations in static and fatigue tensile tests on unidirectional composite materials: A review
Fazlali, B.; Lomov, S. V.; Swolfs, Y.
Vol. 273, Mar 2024, Article No. 111215

2024/986
Academic research for composite aerostructures - A personal perspective
Butler, R.
Vol. 273, Mar 2024, Article No. 111239

2024/987
Mechanical properties and scratch recovery of nanoclay/polyester composite coatings for pre-coated metal (PCM) sheets
Lin, W.; et al.
Vol. 273, Mar 2024, Article No. 111217

2024/988
Bioinspired semi-flexible hydrogel with anti-inflammatory potential for natural tissue-mimicking bone regeneration
Lee, J. S.; et al.
Vol. 273, Mar 2024, Article No. 111223

2024/989
Green strategy based on supercritical-fluid foaming for fabricating rigid microcellular thermoplastic polyimide foams with ultrahigh compressive strength
Liu, H.; et al.
Vol. 273, Mar 2024, Article No. 111204

2024/990
A combined engineering of hollow and core-shell structures for C@MoS2 microcapsules toward high-efficiency electromagnetic absorption
Liu, Y.; et al.
Vol. 273, Mar 2024, Article No. 111244

2024/991
Hierarchically heterogeneous strategy for Ti2AlC/TiAl composite with superior mechanical properties
Liu, P.; et al.
Vol. 273, Mar 2024, Article No. 111259

2024/992
Enhanced interfacial property and thermal conductivity of pitch-based carbon fiber/epoxy composites via three-layer assembly of PDI/GN/ PDI interphase
Jiang, X.; et al.
Vol. 273, Mar 2024, Article No. 111238

2024/993
Fabrication of room temperature self-healing, robust superhydrophobic coatings via spraying dual cross-linking supramolecular silicone polymer/ SiO2 composite
Tao, J.; et al.
Vol. 273, Mar 2024, Article No. 111245

2024/994
A 3D printable gelatin methacryloyl/chitosan hydrogel assembled with conductive PEDOT for neural tissue engineering
Han, Y.; et al.
Vol. 273, Mar 2024, Article No. 111241

2024/995
In-situ TiCxNy nanoparticle reinforced crack-free CoCrFeNi medium-entropy alloy matrix nanocomposites with high strength and ductility via laser powder bed fusion
Zhang, Y.; et al.
Vol. 273, Mar 2024, Article No. 111237

2024/996
Boron carbide-based composites densified via Ti3SiC2 boronizing with excellent mechanical properties and amorphization tolerance
Xiong, Z.; et al.
Vol. 273, Mar 2024, Article No. 111264

2024/997
Composite metamaterial antenna with super mechanical and electromagnetic performances integrated by three-dimensional weaving technique
Li, W.; et al.
Vol. 273, Mar 2024, Article No. 111265

2024/998
3D printed sequence-controlled copolyimides with high thermal and mechanical performance
Du, X.; et al.
Vol. 273, Mar 2024, Article No. 111262

2024/999
An alternative method to evaluate the micromechanics tensile strength properties of natural fiber strand reinforced polyolefin composites. The case of hemp strand-reinforced polypropylene
Espinach, F. X.; et al.
Vol. 273, Mar 2024, Article No. 111211

2024/1000
Surface-activated 3D-printed PEEK implant enhances anti-infection and osteogenesis
Wang, Z.; et al.
Vol. 273, Mar 2024, Article No. 111258

2024/1001
Phosphorus-containing curing agents with dynamic bonds endowing epoxy resins with flame retardancy and remolding capability
Liu, X.; et al.
Vol. 273, Mar 2024, Article No. 111260

2024/1002
One-step construction of three-dimensional disordered graphene-like pyrolytic carbon composites by oxygen controllable chemical vapor deposition
Xiao, C.; et al.
Vol. 273, Mar 2024, Article No. 111266

2024/1003
Polysaccharide hybrid scaffold encapsulated endogenous factors for microfracture enhancement by sustainable release and cell recruitment
Li, Z.; et al.
Vol. 273, Mar 2024, Article No. 111235

2024/1004
That’s how the preform crumples: Wrinkle creation during forming of thick binder-stabilised stacks of non-crimp fabrics
Broberg, P. H.; et al.
Vol. 273, Mar 2024, Article No. 111269

2024/1005
Osteoimmunomodulatory bioinks for 3D bioprinting achieve complete regeneration of critical-sized bone defects
Yu, X.; et al.
Vol. 273, Mar 2024, Article No. 111256

2024/1006
Screen-printed piezoelectric composites for vibrational energy harvesting in combination with structural composite laminates for powering a sensing node
Chen, B.; et al.
Vol. 273, Mar 2024, Article No. 111274

2024/1007
Damage tolerance of basalt fiber reinforced multiscale composites: Effect of nanoparticle morphology and hygrothermal aging
Sukur, E. F.; et al.
Vol. 273, Mar 2024, Article No. 111234

2024/1008
Injectable, stretchable, and conductance-stable fiber for myocardial infarction repair
Li, Y.; et al.
Vol. 273, Mar 2024, Article No. 111242

2024/1009
Process characteristics, damage mechanisms and challenges in machining of fibre reinforced thermoplastic polymer (FRTP) composites: A review
Ge, J.; et al.
Vol. 273, Mar 2024, Article No. 111247

2024/1010
A partial dissolution-regeneration strategy for preparing water-resistant composite film of cellulose I and cellulose II with high light transmittance and adjustable haze
Zhang, L.; Huang, Y.; Wu, M.
Vol. 274, Apr 2024, Article No. 111285

2024/1011
Reformable and sustainable thermosetting carbon fiber composites from epoxy vitrimer
Barnett, P. R.; et al.
Vol. 274, Apr 2024, Article No. 111270

2024/1012
Superior shear strength
subject to the regulation of plastic toughness in K4169 alloy/TiAl intermetallic joints vacuum brazed with gradient composite amorphous filler metals
Zhang, L.; et al.
Vol. 274, Apr 2024, Article No. 111288

2024/1013
3D-printed conical structure absorber based on NFG/Fe3Si/SiCnw ternary composites for multifunctional integrated electromagnetic microwave absorption
Deng, K.; et al.
Vol. 274, Apr 2024, Article No. 111243

2024/1014
A hydrogel derived from skin secretion of Andrias davidianus to facilitate bone regeneration
Zhang, Q.; et al.
Vol. 274, Apr 2024, Article No. 111261

2024/1015
Nacre-inspired hierarchical framework enables tough and impact-monitoring epoxy nanocomposites
Li, D.; et al.
Vol. 274, Apr 2024, Article No. 111246

2024/1016
An ultra-broadband biomimetic microwave blackbody integrating superior mechanical properties inspired by lepidopteran wing scales
Chen, S.; et al.
Vol. 274, Apr 2024, Article No. 111279

2024/1017
A robust anti-icing/de-icing and self-healing coating based on efficient photothermal Bi2S3/Ti3C2Tx nanofillers
Du, C.; et al.
Vol. 274, Apr 2024, Article No. 111255

2024/1018
Simultaneous toughening and strengthening of CF/EP composites through bi-component thermoplastics with hybrid phases between composite layers
Xue, Y.; et al.
Vol. 274, Apr 2024, Article No. 111286

2024/1019
An accurate forming model for capturing the nonlinear material behaviour of multilayered binder-stabilised fabrics and predicting fibre wrinkling
Broberg, P. H.; et al.

Vol. 274, Apr 2024, Article No. 111268

2024/1020
End group capturing in polyurea elastomer by using aromatic dianhydrides for flame retardance
Deng, H.; et al.
Vol. 274, Apr 2024, Article No. 111276

2024/1021
The effect of laser assisted tape placement processing conditions on microstructural evolution, residual stress and interlaminar shear strength of carbon fibre/PEEK laminates
Ma, H.; Bandaru, A. K.; Weaver, P. M.
Vol. 274, Apr 2024, Article No. 111293

2024/1022
Metal-electronegativity-induced sulfur-vacancies and heterostructures of MnS1-x/ZnS-NC@C with dual-carbon decoration for high-performance sodium-ion storage
Zhang, H.; et al.
Vol. 274, Apr 2024, Article No. 111267

2024/1023
Stability of crystallographic texture and mechanical anisotropy toward Al2O3/YAG eutectic ceramic composite using single crystalline seeds
Liu, Y.; et al.
Vol. 274, Apr 2024, Article No. 111263

2024/1024
One-pot solvent-free green strategy to fabricate ultra-efficient polyphosphoester flame retardant for Poly (Lactic acid)
Bai, Z.; et al.
Vol. 274, Apr 2024, Article No. 111236

2024/1025
Tadpole-like bottlebrush polymer-modified multiwalled carbon nanotubes: A strategy for interface-strengthened polymer nanocomposites with exceptional performance
Deng, T.; et al.
Vol. 274, Apr 2024, Article No. 111275

2024/1026
Bio-based pH-responsive microcapsules derived from Schiff base structures for acid rain protection
Chen, Q.; et al.
Vol. 274, Apr 2024, Article No. 111289

2024/1027
Thermal-, magnetic-, and light-responsive 4D printed SMP composites with multiple shape memory effects and their promising applications
Lin, C.; et al.
Vol. 274, Apr 2024, Article No. 111257

2024/1028
Enhancing the electromagnetic interference shielding of epoxy resin composites with hierarchically structured MXene/graphene aerogel
He, Z.; et al.
Vol. 274, Apr 2024, Article No. 111230

2024/1029
Recycling of MoSi2-based industrial solid wastes for the fabrication and high-temperature oxidation behavior of MoSi2–ZrSi2–SiC composite coating
Zhu, L.; et al.
Vol. 274, Apr 2024, Article No. 111281

2024/1030
Biomaterials for diabetic bone repair: Influencing mechanisms, multi-aspect progress and future prospects
Wang, B.; et al.
Vol. 274, Apr 2024, Article No. 111282

2024/1031
Optical wood with switchable solar transmittance for all-round thermal management
Gao, H.; et al.
Vol. 275, Apr 2024, Article No. 111287

2024/1032
Molecular-level network engineering of crosslinker towards high-performance carbon nanotube fiber
Park, J. S.; et al.
Vol. 275, Apr 2024, Article No. 111338

2024/1033
Fabrication of carbon nanotube epoxy prepreg towards lightweight structural composites
Kim, J.; et al.
Vol. 275, Apr 2024, Article No. 111329

2024/1034
Mechanically robust multifunctional starch films reinforced by surface-tailored nanofibrillated cellulose
Tian, J.; et al.
Vol. 275, Apr 2024, Article No. 111339

2024/1035
A novel 3D topological metamaterial for controllability of polarization-dependent multilayer elastic waves
Wang, G.; et al.
Vol. 275, Apr 2024, Article No. 111341

2024/1036
Calcium crosslinked macroporous bacterial cellulose scaffolds with enhanced in situ mineralization and osteoinductivity for cranial bone regeneration
Xun, X.; et al.
Vol. 275, Apr 2024, Article No. 111277

2024/1037
Highly adhesive self-reinforce hydrogel for the amelioration of intervertebral disc degeneration: Eliminating reactive oxygen species and regulating extracellular matrix
Li, Y.; et al.
Vol. 275, Apr 2024, Article No. 111280

2024/1038
Synthesis of conducting polymer intercalated sodium vanadate nanofiber composites as active materials for aqueous zinc-ion batteries and NH3 gas sensors at room temperature
Lee, S. H.; et al.
Vol. 275, Apr 2024, Article No. 111305

2024/1039
Winding pattern design of composite cylinders considering the effect of fiber stacking
Dai, Y.; et al.
Vol. 275, Apr 2024, Article No. 111306

2024/1040
Antimicrobial peptides loaded collagen nanosheets with enhanced antibacterial activity, corneal wound healing and M1 macrophage polarization in bacterial keratitis
Huang, H.; et al.
Vol. 275, Apr 2024, Article No. 111283

2024/1041
Accuracy enhancement for airbag deployment simulations considering the strain rate and temperature-dependent mechanical properties of thermoplastic olefin and polypropylene
Lee, S.; et al.
Vol. 275, Apr 2024, Article No. 111292

2024/1042
Achieving RCS reduction via scattering and absorption mechanisms using a chessboard structured composite
Jiang, Q.; et al.
Vol. 275, Apr 2024, Article No. 111312

2024/1043
Recycling of CF-ABS machining waste for large format additive manufacturing
Walker, R.; et al.
Vol. 275, Apr 2024, Article No. 111291

2024/1044
Study on HAZ extension characteristics during laser ablation of CFRP based on dimensional analysis
Liang, H.; et al.
Vol. 275, Apr 2024, Article No. 111295

2024/1045
Nanostructure and damage characterisation of bitumen under a low cycle strain-controlled fatigue load based on molecular simulations and rheological measurements
Gao, Y.; et al.
Vol. 275, Apr 2024, Article No. 111326

2024/1046
Bio-inspired design and unusual mechanical properties of 3D horseshoe-shaped soft network metamaterials
Zhou, J.; et al.
Vol. 275, Apr 2024, Article No. 111284

2024/1047
Comparative study on the mechanical behaviors of compression molded, additively manufactured, and injection molded recycled carbon fiber reinforced rHDPE composites
Angulo, C.; et al.
Vol. 275, Apr 2024, Article No. 111323

2024/1048
Directionally induced high-density secondary interaction for enhancing the bonding reliability of titanium alloy and CFRTP via functional Schiff base-contained polymer
Su, J.; et al.
Vol. 275, Apr 2024, Article No. 111316

2024/1049
Multiscale-based multiaxial fatigue model of short fiber reinforced polymer composites under high-cycle proportional loading
Zhang, L.; et al.
Vol. 275, Apr 2024, Article No. 111308

2024/1050
Experimental and numerical study of thermoforming-induced deformation in glass fiber/polyetherimide thermoplastic wing leading edge
Zhai, H.; et al.
Vol. 275, Apr 2024, Article No. 111319

2024/1051
Mechanical performance and radar-absorption capacity of carbon Material–Reinforced polymethacrylimide foam: Preparation, comparison, and design
Song, S.; et al.
Vol. 275, Apr 2024, Article No. 111317

2024/1052
Optimisation of ultrasonic welding process of carbon/epoxy composites using Nylon-based or PES thermoplastic interlayers
Calabrese, L.; et al.
Vol. 275, Apr 2024, Article No. 111318

2024/1053
Failure of 3D-printed composite continuous carbon fibre hexagonal frames
Bokharaie, B.; et al.
Vol. 275, Apr 2024, Article No. 111307

2024/1054
Fiber dispersion as a quality assessment metric for pultruded thermoplastic composites
Elderfield, N.; Cook, O.; Wang, J. C. H.
Vol. 275, Apr 2024, Article No. 111321

2024/1055
Fibre orientation distribution function mapping for short fibre polymer composite components from low resolution/large volume X-ray computed tomography
Anuenhammer, R. M.; et al.
Vol. 275, Apr 2024, Article No. 111313

2024/1056
Architected flexible syntactic foams: Additive manufacturing and reinforcing particle driven matrix segregation
Tewani, H.; et al.
Vol. 275, Apr 2024, Article No. 111315

2024/1057
Electronic metal-support interaction-induced space charge polarization for boosting photoelectrochemical water splitting
Zhang, C.; et al.

Vol. 275, Apr 2024, Article No. 111327

2024/1058
Multimaterial coextrusion (bio)printing of composite polymer biomaterial ink and hydrogel bioink for tissue fabrication
Rodrigues, I. C. P.; et al.
Vol. 275, Apr 2024, Article No. 111337

2024/1059
Fabrication of hollow Ni/NiO/C/MnO2@polypyrrole core-shell structures for high-performance electromagnetic wave absorption
Feng, S.; et al.
Vol. 275, Apr 2024, Article No. 111344

2024/1060
An interface-integrated hydrogel for all-in-one flexible supercapacitor with excellent wide-temperature and self-healing properties
Wang, R.; et al.
Vol. 275, Apr 2024, Article No. 111345

2024/1061
4D printed multifunctional wearable strain sensors with programmable sensing characteristics
Zhang, J.; et al.
Vol. 275, Apr 2024, Article No. 111346

2024/1062
A continuum damage model for Mg/Al composite sheets rolling: Theoretical development and application
Wang, T.; et al.
Vol. 275, Apr 2024, Article No. 111347

2024/1063
Predicting failure in injection-moulded short-fibre subcomponents under varied environmental conditions through fracture mechanics
Fujita, Y.; et al.
Vol. 275, Apr 2024, Article No. 111343

2024/1064
Enhancing mechanical performance and high-temperature lubrication enabled by MoS2/WB2 nanolayered films
Gao, Z.; et al.
Vol. 275, Apr 2024, Article No. 111350

2024/1065
Abundant nucleation sites-available liquid crystal hydrogel mimics bone ECM mineralization to boost osteogenesis
Li, L.; et al.
Vol. 275, Apr 2024, Article No. 111340

2024/1066
A novel machine learning model to design historical-independent health indicators for composite structures
Moradi, M.; Gul, F. C.; Zarouchas, D.
Vol. 275, Apr 2024, Article No. 111328

2024/1067
Adaptive ultrasonic full-matrix imaging of internal defects in CFRP laminates with arbitrary stacking sequences
Yu, Z.; et al.
Vol. 275, Apr 2024, Article No. 111309

2024/1068
The impacts of CaCO3 deposition in natural wood on its viscoelastic properties
Choi, H.; et al.
Vol. 275, Apr 2024, Article No. 111324

2024/1069
Quantitative ultrasonic imaging of weave structure in textile composites
Yang, X.; Kersemans, M.; Fan, Z.
Vol. 275, Apr 2024, Article No. 111310

2024/1070
Controlled interlaminar crack initiation in thin notched laminated thermoplastic composites under impact loading: A first step towards unitary layer recovery
Bruneau, A.; Imbert, M.; May, M.
Vol. 275, Apr 2024, Article No. 111322

2024/1071
Strain-rate dependent mixed-mode traction laws for glass fiber-epoxy interphase using molecular dynamics simulations Chowdhury, S. C.; Gillespie Jr, J. W.
Vol. 275, Apr 2024, Article No. 111351

2024/1072
Novel polybutadiene rubber with long cis-1,4 and syndiotactic vinyl segments (CVBR) for high performance sidewall of all-steel giant off-the-road tire
Zhu, H.; et al.
Vol. 275, Apr 2024, Article No. 111349

2024/1073
Synergistic osteogenesis and angiogenesis in promoting bone repair by levistolide A-induced smad pathway activation
Han, Z.; et al.
Vol. 275, Apr 2024, Article No. 111348

2024/1074
Validation of shape change predictions for stamp forming of carbon fiber thermoplastic composite laminates
Barocio, E.; et al.
Vol. 275, Apr 2024, Article No. 111325

2024/1075
Regulated orientation and exfoliation of flaky fillers by close packing structures in polymer composites for excellent thermal conduction and EMI shielding
Hong, J.; et al.
Vol. 275, Apr 2024, Article No. 111357

2024/1076
An integrated nanofiller spray and nanosecond pulse electrically-assisted method for synergistically interlaminar toughening and in-situ damage monitoring of CFRP composites
Li, M.; et al.
Vol. 275, Apr 2024, Article No. 111355

Computational Mechanics

2024/1077
Numerical simulation of time-dependent behaviors of self-healing hydrogels based on a generalized recursive algorithm
Feng, H.; Jiang, L.
Vol. 73, No. 3, Mar 2024, pp 449-463

2024/1078
An isogeometric analysis framework for ventricular cardiac mechanics
Willems, R.; et al.
Vol. 73, No. 3, Mar 2024, pp 465-506

2024/1079
Variational sensitivity analysis and shape optimisation applied to a non-local, ductile damage model
Guhr, F.; Barthold, F.
Vol. 73, No. 3, Mar 2024, pp 507-531

2024/1080
Three-dimensional plasticity-based topology optimization with smoothed finite element analysis
Li, X.; Zhang, X.; Zhang, Y.
Vol. 73, No. 3, Mar 2024, pp 533-548

2024/1081
Space–time flow computation with boundary layer and contact representation: a 10-year history
Takizawa, K.; Tezduyar, T. E.
Vol. 73, No. 3, Mar 2024, pp 549-578

2024/1082
A micromorphic phase-field model for brittle and quasi-brittle fracture
Bharali, R.; Larsson, F.; Janicke, R.
Vol. 73, No. 3, Mar 2024, pp 579-598

2024/1083
A variationally consistent reproducing kernel enhanced material point method and its applications to incompressible materials
Rodriguez, C.; Huang, T.
Vol. 73, No. 3, Mar 2024, pp 599-618

2024/1084
Fully automated model updating framework for damage detection based on the modified constitutive relation error
Diaz, M.; Charbonnel, P.; Chamoin, L.
Vol. 73, No. 3, Mar 2024, pp 619-638

2024/1085
Extended isogeometric analysis: a two-scale coupling FEM/IGA for 2D elastic fracture problems
Santos, K. F.; Barros, F. B.; Silva, R. P.
Vol. 73, No. 3, Mar 2024, pp 639-665

2024/1086
Stochastic virtual element methods for uncertainty propagation of stochastic linear elasticity
Zheng, Z.; Nackenhorst, U.
Vol. 73, No. 3, Mar 2024, pp 667-684

2024/1087
Non-probabilistic reliability-based topology optimization for two-material structure based on convex set and bounded field mixed model
Zhan,J.; Wang, Z.; Xing, J.
Vol. 73, No. 3, Mar 2024, pp 685-704

2024/1088
A general framework of high-performance machine learning algorithms: application in structural mechanics
Markou, G.; et al.
Vol. 73, No. 4, Apr 2024, pp 705-729

2024/1089
On the continuum mechanics of growing plant-like structures
Platen, J.; Fleischhauer, R.; kaliske, M.
Vol. 73, No. 4, Apr 2024, pp 731-749

2024/1090
An arc-length control technique for solving quasi-static fracture problems with phase field models and a staggered scheme
Zambrano, J.; et al.
Vol. 73, No. 4, Apr 2024, pp 751-772

2024/1091
A multiphase-field approach to small strain crystal plasticity accounting for balance equations on singular surfaces
Prahs, A.; et al.
Vol. 73, No. 4, Apr 2024, pp 773-794

2024/1092
Homogenization assumptions for the two-scale analysis of first-order shear deformable shells
Mester, L.; Klarmann, S.; Klinkel, S.
Vol. 73, No. 4, Apr 2024, pp 795-829

2024/1093
A nonlocal gradient damage model with energy limiter for dynamic brittle fracture
Tran, H. T.; Bui, T. Q.
Vol. 73, No. 4, Apr 2024, pp 831-856

2024/1094
From ductile damage to unilateral contact via a point-wise implicit discontinuity
Daneshyar, A.; Herrmann, L.; Kollmannsberger, S.
Vol. 73, No. 4, Apr 2024, pp 857-872

2024/1095
Concurrent semi-Lagrangian reproducing kernel formulation and stability analysis
Atif, M. M.; Wei-chi, S.
Vol. 73, No. 4, Apr 2024, pp 873-906

2024/1096
Support vector machine guided reproducing kernel particle method for image-based modeling of microstructures
Wang, Y.; et al.
Vol. 73, No. 4, Apr 2024, pp 907-942

2024/1097
A sequential linear programming (SLP) approach for uncertainty analysis-based data-driven computational mechanics
Huang, M.; et al.
Vol. 73, No. 4, Apr 2024, pp 943-965

2024/1098
Topology optimization of self-contacting structures
Frederikse, A. H.; Sigmund, O.; Poulios, K.
Vol. 73, No. 4, Apr 2024, pp 967-981

Construction and building materials

2024/1099
Deciphering the influence of superabsorbent polymers on cement hydration and portlandite formation
Wang, H.; et al.
Vol. 418, Mar 2024, Article No. 135455

2024/1100
Impact of carbon nanotubes on the thermochemical production of road bitumen
Adiko, S.; Chernysheva, E. A.; Gureev, A. A.
Vol. 418, Mar 2024, Article No. 135157

2024/1101
Preparation of calcium sulphoaluminate cement-Portland cement-gypsum based sleeve grouting material: Performance optimization and tensile properties of sleeve connector
Pan, H.; et al.
Vol. 418, Mar 2024, Article No. 135341

2024/1102
Study of the correlation of the mechanical resistance properties of Macael white marble using destructive and non-destructive techniques
Saez-Perez, M. P.; Duran-Suarez, J. A.; Castro-Gomes, J.
Vol. 418, Mar 2024, Article No. 135400

2024/1103
Production of high strength and colored concrete using textile waste reactive dyestuffs as superplasticizers
Erdem, E.; Aydin, G. M.; Kilincarslan, R.
Vol. 418, Mar 2024, Article No. 135382

2024/1104
Design and characterization of carbonate-stone-powder-based foam concrete
Xing, F.; et al.
Vol. 418, Mar 2024, Article No. 135315

2024/1105
Short term ageing of asphalt binder in thin asphalt layers
Connell, J.; Maina, J.; Steyn, W. J.
Vol. 418, Mar 2024, Article No. 135386

2024/1106
Uniaxial compressive behavior of concrete column actively confined with internal Fe-SMA spirals
Yeon, Y.; Ji, S.; Hong, K.
Vol. 418, Mar 2024, Article No. 135393

2024/1107
Study on curing degree of emulsified asphalt chip seal based on the comprehensive electrical properties index
Zeng, Q.; et al.
Vol. 418, Mar 2024, Article No. 135401

2024/1108
Pullout resistance of waste fishing net embedded in the interface between the concrete and fibrous mortar matrix: Test method and experimental investigation
Truong, V. D.; et al.
Vol. 418, Mar 2024, Article No. 135397

2024/1109
Experimental investigation on bond properties between rebar and concrete considering rebar corrosion and concrete deterioration caused by sulfate attack
Song, Y.; et al.
Vol. 418, Mar 2024, Article No. 135352

2024/1110
Energy efficient sustainable concrete for multifunctional applications
Abden, M. J.; et al.
Vol. 418, Mar 2024, Article No. 135213

2024/1111
Seismic response and failure mechanism of ordinary concrete and UHTCC short columns reinforced with negative Poisson's ratio steel bars
Tao, Z.; et al.
Vol. 418, Mar 2024, Article No. 135402

2024/1112
Uni- and tri-axial tests and property characterization for thermomechanical effect on hydrated lime modified asphalt concrete
Ashaibi, A.; et al.
Vol. 418, Mar 2024, Article No. 135307

2024/1113
A novel method for characterizing the random distribution of mortar thickness in asphalt mixtures
Wang, X.; et al.
Vol. 418, Mar 2024, Article No. 135319

2024/1114
Effect of grouting on damage and fracture characteristics of fractured rocks under mode I loading
Hu, Q.; et al.
Vol. 418, Mar 2024, Article No. 135376

2024/1115
Failure mechanism of a green substratum filling material based on digital scatter analysis
Li, J.; et al.
Vol. 418, Mar 2024, Article No. 135288

2024/1116
The effect of freeze-thaw cycles and wind erosion on the characteristics of microbial solidified engineering residue
Zhang, M.; et al.
Vol. 418, Mar 2024, Article No. 135374

2024/1117
Finite element method-based numerical study utilizing experimental data on chloride solution transport in concrete under hydraulic pressure
Park, J.; Jung, H.
Vol. 418, Mar 2024, Article No. 135270

2024/1118
Effect of recycled brick powder with various particle features on early-age hydration, water state, and rheological properties of blended cement paste in the context of 3D Printing
Jia, L.; et al.
Vol. 418, Mar 2024, Article No. 135428

2024/1119
A monitoring method of rail fastener reaction force based on iron pad strain
Li, P.; et al.
Vol. 418, Mar 2024, Article No. 135169

2024/1120
Accuracy analysis on CFRP-RC interfacial defects detected using electrical measurement: Influence of steel reinforcement
Yu, Z.; et al.
Vol. 418, Mar 2024, Article No. 134977

2024/1121
Preparation of aragonite whisker-rich materials by wet carbonation of magnesium slag: A sustainable approach for CO_2 sequestration and reinforced cement
Zhang, D.; et al.
Vol. 418, Mar 2024, Article No. 135429

2024/1122
Long-lasting anti-corrosion of superhydrophobic coating by synergistic modification of graphene oxide with polydopamine and cerium oxide
Xie, C.; et al.
Vol. 418, Mar 2024, Article No. 135283

2024/1123
Water distribution characteristics of capillary absorption in internally cured concrete with superabsorbent polymers
Zheng, S.; et al.
Vol. 418, Mar 2024, Article No. 135446

2024/1124
Improvement on durability of concrete by early age continuous loading treatment
Zeng, Y.; et al.
Vol. 418, Mar 2024, Article No. 135392

2024/1125
Experimental study on dry-wet durability and water stability properties of fiber-reinforced and geopolymer-stabilized loess
Wu, Z.; et al.
Vol. 418, Mar 2024, Article No. 135379

2024/1126
Resourceful modification mechanism of modified electrolytic aluminum spent refractory material and its long-term safety performance assessment
Li, J.; et al.
Vol. 418, Mar 2024, Article No. 135254

2024/1127
Modeling damage caused by combined thermal and traffic loading using viscoelastic continuum damage theory
Zeng, Z.; et al.
Vol. 418, Mar 2024, Article No. 135425

2024/1128
Effect of carbon sequestration methods on uptake potential and characteristics of ordinary portland cement-based concrete
Saikia, S. K.; Rajput, A. S.
Vol. 418, Mar 2024, Article No. 135330

2024/1129
Research on proportion and performance optimization of pure gangue backfilling slurry based on multi-objective differential evolution algorithm
Dong, C.; et al.
Vol. 418, Mar 2024, Article No. 135432

2024/1130
Effect of GFRP bar diameter and concrete cover on bond and development length in UHPFRC
Kauffman, L.; Fam, A.
Vol. 418, Mar 2024, Article No. 135445

2024/1131
Construction potential of rice husk ash as eco-friendly cementitious material in a low-water demand for self-compacting concrete
Plando, F. R. P.; Maquiling, J. T.
Vol. 418, Mar 2024, Article No. 135407

2024/1132
Hardwood and softwood timber - natural stone composite connections
Sebastian, W.; Cao, C.
Vol. 418, Mar 2024, Article No. 134707

2024/1133
Optimizing geopolymer mortar for shotcrete applications by focusing on flowability and early-age mechanical characteristics
Zou, H. Y.; et al.
Vol. 418, Mar 2024, Article No. 135290

2024/1134
Experimental study on shear performance of nail and screw-laminated timber-steel composite and timber-timber systems using low-grade timber and mechanical fasteners
Shahin, A.; et al.
Vol. 418, Mar 2024, Article No. 135403

2024/1135
Effect of maintenance environment on the mechanical property and pore structure of cement paste mixed by seawater
Qi, W.; et al.
Vol. 418, Mar 2024, Article No. 135280

2024/1136
Experimental analysis of blistering and water bleeding on asphalt pavements
Moretti, L.; et al.
Vol. 418, Mar 2024, Article No. 135306

2024/1137
A comparative study on the pullout behavior of hooked-end straight and arc-shaped steel fibers from brittle SIFCON matrices under the influence of adjacent fibers

Li, Y.; et al.
Vol. 418, Mar 2024, Article No. 135311

2024/1138
Toughness and strength of PVA-fibre reinforced magnesium phosphate cement (FRMPC) within 24 h
Liu, J.; et al.
Vol. 418, Mar 2024, Article No. 135339

2024/1139
Multi-scale study on steel fiber reinforcement mechanism and uniaxial tension constitutive relationship of UHPFRC containing stone powder
Yang, J.; et al.
Vol. 418, Mar 2024, Article No. 135336

Earthquakes and Structures

2024/1140
Whole-working history analysis of seismic performance state of rocking wall moment frame structures based on plastic hinge evolution
Su, X.; et al.
Vol. 26, No. 3, Mar 2024, pp 175-189

2024/1141
Probabilistic seismic risk assessment of a masonry tower considering local site effects
Saygili, O.
Vol. 26, No. 3, Mar 2024, pp 191-201

2024/1142
Experimental and numerical investigation on the seismic behavior of the sector lead rubber damper
Xu, X.; et al.
Vol. 26, No. 3, Mar 2024, pp 203-218

2024/1143
Input energy spectrum damping modification factors
Merter, O.; Ucar, T.
Vol. 26, No. 3, Mar 2024, pp 219-228

2024/1144
Factor analysis of subgrade spring stiffness of circular tunnel
Guo, X.; et al.
Vol. 26, No. 3, Mar 2024, pp 229-237

2024/1145
Seismic response analysis of buried oil and gas pipelines-soil coupled system under longitudinal multi-point excitation
Dai, J.; et al.
Vol. 26, No. 3, Mar 2024, pp 239-249

2024/1146
Thermal post-buckling behavior of imperfect graphene platelets reinforced metal foams plates resting on nonlinear elastic foundations
Li, Y.; et al.
Vol. 26, No. 4, Apr 2024, pp 251-259

2024/1147
Seismic behavior of deep-sea pipeline after global buckling under active control
Wang, J.; et al.
Vol. 26, No. 4, Apr 2024, pp 261-267

2024/1148
Seismic fragility analysis of corroded RC pier strengthened by engineered cementitious composites
Liang, Y.; et al.
Vol. 26, No. 4, Apr 2024, pp 269-283

2024/1149
Random vibration-based investigation of required separation gap between adjacent buildings
Soleymani, A.; Kontoni, D. N.; Jahangir, H.
Vol. 26, No. 4, Apr 2024, pp 285-297

2024/1150
MCST bending formulation of a cylindrical micro-shell based on TSDT
Arefi, M.
Vol. 26, No. 4, Apr 2024, pp 299-309

2024/1151
Study on the influence of structural and ground motion uncertainties on the failure mechanism of transmission towers
Fu, Z.; et al.
Vol. 26, No. 4, Apr 2024, pp 311-326

Experimental Mechanics

2024/1152
Review: High Speed Temperature Measurements Under Dynamic Loading
Goviazin, G. G.; Nieto-Fuentes, J. C.; Rittel, D.
Vol. 64, No. 3, Apr 2024, pp 295-304

2024/1153
Non-Associated Flow Rule Constitutive Modeling Considering Anisotropic Hardening for the Forming Analysis of Orthotropic Sheet Metal
Zhang, Y.; et al.
Vol. 64, No. 3, Apr 2024, pp 305-323

2024/1154
A New Brazilian Disc Test Procedure for the Elastic Moduli of Orthotropic C/C-SiC Composites
Padan, R.; et al.
Vol. 64, No. 3, Apr 2024, pp 325-339

2024/1155
A Label-Free Measurement Method for Plane Stress States in Optical Isotropic Films with Spectroscopic Ellipsometry
Sun, X.; et al.
Vol. 64, No. 3, Apr 2024, pp 341-352

2024/1156
Unique Identification of Stiffness Parameters in Hyperelastic Models for Anisotropic, Deformable, Thin Materials Based on a Single Experiment - A Feasibility Study Based on Virtual Full-Field Data
Makhool, L.; Balzani, D.
Vol. 64, No. 3, Apr 2024, pp 353-375

2024/1157
Determination of Young's Modulus of PET Sheets from Lamb Wave Velocity Measurement
Lu, H.; Menary, G.
Vol. 64, No. 3, Apr 2024, pp 377-391

2024/1158
Layer Jamming of Magnetorheological Elastomers for Variable Stifness in Soft Robots
Atakuru, T.; Zungor, G.; Samur, E.
Vol. 64, No. 3, Apr 2024, pp 393-404

2024/1159
Path-Integrated Stereo X-Ray Digital Image Correlation: Resolving the Violation of Conservation of Intensity
Jones, E.
Vol. 64, No. 3, Apr 2024, pp 405-423

2024/1160
Development of an Automated Experimental System for Thermomechanical and Electrical Characterization of NiTi Shape Memory Alloy
Rodino, S.; et al.
Vol. 64, No. 3, Apr 2024, pp 425-440

2024/1161
Residual Stress Determination of Cast Aluminium Benchmark Components Using Strain Relief Techniques
Cai, Z.; et al.
Vol. 64, No. 3, Apr 2024, pp 441-452

2024/1162
Development and Analysis of an On-Road Torque Measurement Device for Trucks
Hyttinen, J.; et al.
Vol. 64, No. 4, Apr 2024, pp 455-466

2024/1163
Improvement in Calibration Procedure in Nanoindentation: An Indenter Bluntness Indicator
Chicot, D.; et al.
Vol. 64, No. 4, Apr 2024, pp 467-485

2024/1164
Stress Evaluation Through the Layers of a Fibre-Metal Hybrid Composite by IHD: An Experimental Study
Nobre, J. P.; et al.
Vol. 64, No. 4, Apr 2024, pp 487-500

2024/1165
Near Edge Residual Stress Measurement Using Incremental Hole Drilling
Olson, M. D.; Dewald, A. T.; Watanabe, B. T.
Vol. 64, No. 4, Apr 2024, pp 501-517

2024/1166
An Improved Strain Field Reconstruction Method Based on Digital Twin for Test Monitoring
Wang, B.; et al.
Vol. 64, No. 4, Apr 2024, pp 519-537

2024/1167
Biaxial Extension of Cruciform Specimens: Embedding Equilibrium into Design and Constitutive Characterization
Vitucci, G.
Vol. 64, No. 4, Apr 2024, pp 539-550

2024/1168
Digital Image Correlation at Extreme Temperatures Using Shortwave Ultraviolet (UV-C) Lights and Filters
Dewanjee, P.; et al.
Vol. 64, No. 4, Apr 2024, pp 551-563

2024/1169
Residual Stress Measurements in Tensile Armours of Flexible Pipes by the Contour and X-Ray Diffraction Methods
Diehl, I. L.; et al.
Vol. 64, No. 4, Apr 2024, pp 565-574

2024/1170
Improving Deep Learning-Based Digital Image Correlation with Domain Decomposition Method
Chi, Y.; Liu, Y.; Pan, B.
Vol. 64, No. 4, Apr 2024, pp 575-586

Experimental Techniques

2024/1171
Numerical and Experimental Study of Wind Effect on the Storage Tanks Based the Tank Adjacency
Davarzani, H. R.; et al.
Vol. 48, No. 2, Apr 2024, pp 191-204

2024/1172
Influence of Slip Table of the Shaker System on the Experimentally Obtained Fundamental Lateral Mode Frequency of a Spacecraft
Renji, K.
Vol. 48, No. 2, Apr 2024, pp 205-217

2024/1173
Analysis of Traction Coefficient Subject to Rail Cleaning Effect Based on Tribomachine Measurements
Bernal, E.; et al.
Vol. 48, No. 2, Apr 2024, pp 219-228

2024/1174
A Comparative Study of the Static and Dynamic Characteristics of Jute and Glass Fiber-Reinforced Polyester Composites
Rizal, M.; Mubarak, A. Z.; Alhaidar, T. R.
Vol. 48, No. 2, Apr 2024, pp 229-237

2024/1175
The Effects of Aging Process After Solution Heat Treatment on Drilling Machinability of Corrax Steel
Guldibi, A. S.; et al.
Vol. 48, No. 2, Apr 2024, pp 239-257

2024/1176
High-Order Time-Domain DIC Algorithm Based on a Nonlinear Optical Flow Equation
Dai, S.; et al.
Vol. 48, No. 2, Apr 2024, pp 259-271

2024/1177
Extracting Time-Varying Dynamic Characteristics of a Typical TPS Plate via Thermal-Vibration Experiment
Xue, C.; et al.

Vol. 48, No. 2, Apr 2024, pp 273-284

2024/1178
An Experimental Study of a Steady Plane Wall Jet with Different Reynolds Numbers, Coflow Stream and Surface Conditions
Zhong, YL.; et al.
Vol. 48, No. 2, Apr 2024, pp 285-298

2024/1179
Low-Velocity Impact Damage Quantification on Sandwich Panels by Thermographic and Ultrasonic Procedures
Pirinu, A.; et al.
Vol. 48, No. 2, Apr 2024, pp 299-322

2024/1180
Double Stage Friction Stir Spot Extrusion Welding: a Novel Manufacturing Technique for Joining Sheets
Abdullah, I. T.; Mejbel, M. K.; Al-bhadle, B. M. A.
Vol. 48, No. 2, Apr 2024, pp 323-342

2024/1181
Experimental Study of Helical Milling Carbon Fiber Reinforced Plastics by Variable Parameters
Jiao, A.; et al.
Vol. 48, No. 2, Apr 2024, pp 343-357

2024/1182
Locating Impacts Through Structural Vibrations Using the FEEL Algorithm Without a Known Input Force
Davis, B. T.; MejiaCruz, Y.
Vol. 48, No. 2, Apr 2024, pp 359-368

2024/1183
Impact-Pose Estimation Using ArUco Markers in Structural Dynamics
Cepon, G.; et al.
Vol. 48, No. 2, Apr 2024, pp 369-380

2024/1184
In-Situ Magnetic Barkhausen Noise Measurements to Identify Elastic-Plastic Deformation and Failure in Different Steels
Chai, J.; et al.
Vol. 48, No. 2, Apr 2024, pp 381-392

International Journal of Steel Structures

2024/1185
The Effect of Plan Geometry on Progressive Collapse of Tall Buildings with Diagrid Structure Based on Nonlinear Static and Dynamic Analyses
Shokoohimatin, M.; Hosseini, M.; Nezamabadi, M. F.
Vol. 24, No. 2, Apr 2024, pp 217-230

2024/1186
Effect of Axial Misalignments in Fillet Welded Cruciform Joint Under Static Loading
Paul, B.; et al.
Vol. 24, No. 2, Apr 2024, pp 231-245

2024/1187
Evaluation of Thickness Effect on Fatigue Life Variation of Longitudinal Welded Gusset Joint
Putri, C. A.; et al.
Vol. 24, No. 2, Apr 2024, pp 246-255

2024/1188
Research on Bending Stiffness of the New Sprayer Joint
Li, R.; et al.
Vol. 24, No. 2, Apr 2024, pp 256-263

2024/1189
A Review of Research on Supported Transmission Line Tower Failure Studies: Analysis, Tower Testing and Retrofitting
Chatterjee, A.; et al.
Vol. 24, No. 2, Apr 2024, pp 264-279

2024/1190
State-of-the-Art Review: Seismic Design and Performance Assessment of Special Concentrically Braced Frames Developed for Complex Industrial Building Structures
Wasse, A. D.; et al.
Vol. 24, No. 2, Apr 2024, pp 280-295

2024/1191
Effect of External Ring Stiffener on the Chord Members of Cold-Formed Steel T-Joints Under Combined Axial Compression and Bending
Sangeetha, P.; et al.
Vol. 24, No. 2, Apr 2024, pp 296-309

2024/1192
Residual Mechanical Properties of Q235FR Steel Exposed to High-temperatures
Yang, S.; Sun, J.; Xu, Z.
Vol. 24, No. 2, Apr 2024, pp 310-323

2024/1193
Seismic Resilience Assessment of the Hybrid Bridge Pier Based on Fragility Analysis
Sun, J.; Xu, W.; Tan, Z.
Vol. 24, No. 2, Apr 2024, pp 324-338

2024/1194
Compressive Behaviour of Diagonally Stiffened Concrete Filled Steel Tubular Stub Columns with Reinforcement Stiffeners
Singh, H.; Tiwary, A. K.
Vol. 24, No. 2, Apr 2024, pp 339-353

2024/1195
Bond Behavior of Concrete-Filled Steel Tube with Molybdenum Tailing
Lin, S.; Liu, F.; Bai, Q.
Vol. 24, No. 2, Apr 2024, pp 354-365

2024/1196
Effect of Strut Stiffness on Seismic Performance of Fully Integral Steel Bridge with a Strut-Braced Pier
Choi, B.; Kwak, J.; Diep, H. T.
Vol. 24, No. 2, Apr 2024, pp 366-376

2024/1197
Study on Detailing of Structural Steel Section on Lateral Behavior of SRC-RC Transfer Columns
Jain, A.; Sahoo, D. R.
Vol. 24, No. 2, Apr 2024, pp 377-392

2024/1198
Experimental and Numerical Analysis on Bending Behavior of Hybrid Bridge Deck System Composed of Transversely Connected OSD and Composite Deck
Dai, C.; et al.
Vol. 24, No. 2, Apr 2024, pp 393-404

2024/1199
Impact resistance and damage assessment of steel beams with different web openings
Chen, H.; et al.
Vol. 24, No. 2, Apr 2024, pp 405-416

International Journal of Structural Stability and Dynamics

2024/1200
Second-Order Generalized Plastic Hinge Method for Ultimate Bearing Capacity Estimation of Unbraced Steel Frames
Yang, L.; et al.
Vol. 24, No. 5, Mar 2024, Article No. 2450045

2024/1201
Intelligent Surface Cracks Detection in Bridges Using Deep Neural Network
Zhang, X.; et al.
Vol. 24, No. 5, Mar 2024, Article No. 2450046

2024/1202
Vibration Reduction Performanceof a New Tuned Mass Damper with Pre-StrainedSuperelastic SMA Helical Springs
Lv, H.; Huang, B.
Vol. 24, No. 5, Mar 2024, Article No. 2450047

2024/1203
Global Optimization of Medium Low-Speed Maglev Train-Bridge Dynamic System Based on Multi-Objective Evolutionary Algorithm
Li, D.; et al.
Vol. 24, No. 5, Mar 2024, Article No. 2450049

2024/1204
Seismic Performance Analysis of the Two-DimensionalIsolation Device for Double-Layer Grid Structure

Zhang, T.; et al.
Vol. 24, No. 5, Mar 2024, Article No. 2450051

2024/1205
An Eigensystem Realization Algorithm for Identification of Modal Parameters of Nonviscous Damping Structure System
Shen, R.; et al.
Vol. 24, No. 5, Mar 2024, Article No. 2450052

2024/1206
Development and Application of Eddy Current Damping-Based Tuned Mass Damper for Wind-Induced Vibration Control of Transmission Tower
Lei, X.; et al.
Vol. 24, No. 5, Mar 2024, Article No. 2450053

2024/1207
Structural Modal Parameters Identification Under Ambient Excitation Using Optimized Symplectic Geometry Mode Decomposition
Hu, F.; et al.
Vol. 24, No. 5, Mar 2024, Article No. 2450054

2024/1208
Nonlinear Dynamic Characteristics of Rotating Thick Ring on the Elastic Foundation Based on Plane Stress Theory
Fan, B.; Wang, Z.; Wang, Q.
Vol. 24, No. 5, Mar 2024, Article No. 2450055

2024/1209
Dynamic Response of Continuous Uphill Pavement with Multi-Layer Plate on Viscoelastic Half-Space Foundation
Li, S.; et al.
Vol. 24, No. 5, Mar 2024, Article No. 2450060

2024/1210
On Nonlinear Vibration of Piezo-Electrically Multiscale Hybrid Nanocomposite Sandwich Plate Including an Auxetic Core Based on HSDT
Mahinzare, M.; Rastgoo, A.; Ebrahimi, F.
Vol. 24, No. 5, Mar 2024, Article No. 2450066

2024/1211
Rapid Assessment of Seismic Risk for Railway Bridges Based on Machine Learning
Huang, Y.; He, J.; Zhu, Z.
Vol. 24, No. 6, Mar 2024, Article No. 2450056

2024/1212
Dynamic Analysis of Coupled Train and Cracked Bridge Systems Using Multiscale Finite Element Modeling
Li, H.; Wang, T.; Yan, H.
Vol. 24, No. 6, Mar 2024, Article No. 2450057

2024/1213
Performance Evaluation of Inerter-Based Dampers for Bridge Flutter Control: A Comparative Study
Feng, Z.; et al.
Vol. 24, No. 6, Mar 2024, Article No. 2450058

2024/1214
Effect of Soil–Structure Interaction on Inelastic Displacement Ratios of Bridge Structures Subjected to Pulse-Like Ground Motions
Sung, Y.; et al.
Vol. 24, No. 6, Mar 2024, Article No. 2450059

2024/1215
Vibration and Stability Analysis of a Spinning Hollow Functionally Graded Beam with Exponentially Varying Cross-Section
Wang, G.; et al.
Vol. 24, No. 6, Mar 2024, Article No. 2450061

2024/1216
Buckling of Thin-Walled Cylindrical Shell Structures with Axially Variable Elastic Modulus Under Axial Compression
Yang, L.; et al.
Vol. 24, No. 6, Mar 2024, Article No. 2450062

2024/1217
Longitudinal Seismic Response of a Pipe Pile Embedded in Saturated Thermoelastic Ground Subjected to Rayleigh Waves
Liu, H.; et al.
Vol. 24, No. 6, Mar 2024, Article No. 2450063

2024/1218
Dynamic Amplification Factors of an Arch Bridge Under Random Traffic Flows
Wang, B.; et al.
Vol. 24, No. 6, Mar 2024, Article No. 2450064

2024/1219
Performance of Floating Slab Track with Rubber Vibration Isolator
Deng, S.; et al.
Vol. 24, No. 6, Mar 2024, Article No. 2450065

2024/1220
Prediction Framework of Vortex-Induced Vibration of Steel Tubes in Transmission Towers Based on Generalized Wake Oscillator Model
Li, J.; Li, Z.; Wang, T.
Vol. 24, No. 6, Mar 2024, Article No. 2450066

2024/1221
Linear and Nonlinear Vibration of Axially Loaded Timoshenko Beam with Elastic Supports: Effects of Transition Parameter
Li, Z.; et al.
Vol. 24, No. 6, Mar 2024, Article No. 2450067

2024/1222
A Drive-By Methodology for Rapid Inspection of HSR Bridge Substructures Using Dynamic Responses of Passing Marshaling Trains
Wang, C.; et al.
Vol. 24, No. 6, Mar 2024, Article No. 2450068

2024/1223
Model Updating Method for Jacket Platform Considering Different Component Degradation Based on Deep Learning
Li, Y.; et al.
Vol. 24, No. 7, Apr 2024, Article No. 2450070

2024/1224
Characterization of Dynamic Mechanical Properties of Viscoelastic Damper Based on Physics-Constrained Data-Driven Approach
Li, Q.; et al.
Vol. 24, No. 7, Apr 2024, Article No. 2450071

2024/1225
Temperature-Dependent Vibration Characteristics of Porous FG Material Plates Utilizing FSDT
Kumar, V.; Singh, S. J.; Harsha, P.
Vol. 24, No. 7, Apr 2024, Article No. 2450072

2024/1226
Adaptive Flexible Controller Frequency Optimization for Reducing Structural Response of a 10 Mw Floating Offshore Wind Turbine
Zhang, R.; et al.
Vol. 24, No. 7, Apr 2024, Article No. 2450073

2024/1227
Damage Assessment of Multi-Box Structures Subjected to Internal Blast Loadings
Li, L.; et al.
Vol. 24, No. 7, Apr 2024, Article No. 2450074

2024/1228
Finite Element-Based Free Vibration and Deflection Analysis of Bio-Composites Hybrid Laminated Skew Plates Using Experimental Elastic Properties
Sahu, D. P.; Prusty, J. K.; Mohanty, S. C.
Vol. 24, No. 7, Apr 2024, Article No. 2450075

2024/1229
Vibration Characteristics of Mistuned Blisk with Chordwise Variable Thickness Blades Subjected to Aerodynamic Prestress
Song, R.; et al.
Vol. 24, No. 7, Apr 2024, Article No. 2450076

2024/1230
Impact of the Porosity and Elastic Foundation on Frequency and Buckling Response of Bidirectional Functionally Graded Piezoelectric Porous Plate
Harsha, A.; Kumar, P.
Vol. 24, No. 7, Apr 2024, Article No. 2450077

2024/1231
Analytic Solution for Free Vibrations of Folded Plate Structures
Deutsch, A.; Eisenberger, M.

Vol. 24, No. 7, Apr 2024, Article No. 2450078

2024/1232
Experimental and Numerical Study on Damage Characteristics of the Shield Tunnel Segment Under Blast Impact Loading
Zahng, Z.; et al.
Vol. 24, No. 7, Apr 2024, Article No. 2450079

2024/1233
Nonlinear Inelastic Stability Behavior of High-Strength Stainless Steel I-Beams with Sinusoidal Web Openings
Carvalho, A. S.; et al.
Vol. 24, No. 7, Apr 2024, Article No. 2450080

2024/1234
An Analytical Solution on Vibration Reduction and Shear Force Mitigation of Cantilever Mindlin Plates Using Orthogonal Ribs
Guo, H.; Zhang, K.; Lin, T. R.
Vol. 24, No. 7, Apr 2024, Article No. 2450082

2024/1235
Ensemble Learning-Based Seismic Response Prediction of Isolated Structure Considering Soil–Structure Interaction
Fu, B.; Liu, X.; Chen, J.
Vol. 24, No. 8, Apr 2024, Article No. 2450081

2024/1236
Nonlinear Damping and Vibration Assessment of Sandwich Beam with Composite Faces and Viscoelastic Core Layer
Al-Dulaijan, S. U.; et al.
Vol. 24, No. 8, Apr 2024, Article No. 2450083

2024/1237
An Improved Stochastic Averaging on the Piezoelectric Vibrational Harvester Model with Stiffness and Inertia Nonlinearities
Li, Y.; Ge, G.
Vol. 24, No. 8, Apr 2024, Article No. 2450084

2024/1238
Bridge Damage Identification Using Rotation Influence Line Under Random Vehicle Loads
Liu, C.; et al.
Vol. 24, No. 8, Apr 2024, Article No. 2450085

2024/1239
On the Static Instability of FG-GNP-Reinforced Composite Cylindrical Shells Under Thermo-Mechanical Loading
Jia, Y.
Vol. 24, No. 8, Apr 2024, Article No. 2450086

2024/1240
Dynamic Analysis of Elastically Supported Functionally Graded Sandwich Beams Resting on Elastic Foundations Under Moving Loads
Chen, W.; Lin, C.
Vol. 24, No. 8, Apr 2024, Article No. 2450087

2024/1241
Frequency Variation and Dynamic Behavior in a Moving Mass-Plate System
Yang, J. P.; Huang, S.; Yau, J. D.
Vol. 24, No. 8, Apr 2024, Article No. 2450088

2024/1242
Seismic Isolation Measures of Plate-Shell Integrated Concrete Liquid-Storage Structure
Qi, L.; et al.
Vol. 24, No. 8, Apr 2024, Article No. 2450090

2024/1243
Implementation and Verification of Real-TimeHybrid Simulation for the Dynamic PerformanceAssessment of Base-Isolated Structures
Liu, Y. H.; et al.
Vol. 24, No. 8, Apr 2024, Article No. 2450091

2024/1244
A Novel Split-Type Two-Axle Vehicle Modelfor Bridge Indirect Measurement
Zhu, J.; Shi, T.
Vol. 24, No. 8, Apr 2024, Article No. 2450092

2024/1245
Size-Dependent Electro-Thermal Buckling Analysisof Flexoelectric Microbeams
Beni, Y. T.
Vol. 24, No. 8, Apr 2024, Article No. 2450093

2024/1246
A Hybrid Genetic Algorithm-Based Parameter IdentificationMethod for Nonlinear Hysteretic Systemwith Experimental Verification
Lu, Z.; et al.
Vol. 24, No. 8, Apr 2024, Article No. 2450099

2024/1247
Experimental Study on Impulse-Induced Liquid SloshingModes and Frequencies in Rectangular Tanks
Hsu, W.; et al.
Vol. 24, No. 8, Apr 2024, Article No. 2550040

2024/1248
Out-of-Plane Instability and Vibrationsof a Flexible Circular Arch Under a Moving Load
Zhao, X.; Heijden, G. H. M.
Vol. 24, No. 8, Apr 2024, Article No. 2550049

Journal of The Institution of Engineers (India): Series A

2024/1249
A Machine Learning-Based User-Friendly Approach for Prediction of Traffic-Induced Vibrations and its Application for Parametric Study
Javaid, M. F.; et al.
Vol. 105, No. 1, Mar 2024, pp 1-13

2024/1250
A Parametric Study on Composite Panel Subjected to Compression Load
Kumar, S.; Suman, S. K.; Ranjan, A.
Vol. 105, No. 1, Mar 2024, pp 15-24

2024/1251
Behavior of the Column Stubs of Telecommunication Towers Strengthened with Different Types of FRP Fabrics
Mohamed, M. S. M.; Hanna, N. F.; Ayash, N. M.
Vol. 105, No. 1, Mar 2024, pp 25-35

2024/1252
Compressive Strength and Elasticity of Masonry Prisms with Clay Brick and Flyash Brick
Mishra, R.; Kumar, P.
Vol. 105, No. 1, Mar 2024, pp 37-48

2024/1253
Critical Analysis of PM2.5 in Delhi Region to Strategize Effective Air Pollution Management Plan
Jha, A. K.; Suman; Mishra, S. K.
Vol. 105, No. 1, Mar 2024, pp 49-59

2024/1254
Design of Concrete Colour Reference Charts for Monitoring of Deterioration in Concrete Structures
Reddy, V. G. P.; et al.
Vol. 105, No. 1, Mar 2024, pp 61-75

2024/1255
Experimental Investigation on the Behavior of Steel Angle and Strip Jacketed RC Column Under Eccentric Loading
Sen, D.; Begum, M.
Vol. 105, No. 1, Mar 2024, pp 77-89

2024/1256
Identifying Factors Causing Motorcycle Crashes Among Young Adults in India Using Modified Motorcycle Rider Behavior Questionnaire
Kumar, A.; et al.
Vol. 105, No. 1, Mar 2024, pp 91-104

2024/1257
Influence of Diagonal Prop Bar on the Behavior of Stiffened Concrete-Filled Steel Tube Columns
Singh, H.; Tiwary, A. K.
Vol. 105, No. 1, Mar 2024, pp 105-128

2024/1258
Investigation on Flexural Behavior of Conventionally Reinforced, Steel Fiber-Reinforced, and Post-tensioned Geopolymer Concrete Beams

Srinivasamurthy, L.; Nataraja, M. C.; Srinivasan, K.
Vol. 105, No. 1, Mar 2024, pp 129-150

2024/1259
Mechanical and Fracture Behavior of Concrete Material Derived from CDA, Crumb Rubber Particles and Inclusion of Basalt Fiber
Puram, A.; et al.
Vol. 105, No. 1, Mar 2024, pp 151-165

2024/1260
Modeling and Optimization of Specific Cutting Energy Required for Cutting Napier Grass Using RSM
Powar, R. V.; et al.
Vol. 105, No. 1, Mar 2024, pp 167-175

2024/1261
Probabilistic Analysis of Pile Foundation in Cohesive Soil
Mustafa, R.; et al.
Vol. 105, No. 1, Mar 2024, pp 177-193

Journal of Intelligent Material Systems and Structures

2024/1262
Experimentation and simulation study of electromechanical response characteristics of a 2-2 type cement-based piezoelectric composite sensor
Dong, H.; et al.
Vol. 35, No. 4, Mar 2024, pp 370-379

2024/1263
Health monitoring of steel structures using surface mountable and detachable PZT sensor
Singh, S. K.; Shanker, R.; Ranjan, A.
Vol. 35, No. 4, Mar 2024, pp 380-392

2024/1264
Numerical analysis of the dynamic characteristics of a fractional-order viscoelastic beam with fixed supports at both ends
Li, H.; et al.
Vol. 35, No. 4, Mar 2024, pp 393-409

2024/1265
Parameter estimation of transfer function of viscous clutch with electrorheological fluid and torque control
Musialek, I.; et al.
Vol. 35, No. 4, Mar 2024, pp 410-423

2024/1266
A micromechanical modeling approach for predicting the piezoelectric and mechanical properties of piezoelectric fiber-reinforced multiphase composites containing CNT/GNP hybrids
Zhou, Y.; et al.
Vol. 35, No. 4, Mar 2024, pp 424-439

2024/1267
A hybrid self-centering seismic damper: Finite element modeling and parametric analysis
Cao, S.; et al.
Vol. 35, No. 4, Mar 2024, pp 440-457

2024/1268
Magnetostrictive energy conversion ability of Iron Cobalt Vanadium alloy sheet: Experimental and theoretical evaluation
Zangho, B. F. T.; et al.
Vol. 35, No. 4, Mar 2024, pp 458-470

2024/1269
Modeling and experimental study of a miniaturized magnetorheological valve with high performance
Ntella, S. L.; Koechli, C.; Perriard, Y.
Vol. 35, No. 4, Mar 2024, pp 471-481

2024/1270
Asymmetric two-dimensional poroelastic analysis of heterogeneous smart discs considering hygrothermal loading
Eldeeb, A. M.; et al.
Vol. 35, No. 5, Mar 2024, pp 517-537

2024/1271
A bio-inspired shape memory alloy-based smart fin system for adaptive thermal management
Pandey, S. R.; Bhattacharya, B.

Vol. 35, No. 5, Mar 2024, pp 538-555

2024/1272
Attenuation characteristics of concrete using smart aggregate transducers: Experiments and numerical simulations of P-wave propagation
Sun, X.; Fan, S.; Liu, C.
Vol. 35, No. 5, Mar 2024, pp 556-572

2024/1273
Design, theoretical modeling, and experimental analysis of a magnetorheological damper with radial damping gap
Yan, J.; Dong, L.
Vol. 35, No. 5, Mar 2024, pp 573-586

2024/1274
Experimental and numerical investigation of the bonding conditions of piezoelectric sensors under high compressive strains on structures
Negi, P.; Kaur, N.; Kumar, P.
Vol. 35, No. 5, Mar 2024, pp 587-604

2024/1275
Impact behavior of a novel magnetorheological energy absorber based on wedge-shaped squeeze flow model
Li, Z.; Fu, B.; Liao, C.
Vol. 35, No. 6, Apr 2024, pp 607-620

2024/1276
Medium-high frequency vibration control of an industrial pipeline using squeeze-mode magnetorheological dampers
Dong, X.; et al.
Vol. 35, No. 6, Apr 2024, pp 621-632

2024/1277
Monitoring damage of concrete beams via self-sensing cement mortar coating with carbon nanotube-nano carbon black composite fillers
Qiu, L.; et al.
Vol. 35, No. 6, Apr 2024, pp 633-648

2024/1278
Pseudo-Active Actuators With Positive-Negative Dampings
Bai, X. F.; Chen, J.
Vol. 35, No. 6, Apr 2024, pp 649-660

2024/1279
Experimental investigation of a novel high performance multi-walled carbon nano-polyvinylpyrrolidone/silicon-based shear thickening fluid damper
Sun, L.; Wang, G.; Zhang, C.
Vol. 35, No. 6, Apr 2024, pp 661-672

2024/1280
Modal signal analysis of parabolic shell structures with flexoelectric sensors
Zhang, J.; Fan, M.; Tzou, H.
Vol. 35, No. 7, Apr 2024, pp 675-688

2024/1281
Analysis and experimentation of variable gap magnetorheological transmission device driven by electromagnetic force
Gong, H.; Huang, J.
Vol. 35, No. 7, Apr 2024, pp 689-704

2024/1282
Optimized piezo-shunted metadamping towards the high-stiff high-damped metamaterial
Bera, K. K.; Biswas, S.; Banerjee, A.
Vol. 35, No. 7, Apr 2024, pp 705-717

2024/1283
Development of a bipedal piezoelectric actuator with flexible mechanism based on the frog-leg inspiration
Cheng, T.; et al.
Vol. 35, No. 7, Apr 2024, pp 718-726

2024/1284
VIV array for wind energy harvesting
Chen, S.; et al.
Vol. 35, No. 7, Apr 2024, pp 727-739

Journal of Pressure Vessel Technology

2024/1285
Thermo-fluid-coupled analysis of double fillet welds on tube membrance panels during submerged arc welding
Koo, B. S.
Vol. 146, No. 2, Apr 2024, Article No. 21001

2024/1286
A unified fracture model for X65 pipeline material under various constraints using the extended finite element method (XFEM)
Shahzamanian, M. M.
Vol. 146, No. 2, Apr 2024, Article No. 21301

2024/1287
Large deformation dynamic characteristics of cracked laminated panel and improvement of stiffness using shape memory alloy fiber
Kumar, E. K.; Pattanayak, P.; Panda, S. K.
Vol. 146, No. 2, Apr 2024, Article No. 21302

2024/1288
Analytical formulation to predict residual stresses in thick-walled cylinders subjected to hoop winding, shrink-fit, and conventional and reverse autofrettages.
Vol. 146, No. 2, Apr 2024, Article No. 21501

2024/1289
Corrosion fatigue behavoiur of 6000HP fracture pump of the valve body under different plunger stroke times and acid fracture fluid environment
Wang, G.; et al.
Vol. 146, No. 2, Apr 2024, Article No. 21502

2024/1290
Failure pressure evaluation of corroded pipeline using semi-empirical and finite element analysis
Torres, J. V. S.; et al.
Vol. 146, No. 2, Apr 2024, Article No. 21503

2024/1291
Comparative Analysis of Bursting Pressure Prediction Methods for Steam Generator Tube With Volume Defect
Han, Y.; Huang, S.; Hui, H.
Vol. 146, No. 2, Apr 2024, Article No. 21701

Journal of Sandwich Structures & Materials

2024/1292
Structural optimization and experimental study on the Ti-alloy kagoma structure formed by the superplastic forming/diffusion bonding process
Wu, D.; et al.
Vol. 26, No. 3, Mar 2024, pp 303-316

2024/1293
Global bucking behavior of a sandwich beam with graded lattice cores
Zhang, H.; et al.
Vol. 26, No. 3, Mar 2024, pp 317-335

2024/1294
On finite group velocity in composite plates
Kuznetsoy, S.
Vol. 26, No. 3, Mar 2024, pp 336-349

2024/1295
Impact analysis of compression preloaded honeycomb sandwich structures
Fischer, C.; et al.
Vol. 26, No. 3, Mar 2024, pp 350-372

2024/1296
Tensile properties of transversely isotropic closed-cell PVC foam under quasi-static and dynamic loadings
Tang, Y.; et al.
Vol. 26, No. 3, Mar 2024, pp 373-395

2024/1297
Optimization on compressive strength of sandwich plates with internal arborescent microstructure
Wirowski, A.; Kowalczyk, I.
Vol. 26, No. 3, Mar 2024, pp 396-414

Journal of Vibration and Control

2024/1298
Characteristic study of pyroshock propagation in a structure using a pyroshock simulator
Kim, B.; Lee, J.
Vol. 30, No. 5-6, Mar 2024, pp 960-972

2024/1299
Bearing fault diagnosis method based on variational mode decomposition optimized by CS-PSO
Liu, R.; et al.
Vol. 30, No. 5-6, Mar 2024, pp 973-987

2024/1300
Bandwidth widening for sound absorption of a flexible microoperforated panel backed by a multi-frequency panel-type resonator
Yeang, W. Y.; Halim, D.
Vol. 30, No. 5-6, Mar 2024, pp 988-1001

2024/1301
Correlation transmissibility damage indicator for deterioration performance analysis of hydropower generator unit
Tong, K.; et al.
Vol. 30, No. 5-6, Mar 2024, pp 1002-1012

2024/1302
Transfer learning evaluation based on optimal convolution neural networks architecture for bearing fault diagnosis applications
Alabsi, M.; et al.
Vol. 30, No. 5-6, Mar 2024, pp 1013-1022

2024/1303
Modeling and characteristics study of double-diamond bionic vibration isolation system with inerter
Song, Y.; et al.
Vol. 30, No. 5-6, Mar 2024, pp 1023-1035

2024/1304
Automatic modal identification based on similarity filtering and fuzzy clustering
Jiang, D.; et al.
Vol. 30, No. 5-6, Mar 2024, pp 1036-1047

2024/1305
Study on dynamic characteristics of composite plates under non-uniform gradient temperature along the thickness
Duan, B.; et al.
Vol. 30, No. 5-6, Mar 2024, pp 1048-1062

2024/1306
Vibro-acoustic response of ribbed-panel-cavity systems due to an internal sound source excitation
Zhang, K.; et al.
Vol. 30, No. 5-6, Mar 2024, pp 1063-1079

2024/1307
The optimum enhanced viscoelastic tuned mass dampers: Exact closed-form expressions
Chowdhury, S.; Banerjee, A.; Adhikari, S.
Vol. 30, No. 5-6, Mar 2024, pp 1080-1102

2024/1308
Unbalanced vibration control of active magnetic bearing using an active disturbance rejection notch decoupling technique
Li, B.
Vol. 30, No. 5-6, Mar 2024, pp 1103-1116

2024/1309
Neural network–based active control of a rigid–flexible spacecraft with bounded input
Fu, Y.
Vol. 30, No. 5-6, Mar 2024, pp 1117-1132

2024/1310
Chattering-free terminal sliding-mode tracking control for uncertain nonlinear systems with disturbance compensation
Zou, X.; et al.
Vol. 30, No. 5-6, Mar 2024, pp 1133-1142

2024/1311
Fault-tolerant attitude control for liquid-filled flexible spacecraft without angular velocity measurements based on disturbance observer
Song, X.; et al.
Vol. 30, No. 5-6, Mar 2024, pp 1143-1158

2024/1312
Thermoacoustic response of polymethyl methacrylate composite shells reinforced by carbon nanotube resting on Winkler–Pasternak elastic foundation
Tarkashvand, A.; et al.
Vol. 30, No. 5-6, Mar 2024, pp 1159-1178

2024/1313
Compound faults diagnosis of rotating machinery via enhanced two-layer sliding correlated kurtosis
Zhang, C.; et al.
Vol. 30, No. 5-6, Mar 2024, pp 1179-1189

2024/1314
Stabilization of nonlinear fractional order faulty systems with time-varying delay
Mahmoudabadi, P.; Tavakoli-Kakhki, M.
Vol. 30, No. 5-6, Mar 2024, pp 1190-1199

2024/1315
Design and efficiency evaluation of a new wearable device for multi-degree suppression of hand pathological tremor
Yousef, M.; et al.
Vol. 30, No. 5-6, Mar 2024, pp 1200-1213

2024/1316
Composite collaborative acoustic metamaterials: Isolating shaft vibration of guide roller in printing machine
Lei, X.; et al.
Vol. 30, No. 5-6, Mar 2024, pp 1214-1226

2024/1317
Anti-sway control of variable rope length container crane based on phase plane trajectory planning
Huang, W.; et al.
Vol. 30, No. 5-6, Mar 2024, pp 1227-1240

2024/1318
A Rolling Bearing Fault Diagnosis Method via 2D Feature Map of CSCoh After Denoising and MSCNN Under Different Conditions
Chen, X.; et al.
Vol. 30, No. 5-6, Mar 2024, pp 1241-1253

2024/1319
Robust H∞ output consensus of heterogeneous nonlinear multi-agent systems with external disturbance and unknown time-delay based on distributed Lyapunov-based MPC
Rahimi, N.; Binazadeh, T.
Vol. 30, No. 5-6, Mar 2024, pp 1254-1274

2024/1320
Parametric optimization of the Eddy current dampers applied to a suspension bridge considering bi-directional earthquakes
Hu, S.; et al.
Vol. 30, No. 5-6, Mar 2024, pp 1275-1285

2024/1321
Suppress chatter in milling of thin-walled parts via fixture with active support
Dong, X.; et al.
Vol. 30, No. 5-6, Mar 2024, pp 1286-1296

2024/1322
Performance evaluation of an improved non-singular sliding mode attitude control of a perturbed quadrotor: Experimental validation
Hassani, H.; Mansouri, A.
Vol. 30, No. 5-6, Mar 2024, pp 1297-1312

2024/1323
A novel adaptive robust control for trajectory tracking of mobile robot with uncertainties
Xiao, W.; et al.
Vol. 30, No. 5-6, Mar 2024, pp 1313-1325

2024/1324
Robust control of vehicle suspension systems with friction non-linearity for ride comfort enhancement
Ozbek, C.; Burkan, R.; Yagiz, N.
Vol. 30, No. 5-6, Mar 2024, pp 1326-1338

2024/1325
A Lagrangian approach for the railway vehicle with gear system coupled model considering

wheel polygonal faults under traction conditions
Zhao, Y.; et al.
Vol. 30, No. 5-6, Mar 2024, pp 1339-1352

2024/1326
A harmonic balance solution for the intrinsic 1D nonlinear equations of the beams
Siami, A.; Nitzsche, F.
Vol. 30, No. 5-6, Mar 2024, pp 1353-1367

2024/1327
Acoustic propagation through a duct metamaterial attached with periodic multi-resonant cavities
Liu, J.; et al.
Vol. 30, No. 5-6, Mar 2024, pp 1368-1377

2024/1328
Vibration and stability analysis of a spinning shaft with arbitrary boundaries subjected to partial load
Guang-ding, W.; et al.
Vol. 30, No. 5-6, Mar 2024, pp 1378-1390

2024/1329
Analyses of synchronous motion characteristics for a two-rigid-body vibration system with three co-rotating eccentric rotors mounted on two different rigid bodies
Yu, L.; Hou, Y.
Vol. 30, No. 7-8, Apr 2024, pp 1405-1421

2024/1330
Low-frequency sound insulation of honeycomb membrane-type acoustic metamaterials with different interlayer characteristics
Li, Y.; Yan, J.; zhang, Y.
Vol. 30, No. 7-8, Apr 2024, pp 1422-1437

2024/1331
A combined method to identify the rail irregularity at welded region
Lou, P.; Chen, Y.; Li, Z.
Vol. 30, No. 7-8, Apr 2024, pp 1438-1448

2024/1332
The optimum design of particle tuned mass damper for structural seismic control considering soil-structure interaction
Liu,S.; et al.
Vol. 30, No. 7-8, Apr 2024, pp 1449-1463

2024/1333
Investigation on the tunable bi-stable clustered energy conversion inspired dynamic vibration absorbers: A theoretical study
Huang, X.; Zhang,X.; Yang, B.
Vol. 30, No. 7-8, Apr 2024, pp 1464-1478

2024/1334
Online frequency estimation of periodic disturbance based on FFT algorithm with application in repetitive control
Moghadam, H.; Vasegh, N.; Mousavi, S. M. S.
Vol. 30, No. 7-8, Apr 2024, pp 1479-1486

2024/1335
Test and analysis of multi-cavity particle damper for horizontal vibration control of pipeline structures
Wang, B.; et al.
Vol. 30, No. 7-8, Apr 2024, pp 1487-1501

2024/1336
Fault identification with limited labeled data
Berenji, A.; Taghiyarrenani, Z.; Bastami, A. R.
Vol. 30, No. 7-8, Apr 2024, pp 1502-1510

2024/1337
Research on dynamic characteristics of a novel triple-magnet magnetic suspension dynamic vibration absorber
Chen, X.; et al.
Vol. 30, No. 7-8, Apr 2024, pp 1511-1523

2024/1338
Modeling and control of robotic manipulators equipped with the flexible cable-pulley based gravity compensation mechanism
Arezoo, K.; et al.
Vol. 30, No. 7-8, Apr 2024, pp 1524-1547

2024/1339
Parameters optimization of three-element dynamic vibration absorber with inerter and grounded stiffness
Baduidana, M.; Kenfack-Jiotsa, A.
Vol. 30, No. 7-8, Apr 2024, pp 1548-1565

2024/1340
Unbalance identification for a practical turbofan engine using augmented Kalman filter improved with the convergence criterion
Zhou, L.; et al.
Vol. 30, No. 7-8, Apr 2024, pp 1566-1579

2024/1341
Fixed time sliding mode control for disturbed robotic manipulator
Anjum, Z.; et al.
Vol. 30, No. 7-8, Apr 2024, pp 1580-1593

2024/1342
L-kurtosis-based optimal wavelet filtering and its application to fault diagnosis of rolling element bearings
Ming, A.; et al.
Vol. 30, No. 7-8, Apr 2024, pp 1594-1603

2024/1343
Fractional-Order sliding mode control of a 4D memristive chaotic system
Gokyildirim, A.; Calgan, H.; Demirtas, M.
Vol. 30, No. 7-8, Apr 2024, pp 1604-1620

2024/1344
Modal parameter identification in civil structures via Hilbert transform ensemble with improved empirical wavelet transform
Qin, S.; et al.
Vol. 30, No. 7-8, Apr 2024, pp 1621-1634

2024/1345
Adaptive backstepping control design for ATMD systems in nonlinear structures with nonlinear disturbance and parametric uncertainties
Umutlu, R. C.; et al.
Vol. 30, No. 7-8, Apr 2024, pp 1635-1646

2024/1346
Adaptive neural network independent joint-based control for an ODE-PDE rigid-flexible manipulator with multiple constraints
Liu, S.; et al.
Vol. 30, No. 7-8, Apr 2024, pp 1647-1658

2024/1347
Performance study of model predictive control with reference prediction for real-time hybrid simulation
Zeng, C.; Guo,
Vol. 30, No. 7-8, Apr 2024, pp 1659-1673

2024/1348
Two elastic supporting models to simulate the submerged floating tunnel and their equivalence on the free/forced vibrations
Yi, Z.; et al.
Vol. 30, No. 7-8, Apr 2024, pp 1674-1689

2024/1349
Generalized fractional-order Legendre wavelet method for two dimensional distributed order fractional optimal control problem
Kumar, N.; Mehra, M.
Vol. 30, No. 7-8, Apr 2024, pp 1690-1705

2024/1350
Investigation of the effects of frequency veering phenomenon in a pre-twisted and double-tapered rotating Timoshenko beam
Sachin, D.; Degalhal, M. R.
Vol. 30, No. 7-8, Apr 2024, pp 1706-1720

2024/1351
H∞ performance tracking and group consensus of delayed multiagent systems under attack
Nasir, M.; et al.
Vol. 30, No. 7-8, Apr 2024, pp 1721-1736

2024/1352
Finding the exact value of the maximum allowable upper bound of the delay parameters in the multiple-delay LTI systems
Abolpour, R.; Dehghani, M.

Vol. 30, No. 7-8, Apr 2024, pp 1737-1745

2024/1353
A statistical and reliability approach to vibration-based health monitoring in composite structures
Nobari, A. E. S.; Aliabadi, M. H. F.
Vol. 30, No. 7-8, Apr 2024, pp 1746-1758

2024/1354
An efficient underwater absorber using pentamode metamaterials for broadband frequency
Jia, X.; et al.
Vol. 30, No. 7-8, Apr 2024, pp 1759-1771

2024/1355
Optimization of sound-absorbing and insulating structures with 3D printed recycled plastic and tyre rubber using the TOPSIS approach
Astrauskas, T.; Grubliauskas, R.; Janusevicius, T.
Vol. 30, No. 7-8, Apr 2024, pp 1772-1782

2024/1356
Output feedback attitude control of flexible spacecraft under actuator misalignment and input nonlinearities
Javaid, U.; et al.
Vol. 30, No. 7-8, Apr 2024, pp 1783-1801

2024/1357
Improving soundproof characteristics of an FG-CNT–reinforced composite structure by adding a coating magneto-electro-elastic layer
Ghassabi, M.; Motaharifar, F.; Talebitooti, R.
Vol. 30, No. 7-8, Apr 2024, pp 1802-1017

2024/1358
Multi-objective parameter optimization of ultrasonic vibration–assisted micro-EDM of Ti-6Al-4V alloys
Xu, J.; et al.
Vol. 30, No. 7-8, Apr 2024, pp 1818-1828

2024/1359
UAV-based operational modal analysis method using improved homography-based perspective rectification method
Luo, J.; et al.
Vol. 30, No. 7-8, Apr 2024, pp 1829-1840

2024/1360
Reliability analysis for product package via probability density function of acceleration random response
Yang, S.; Liu, Z.
Vol. 30, No. 7-8, Apr 2024, pp 1841-1854

Materials and Structures

2024/1361
Water vapour permeability of inorganic construction materials
Hall, C.; Lo, G. J.; Hamilton, A.
Vol. 57, No. 2, Mar 2024, pp 39

2024/1362
Seismic performance of a new type of RC shear walls confined with high-strength rectangular spiral reinforcements
Zhao, H.; et al.
Vol. 57, No. 2, Mar 2024, pp 38

2024/1363
Textile reinforced mortar (TRM) as a barrier for concrete structures subjected to carbonation and chloride attack: experimental investigation and analytical modelling
Karakasis, I. C.; et al.
Vol. 57, No. 2, Mar 2024, pp 37

2024/1364
Evolution of self-healing performance of UHPC exposed to aggressive environments and cracking/healing cycles
Xi, B.; Ferrara, L.
Vol. 57, No. 2, Mar 2024, pp 36

2024/1365
Hydration and microstructure of calcium sulfoaluminate-Portland cement binder systems for set-on-demand applications

Tao, Y.; et al.
Vol. 57, No. 2, Mar 2024, pp 35

2024/1366
Simplified methodology for fatigue analysis of reinforced asphalt systems
Oreskovic, M.; et al.
Vol. 57, No. 2, Mar 2024, pp 34

2024/1367
Non-linear analysis of rectangular cross-sections with different reinforcements: dimensionless closed form solution
Belliazzi, S.; et al.
Vol. 57, No. 2, Mar 2024, pp 33

2024/1368
Property deterioration in reactive elastomeric terpolymer modified binders during storage at elevated temperatures
Sharma, A.; et al.
Vol. 57, No. 2, Mar 2024, pp 32

2024/1369
Tensile strength retention of glass fibre-reinforced stirrups subjected to aggressive solutions: effect of environmental condition, stirrup shape and stirrup diameter
Hajmoosa, A.; et al.
Vol. 57, No. 2, Mar 2024, pp 31

2024/1370
Research on the durability of FRP-bonded concrete beams subjected to a performance probabilistic design method
Zou, Y.; Ji, Y.; Li, W.
Vol. 57, No. 2, Mar 2024, pp 30

2024/1371
Performance evaluation of axially loaded BFRP-reinforced concrete members confined with hybrid helix-ties
Elhag, A. B.; et al.
Vol. 57, No. 2, Mar 2024, pp 29

2024/1372
Raman identification of CaCO3 polymorphs in concrete prepared with carbonated recycled concrete aggregates
Marchetti, M.; et al.
Vol. 57, No. 2, Mar 2024, pp 28

2024/1373
Development and properties of porous warm mix agent-loaded composite flame retardant and its suppressions on bituminous combustion and volatile release
Xia, W.; Teng, W.; Xu, T.
Vol. 57, No. 2, Mar 2024, pp 27

2024/1374
Flexural behavior of FRP bars reinforced seawater coral aggregate concrete beams incorporating alkali-activated materials
Zhang, B.; et al.
Vol. 57, No. 2, Mar 2024, pp 26

2024/1375
Properties and relationships of porous concrete based on Griffith's theory: compressive strength, permeability coefficient, and porosity
Hou, F.; et al.
Vol. 57, No. 3, Apr 2024, pp 52

2024/1376
Durability against dry–wet and freeze–thaw cycles of alkali residue-based foamed concrete
Wang, Z.; et al.
Vol. 57, No. 3, Apr 2024, pp 51

2024/1377
The role of intrinsic soil properties in the compressive strength and volume change behavior of unstabilized earth mortars
Meimaroglou, N.; Mouzakis, C.
Vol. 57, No. 3, Apr 2024, pp 50

2024/1378
Assessing the combined water of cement pastes: comparing solvent exchange and silica gel as hydration stoppage methods

Abrao, P. C. R. A.; et al.
Vol. 57, No. 3, Apr 2024, pp 49

2024/1379
Unraveling the nexus between internal structural variability and macro-texture in asphalt mixtures: a mesoscopic investigation
Ren, Z.; et al.
Vol. 57, No. 3, Apr 2024, pp 48

2024/1380
Impact of supplementary cementitious materials on the solid–liquid equilibrium curve of calcium in cement hydrates
Zhang, M.; et al.
Vol. 57, No. 3, Apr 2024, pp 47

2024/1381
Impact of cyclic loading and corrosion on the bond performance of steel–polypropylene hybrid fiber reinforced concrete
Zhang, Q.; et al.
Vol. 57, No. 3, Apr 2024, pp 46

2024/1382
Crack-filling effect of gel on time-dependent mechanical behavior of concrete damaged by alkali–silica reaction
Joo, H. E.; Takahashi, Y.
Vol. 57, No. 3, Apr 2024, pp 45

2024/1383
RILEM recommendation from TC 289-DCM: guideline for designing and operating long-term marine exposure sites
Li, K.; et al.
Vol. 57, No. 3, Apr 2024, pp 44

2024/1384
Effect of elevated temperature exposure on the flexural behavior of steel–polypropylene hybrid fiber-reinforced concrete
Suwanitaya, P.; Chotickai, P.
Vol. 57, No. 3, Apr 2024, pp 43

2024/1385
Experimental and numerical investigation of the tensile strength of lightweight concrete including expanded clay aggregate with emphasis on the double punch test
Sadrinejad, I.; et al.
Vol. 57, No. 3, Apr 2024, pp 41

2024/1386
A minimum strain energy release-based thermal–mechanical damage model for fracture process simulation of quasi-brittle materials under high temperatures
Sun, B.; Guo, T.
Vol. 57, No. 3, Apr 2024, pp 40

Ocean Systems Engineering

2024/1387
Effect of local joint flexibility on the fatigue lfe assessment of jacket-type offshore platform
Asgarian, B.; Kuzehgar, P.; Rezadoost, P.
Vol. 14, No. 1, Mar 2024, pp 1 to 16

2024/1388
Predictive control and modeling of a point absorber wave energy harvesting connected to the grid using a LPMSG-based power converter
Berkani, A.; et al.
Vol. 14, No. 1, Mar 2024, pp 17-52

2024/1389
Experimental and statistical investigation of torque coefficient in optimized surface piercing propeller
Zarezadeh, M.; Nouri, N.M.; Madoliat, R.
Vol. 14, No. 1, Mar 2024, pp 53-72

2024/1390
Predictive control theory and design for offshore platforms
Hung, C. C.; Nguyen, T.; Hsieh, C. Y.
Vol. 14, No. 1, Mar 2024, pp 73-84

2024/1391
Prediction of ocean surface current: Research status, challenges, and opportunities. A review
Aldini, I.; et al.
Vol. 14, No. 1, Mar 2024, pp 85-99

Smart Materials and Structures

2024/1392
High-velocity micromorphological observation and simulation of magnetorheological gel using programmable magneto-controlled microfluidics system and micro-tube dynamic models
Yu, M.; et al.
Vol. 33, No. 3, Mar 2024, Article No. 35001

2024/1393
Radial vibration analysis for piezoceramic shell-stacked spherical transducer with thick walls
Tang, Y.; et al.
Vol. 33, No. 3, Mar 2024, Article No. 35002

2024/1394
Enhanced performance triboelectric nanogenerator based on mullite/PVA composites for self-driven sensing and smart home control
Zhang, P.; et al.
Vol. 33, No. 3, Mar 2024, Article No. 35003

2024/1395
Rigid-flexible coupled origami robots via multimaterial 3D printing
Xue, W.; et al.
Vol. 33, No. 3, Mar 2024, Article No. 35004

2024/1396
Modeling mechanical waves propagation in flexoelectric solids
Zhou, H.; et al.
Vol. 33, No. 3, Mar 2024, Article No. 35005

2024/1397
River valley-inspired, high-sensitivity, and rapid-response capacitive three-dimensional force tactile sensor based on U-shaped groove structure
Xu, D.; et al.
Vol. 33, No. 3, Mar 2024, Article No. 35006

2024/1398
Multi-material 4D printing to realize two-phase morphing in self-actuating structures
Lee, H. M.; et al.
Vol. 33, No. 3, Mar 2024, Article No. 35007

2024/1399
Controlled adsorption of gas molecules by tuning porosity of titanium film
Han, S.; et al.
Vol. 33, No. 3, Mar 2024, Article No. 35008

2024/1400
Electrostatic-driven soft air pump with segmented electrodes
Zhao, J.; et al.
Vol. 33, No. 3, Mar 2024, Article No. 35009

2024/1401
A proof of concept for reliability aware analysis of junctionless negative capacitance FinFET-based hydrogen sensor
Gandhi, N.; et al.
Vol. 33, No. 3, Mar 2024, Article No. 35010

2024/1402
Realizing stretchable energy harvesting film through stretch-buckling conversion of wavy base
Gwak, Y.; et al.
Vol. 33, No. 3, Mar 2024, Article No. 35011

2024/1403
Dynamic control of reflection from a metasurface with distinct modulating mechanisms
Liu, S.; et al.
Vol. 33, No. 3, Mar 2024, Article No. 35012

2024/1404
Adaptive beam with elastic support based on magnetorheological elastomers for modal modulation and vibration suppression
Wang, L.; et al.
Vol. 33, No. 3, Mar 2024, Article No. 35013

2024/1405
Efficient seismic fragility assessment method for a frictional isolated bridge constrained by shape memory alloy cables under pulse-like ground motion
Zhu, Y.; Shu, Y.; Zhong, J.
Vol. 33, No. 3, Mar 2024, Article No. 35014

2024/1406
A novel inclined membrane contact model for analyzing the pneu-net soft actuator lateral wall contact
Liu, T.; Wang, X.
Vol. 33, No. 3, Mar 2024, Article No. 35015

2024/1407
Reconfigurable phononic crystal sensor for liquid detection
Zhu, T.; et al.
Vol. 33, No. 3, Mar 2024, Article No. 35016

2024/1408
A metamaterial-assisted coda wave interferometry method with nonlinear guided waves for local incipient damage monitoring in complex structures
Shan, S.; et al.
Vol. 33, No. 3, Mar 2024, Article No. 35017

2024/1409
Dynamic braille display based on surface-structured PVC gel
Tian, C.; et al.
Vol. 33, No. 3, Mar 2024, Article No. 35018

2024/1410
Thermomechanical description of shape memory alloys using the preisach model
Alvares, T. Q.; et al.
Vol. 33, No. 3, Mar 2024, Article No. 35019

2024/1411
Multimode auxetic piezoelectric energy harvester for low-frequency vibration
He, L.; Kurita, H.; Narita, F.
Vol. 33, No. 3, Mar 2024, Article No. 35020

2024/1412
Temperature and strain monitoring during thermoforming of thermoplastic composite laminates using optical frequency domain reflectometry
Fan, B.; et al.
Vol. 33, No. 3, Mar 2024, Article No. 35021

2024/1413
Nonlinear dynamic morphing of conical bistable dielectric elastomer actuator
Zhang, J.; et al.
Vol. 33, No. 3, Mar 2024, Article No. 35022

2024/1414
Bidisperse magnetorheological fluids with strong magnetorheological response, long-term stability and excellent in-use performance
Nejatpour, M.; et al.
Vol. 33, No. 3, Mar 2024, Article No. 35023

2024/1415
Soft electroadhesive grippers with variable stiffness and deflection motion capabilities
Xiang, C.; et al.
Vol. 33, No. 3, Mar 2024, Article No. 35024

2024/1416
Dynamic measurement of ballistic impact using an optical fibre sensor
Velasco, I.; et al.
Vol. 33, No. 3, Mar 2024, Article No. 35025

2024/1417
Wellbore fracture recognition and fracture parameter identification method using piezoelectric ultrasonic and machine learning
Liu, Z.; et al.
Vol. 33, No. 3, Mar 2024, Article No. 35026

2024/1418
Viscoelasticity, stiffness gradient and their effects on adhesion of an epoxy shape memory polymer
Gong, L.; Wang, X.
Vol. 33, No. 3, Mar 2024, Article No. 35027

2024/1419
Assessment of self-healing performance of cement-based materials incorporating ion chelator and industrial wastes
Wang, R.; et al.
Vol. 33, No. 3, Mar 2024, Article No. 35028

2024/1420
On the optimal planform of a cantilever unimorph piezoelectric vibrating energy harvester
Salman, E.; Lustig, S.; Elata, D.
Vol. 33, No. 3, Mar 2024, Article No. 35029

2024/1421
Adaptive optimal fault-tolerant vibration control and sensitivity analysis of semi-active suspension based on a self-powered magneto-rheological damper
Gao, X.; et al.
Vol. 33, No. 3, Mar 2024, Article No. 35030

2024/1422
Torsional actuation and vari-stiffness characteristics of SMA/basalt hybrid braided composite tubes
Ke, J.; et al.
Vol. 33, No. 3, Mar 2024, Article No. 35031

2024/1423
Investigation of cluster magnetorheological electro-Fenton composite polishing process for single-crystal GaN wafer based on BBD experimental method
Zheng, Q.; et al.
Vol. 33, No. 3, Mar 2024, Article No. 35032

2024/1424
Early bolt looseness monitoring using the leading waves energy in piezoelectric active sensing
Wang, T.; et al.
Vol. 33, No. 3, Mar 2024, Article No. 35033

2024/1425
Aeroelastic metastructure for simultaneously suppressing wind-induced vibration and energy harvesting under wind flows and base excitations
Chen, S.; Xu, C.; Zhao, L.
Vol. 33, No. 3, Mar 2024, Article No. 35034

2024/1426
Design and experiment study of a novel dual-channel independent-coil magnetorheological grease damper
Wang, H.; et al.
Vol. 33, No. 3, Mar 2024, Article No. 35035

2024/1427
Buckling-driven piezoelectric defect-induced energy localization and harvesting using a Rubik's cube-inspired phononic crystal structure
Cao, D.; et al.
Vol. 33, No. 3, Mar 2024, Article No. 35036

2024/1428
Explicit model predictive control of magnetorheological suspension for all-terrain vehicles with road preview
Li, W.; et al.
Vol. 33, No. 3, Mar 2024, Article No. 35037

2024/1429
Mechanistic prediction of folding angles in 4D printed shape memory polymers under varied loading conditions
Li, Y.; Ponnappan, H. K.
Vol. 33, No. 3, Mar 2024, Article No. 35038

2024/1430
Exploring chloride-induced corrosion in reinforced concrete structures through embedded piezo sensor technology: an experimental and numerical study
Morwal, T.; et al.
Vol. 33, No. 3, Mar 2024, Article No. 35039

2024/1431
Hole-edge crack monitoring in attachment lug with large bolt hole based on guided wave and circular piezoelectric sensor array
Shi, L.; et al.
Vol. 33, No. 3, Mar 2024, Article No. 35040

2024/1432
Structural design and multi-objective optimization of a novel asymmetric magnetorheological damper
Liang, H.; et al.
Vol. 33, No. 3, Mar 2024, Article No. 35041

2024/1433
Enhancing sparse regression modeling of hysteresis with optimized PIO algorithm in piezo actuator
Jin, Y.; et al.
Vol. 33, No. 3, Mar 2024, Article No. 35042

2024/1434
Kresling origami-inspired electromagnetic energy harvester with reversible nonlinearity
Yin, P.; et al.
Vol. 33, No. 3, Mar 2024, Article No. 35043

2024/1435
Design and feasibility analysis of magnetorheological flexible joint for upper limb rehabilitation
Li, G.; et al.
Vol. 33, No. 3, Mar 2024, Article No. 35044

2024/1436
A multi-directional and multi-modal galloping piezoelectric energy harvester with tri-section beam
Xia, C.; et al.
Vol. 33, No. 3, Mar 2024, Article No. 35045

2024/1437
Analysis of torsional buckling of a cylindrical sandwich shell with a magnetorheological fluid core layer
Kashipazha, M.; Kheirikhah, M.; Meshkinabadi, S.
Vol. 33, No. 3, Mar 2024, Article No. 35046

2024/1438
Active vibration control for thin curved structures using dielectric elastomer actuators
Hiruta, T.; et al.
Vol. 33, No. 3, Mar 2024, Article No. 35047

2024/1439
Optimizing dispensing performance of needle-type piezoelectric jet dispensers: a novel drive waveform approach
Cao, L.; et al.
Vol. 33, No. 4, Apr 2024, Article No. 045001

2024/1440
High-efficient and intelligent antibacterial face mask integrated with airflow-temperature dual-function sensors for respiratory monitoring and disease prevention
Lan, X.; et al.
Vol. 33, No. 4, Apr 2024, Article No. 045002

2024/1441
Understanding the role of laser processing parameters and position-dependent heterogeneous elastocaloric effect in laser powder bed fused NiTi thin-walled structures
Peng, X.; et al.
Vol. 33, No. 4, Apr 2024, Article No. 045003

2024/1442
Phenomenological studies on magnetic and mechanical remanence effects in magnetorheological fluids
Wiener, T.; et al.
Vol. 33, No. 4, Apr 2024, Article No. 045004

2024/1443
A differentiable actuator extends potential configurations of modular robots
Li, H.; et al.
Vol. 33, No. 4, Apr 2024, Article No. 045005

2024/1444
PVDF piezoelectric sensor based on solution blow spinning fibers for structural stress/strain health monitoring
Zou, X.; et al.
Vol. 33, No. 4, Apr 2024, Article No. 045006

2024/1445
A phase-transition model of reprocessible thermadapt shape memory polymer
Mu, T.; et al.
Vol. 33, No. 4, Apr 2024, Article No. 045007

2024/1446
Bayesian approach of elliptical loci and RAPID for damage localization in wind turbine blade
Lu, J.; et al.
Vol. 33, No. 4, Apr 2024, Article No. 045008

2024/1447
Design and analysis of three-dimensional chiral metamaterials for enhanced torsional compliance
Ji, M.; et al.
Vol. 33, No. 4, Apr 2024, Article No. 045009

2024/1448
Experimental study on vibration control performance of TMD-STF damper
Wei, M.; Lin, K.; Liu, J.
Vol. 33, No. 4, Apr 2024, Article No. 045010

2024/1449
A fast-actuated soft gripper based on shape memory alloy wires
Li, X.; et al.
Vol. 33, No. 4, Apr 2024, Article No. 045011

2024/1450
Design and analysis of a contact-aided flexure hinge (CAFH) with variable stiffness
Dai, S.; Hao, G.; Qiu, L.
Vol. 33, No. 4, Apr 2024, Article No. 045012

2024/1451
Magnetorheological variable stiffness and damping flexible joint with cam working surface for industrial robot
Wu, L.; Dong, X.; Yang, B.
Vol. 33, No. 4, Apr 2024, Article No. 045013

2024/1452
Design and performance analysis of a flexible-hinged piezoelectric driving dispenser
Wu, M.; et al.
Vol. 33, No. 4, Apr 2024, Article No. 045014

2024/1453
Customized deformation behavior of morphing wing through reversibly assembled multi-stable metamaterials
Wang, C.; et al.
Vol. 33, No. 4, Apr 2024, Article No. 045015

2024/1454
Vibration control of giant electrorheological damper combining nonlinear fractional-order controller and extended state observer
Pu, H.; et al.
Vol. 33, No. 4, Apr 2024, Article No. 045016

2024/1455
Analyzing the structural behavior of conducting polymer actuators and its interdependence with the electrochemical phenomenon
Kumar, S.; Yu, A.; Khandelwal, M.
Vol. 33, No. 4, Apr 2024, Article No. 045017

2024/1456
3D-printed passive bellow actuator for portable soft wearable robots
Xia, J.; et al.
Vol. 33, No. 4, Apr 2024, Article No. 045018

2024/1457
Performance analysis of electrical signal output of multi-state flexoelectric structures with parameter uncertainties through quasi-Monte Carlo method
Liu, X.; et al.
Vol. 33, No. 4, Apr 2024, Article No. 045019

2024/1458
Research on a rotary piezoelectric energy harvester based on movable magnets
Han, Y.; et al.
Vol. 33, No. 4, Apr 2024, Article No. 045020

2024/1459
Dual-parameter stretchable, transferable mesh piezoresistive sensor for electronic skin detection of strain and temperature changes
Wang, C.; et al.
Vol. 33, No. 4, Apr 2024, Article No. 045021

2024/1460
Model-based linear control of nonlinear pneumatic soft bending actuators

Wang, J.; et al.
Vol. 33, No. 4, Apr 2024, Article No. 045022

2024/1461
A machine learning-based method for co-design and optimization of microwave-absorbing/load-bearing multifunctional structures
Wang, J.; Zhou, L.; Fan, C.
Vol. 33, No. 4, Apr 2024, Article No. 045023

2024/1462
Harnessing multi-stable piezoelectric systems for enhanced wind energy harvesting
Liu, X.; et al.
Vol. 33, No. 4, Apr 2024, Article No. 045024

2024/1463
Development of a novel nonlinear model and control strategy for soft continuum robots featuring hard magnetoactive elastomers
Moezi, S. A.; Sedaghati, R.; Rakheja, S.
Vol. 33, No. 4, Apr 2024, Article No. 045025

2024/1464
Flutter analysis of laminated fiber-reinforced magnetorheological elastomer sandwich plate resting on an elastic foundation using an improved first-order shear deformation theory Aboutalebi, R.; Eshaghi, M.
Vol. 33, No. 4, Apr 2024, Article No. 045026

2024/1465
Dual-stage theoretical model of magnetorheological dampers and experimental verification
Lei, B.; et al.
Vol. 33, No. 4, Apr 2024, Article No. 045027

2024/1466
A Lamb-wave based SHM for multi-damage localizations in large composite plates by using piezoelectric transducer array
Chen, C.; et al.
Vol. 33, No. 4, Apr 2024, Article No. 045028

2024/1467
An origami-inspired energy absorber
Khazaaleh, S.; Dalaq, A. S.; Daqaq, M. F.
Vol. 33, No. 4, Apr 2024, Article No. 045029

2024/1468
A piecewise inverse finite element method for shape sensing of the morphing wing fishbone
Huang, T.; Dong, T.; Yuan, S.
Vol. 33, No. 4, Apr 2024, Article No. 045030

2024/1469
Multilayer modeling framework for analyzing thermo-mechanical properties and responses of twisted and coiled polymer actuators
Gao, Z.; et al.
Vol. 33, No. 4, Apr 2024, Article No. 045031

2024/1470
Theoretical modeling and experimental investigation of carbon fiber reinforced plastic-based piezoelectric actuator
Cao, T.; et al.
Vol. 33, No. 4, Apr 2024, Article No. 045032

2024/1471
Predictive lumped model for a tunable bistable piezoelectric energy harvester architecture
Benhemou, A.; et al.
Vol. 33, No. 4, Apr 2024, Article No. 045033

2024/1472
Numerical and experimental assessment of tilted-helical fiber orientation effects on deformation of pneumatic soft actuators
Shabani, M.
Vol. 33, No. 4, Apr 2024, Article No. 045034

2024/1473
Experimental study of vibration modes switching based triple frequency-up converting energy harvesting with pre-biased displacement
Xu, J.; et al.
Vol. 33, No. 4, Apr 2024, Article No. 045035

Smart Structures and Systems

2024/1474
Structural system reliability-based design optimization considering fatigue limit state
Biton, N. I. D.; Lee, Y.
Vol. 33, No. 3, Mar 2024, pp 177-188

2024/1475
Operational performance evaluation of bridges using autoencoder neural network and clustering
Jiang, H.; et al.
Vol. 33, No. 3, Mar 2024, pp 189-199

2024/1476
A combined spline chirplet transform and local maximum synchrosqueezing technique for structural instantaneous frequency identification
Yuan, P.; et al.
Vol. 33, No. 3, Mar 2024, pp 201-215

2024/1477
Compact electromagnetic vibration suppressor and energy harvester; an experimental study
Afsharfard, A.; Zoka, H.; Kim, K. C.
Vol. 33, No. 3, Mar 2024, pp 217-225

2024/1478
Real-time online damage localisation using vibration measurements of structures under variable environmental conditions
Lakshmi, K.
Vol. 33, No. 3, Mar 2024, pp 227-241

2024/1479
Modeling of vibration protection by shape memory alloy parts with an account of latent heat
Belyaev, F. S.; et al.
Vol. 33, No. 3, Mar 2024, pp 243-251

2024/1480
Dual-loss CNN: A separability-enhanced network for current-based fault diagnosis of rolling bearings
Cui, L.; et al.
Vol. 33, No. 4, Apr 2024, pp 253-262

2024/1481
Review for vision-based structural damage evaluation in disasters focusing on nonlinearity
Wang, S.; Nishio, M.
Vol. 33, No. 4, Apr 2024, pp 263-279

2024/1482
Nonlinear dynamics of an adaptive energy harvester with magnetic interactions and magnetostrictive transduction
Savi, P. V.; Savi, M. A.
Vol. 33, No. 4, Apr 2024, pp 281-290

2024/1483
Nonlinear intelligent control systems subjected to earthquakes by fuzzy tracking theory
Chen, Z. Y.; et al.
Vol. 33, No. 4, Apr 2024, pp 291-300

2024/1484
Crack growth prediction on a concrete structure using deep ConvLSTM
Kang, M.; An, Y.
Vol. 33, No. 4, Apr 2024, pp 301-311

2024/1485
A deep neural network to automatically calculate the safety grade of a deteriorating building
Kim, S.; et al.
Vol. 33, No. 4, Apr 2024, pp 312-323

Steel and Composite Structures

2024/1486
Temperature-dependent multi-phase-lags theory on a magneto-thermoelastic medium with microtemperatures
Said, S. M.
Vol. 50, No. 5, Mar 2024, pp 489-497

2024/1487
Tests and numerical analysis on octagonal concrete-filled double skinned steel tubular short columns under axial compression
Manigandan, R.
Vol. 50, No. 5, Mar 2024, pp 499-513

2024/1488
Assessment of cold-formed steel screwed beam-column conections: Experimental tests and numerical simulations
Maali, M. S.; et al.
Vol. 50, No. 5, Mar 2024, pp 515-529

2024/1489
Experimental and numerical study on progressive collapse of composite steel-concrete frames
Wang, J.; et al.
Vol. 50, No. 5, Mar 2024, pp 531-548

2024/1490
Seismic performance evaluation of an external steel frame retrofit system
Adane, M.; et al.
Vol. 50, No. 5, Mar 2024, pp 549-562

2024/1491
Effects of hygro-thermal environment on dynamic responses of variable thickness functionally graded porous microplates
Pham, Q.; Nguyen, P.; Tran, V.
Vol. 50, No. 5, Mar 2024, pp 563-581

2024/1492
Optimum design of steel frames against progressive collapse by guided simulated annealing algorithm
Tayfur, B.; Daloglu, A. T.
Vol. 50, No. 5, Mar 2024, pp 583-594

2024/1493
Fresh and hardened properties of expansive concrete utilizing waste aluminum lathe
Ozkilic, Y. O.; et al.
Vol. 50, No. 5, Mar 2024, pp 595-608

2024/1494
Nonlinear free vibration impact on the smart small-scale thermo-mechanical sensors for monitoring the information in sports application
Zhang, Y.; Bagheri, M.
Vol. 50, No. 6, Mar 2024, pp 609-625

2024/1495
Behavior of simple precast high-strength concrete beams connected in the maximum bending moment zone using steel extended endplate connections
Salama, M. I.; et al.
Vol. 50, No. 6, Mar 2024, pp 627-641

2024/1496
Assessment of seismic design coefficients for composite special moment frames with reinforced concrete columns and steel beams: Evaluation of code recommendations
Abadi, E. T. Y.; Kazemi, M. T.
Vol. 50, No. 6, Mar 2024, pp 643-658

2024/1497
Static and fatigue performance of short group studs connector in novel post-combination steel-UHPC composite deck
Xiao, H.; et al.
Vol. 50, No. 6, Mar 2024, pp 659-674

2024/1498
Distortional buckling performance of cold-formed steel lightweight concrete composite columns
Li, Y.; et al.
Vol. 50, No. 6, Mar 2024, pp 675-688

2024/1499
Investigation of damaged formwork timber beam retrofitting with anchoraged CFRP strip under different loading
Turer, A.; et al.
Vol. 50, No. 6, Mar 2024, pp 689-703

2024/1500
Effect of the initial imperfection on the response of the stainless-steel shell structures

Celik, A. I.; Zeybek, O.; Ozkilic, O.
Vol. 50, No. 6, Mar 2024, pp 705-720

2024/1501
An experimental study on a steel multi-slit damper for seismic retrofit of soft-first story structures
Javidan, M. M.; Kim, J.
Vol. 50, No. 6, Mar 2024, pp 721-734

2024/1502
Transient dynamic analysis of sandwich beam subjected to thermal and pulse load
Nassir, L. M.; et al.
Vol. 51, No. 1, Apr 2024, pp 1 to 8

2024/1503
Shear mechanical behavior of prefabricated and assembled multi-key group stud connectors
Fan, L.; et al.
Vol. 51, No. 1, Apr 2024, pp 9 to 24

2024/1504
Application of the optimal fuzzy-based system on bearing capacity of concrete pile
Zhang, K.; Zhang, Y.; Razzaghzadeh, B.
Vol. 51, No. 1, Apr 2024, pp 25-41

2024/1505
Supply chain management and artificial intelligence improve the microstructure and economic evaluation of composite materials
Yang, X.; Li, M.
Vol. 51, No. 1, Apr 2024, pp 43-51

2024/1506
Research on three-point bending fatigue life and damage mechanism of aluminum foam sandwich panel
Xiao, W.; Wang, H.; Song, X.
Vol. 51, No. 1, Apr 2024, pp 53-61

2024/1507
Effects of the stiffness of an inclusion on the mechanical behavior of an aluminum alloy plate with a lateral notch
Abdelmadjid, M.; et al.
Vol. 51, No. 1, Apr 2024, pp 63-72

2024/1508
Using DQ method for vibration analysis of a laminated trapezoidal structure with functionally graded faces and damaged core
Valverde, V.; et al.
Vol. 51, No. 1, Apr 2024, pp 73-91

2024/1509
Seismic performance evaluation of a steel slit damper for retrofit of structures on soft soil
Nasab, M. S. E.; Kim, J.; Ahn, T.
Vol. 51, No. 1, Apr 2024, pp 93-101

2024/1510
A unified consistent couple stress beam theory for functionally graded microscale beams
Wu, C.; Huang, Z.
Vol. 51, No. 2, Apr 2024, pp 103-116

2024/1511
Study on bearing capacity of combined confined concrete arch in large-section tunnel
Bei, J.; et al.
Vol. 51, No. 2, Apr 2024, pp 117-126

2024/1512
An advanced software interface to make OpenSees for thermal analysis of structures more user-friendly
Jeong, S.; e al.
Vol. 51, No. 2, Apr 2024, pp 127-138

2024/1513
Thermoelastic analysis of rotating FGM thick-walled cylindrical pressure vessels under bi-directional thermal loading using disk-form multilayer
Ramezani, F.; Nejad, Z.
Vol. 51, No. 2, Apr 2024, pp 139-151

2024/1514
Shear strengthening of seawater sea-sand concrete beams containing no shear reinforcement using NSM aluminum alloy bars
Ozkilic, Y. O.; et al.

Vol. 51, No. 2, Apr 2024, pp 153-172

2024/1515
Performance-based seismic design of a spring-friction damper retrofit system installed in a steel frame
Gharagoz, M. M.; et al.
Vol. 51, No. 2, Apr 2024, pp 173-183

2024/1516
Investigating wave propagation in sigmoid-FGM imperfect plates with accurate Quasi-3D HSDTs
Nebab, M.; Atmane, H. A.; Bennai, R.
Vol. 51, No. 2, Apr 2024, pp 185-202

2024/1517
Stress-based topology optimization under buckling constraint using functionally graded materials
Nguyen, M.; Lee, D.; Shin, S.
Vol. 51, No. 2, Apr 2024, pp 203-223

Structural Concrete: Journal of the FIB

2024/1518
Design of UHPC prestressed girders for shear
Foster, S. J.; Bentz, E.
Vol. 25, No. 2, Apr 2024, pp 780-795

2024/1519
Bearing capacity of UHPC-NC connection structure in negative moment zone of PC beam bridges
Li, X.; Li, R.; HU, Z.
Vol. 25, No. 2, Apr 2024, pp 796-809

2024/1520
Experimental study on mechanical properties of recycled aggregate concrete with polypropylene fiber under combined compression-shear loading
Liu, Z.; et al.
Vol. 25, No. 2, Apr 2024, pp 810-825

2024/1521
Rocket blast resistance of the fully demountable high performance FRC tongue and groove blocks
Bouzkurt, H. B.; et al.
Vol. 25, No. 2, Apr 2024, pp 826-849

2024/1522
Microscopic mechanism analysis and failure criterion study of glass fiber recycled concrete under three-dimensional compressive stress state
Chen, Y.; et al.
Vol. 25, No. 2, Apr 2024, pp 850-868

2024/1523
Strain rate sensitivity of strain-hardening fiber-reinforced concrete subjected to dynamic direct tensile loading
Vu, V. Y.; et al.
Vol. 25, No. 2, Apr 2024, pp 869-885

2024/1524
Investigation on the influence of fiber fraction and orientation on the mechanical properties of fiber-reinforced concrete slabs
Khan, M. S.; Ibrahim, S. M.; Shariq, M.
Vol. 25, No. 2, Apr 2024, pp 886-903

2024/1525
Properties of steel fiber reinforced mortar-plastic columns with the cross-section in a form of a Cesaro fractal
Katzer, J.; Skoratko, A.; Seitl, S.
Vol. 25, No. 2, Apr 2024, pp 904-915

2024/1526
Study on bending failure and crack characteristics in ductile fiber-reinforced concrete beams
Wang, H.; et al.
Vol. 25, No. 2, Apr 2024, pp 916-934

2024/1527
Experimental characterization of a cost-competitive tailor-made HPFRC mix design for wide application in precast girder of roadway bridges

Ruiz, R.; et al.
Vol. 25, No. 2, Apr 2024, pp 935-955

2024/1528
Influence of fiber orientation on flexural-based design of steel fiber-reinforced concrete slabs: Experimental and numerical program
Aidarov, S.; et al.
Vol. 25, No. 2, Apr 2024, pp 956-972

2024/1529
A modeling strategy for the shear and flexural performance prediction of SFRC beams without stirrups accounting for the variability of properties
Benedito, A. V.; et al.
Vol. 25, No. 2, Apr 2024, pp 973-991

2024/1530
Experimental study and optimal design of UHPC T-shaped beam
Deng, S.; et al.
Vol. 25, No. 2, Apr 2024, pp 992-1005

2024/1531
Shrinkage cracking in restrained FRC members containing conventional reinforcement
Tang, P.; et al.
Vol. 25, No. 2, Apr 2024, pp 1006-1017

2024/1532
A study on HyFRCC consisting of PE and carbon fiber: Investigation of electrical and fracture properties based on orthogonal design
Zhu, J.; Shen, H.; Wel, L.
Vol. 25, No. 2, Apr 2024, pp 1018-1030

2024/1533
Macrosynthetic fibers as replacement of conventional steel reinforcement for concrete of partition walls
Ruiz, M. F.; et al.
Vol. 25, No. 2, Apr 2024, pp 1031-1051

2024/1534
Experiments on shear behavior of reinforced concrete continuous beams strengthened by C-FRCM
Feng, R.; et al.
Vol. 25, No. 2, Apr 2024, pp 1052-1075

2024/1535
Bending moments redistribution in two-span reinforced concrete beams reinforced with FRP bars based on collected data research
Szczepanski, K.; Kotynia, R.
Vol. 25, No. 2, Apr 2024, pp 1076-1091

2024/1536
Effectiveness of FRP confinement for low strength recycled aggregate concrete compressive members having optimized combination of fibers
Raza, A.; et al.
Vol. 25, No. 2, Apr 2024, pp 1092-1104

2024/1537
Structural evaluation of RC overhang cantilever slab strengthened with FRP near-surface mounted (NSM) composites for bridge applications
Mosallam, A. S.; et al.
Vol. 25, No. 2, Apr 2024, pp 1105-1128

2024/1538
Numerical and analytical modeling of SPH-ECC strengthened RC beams
Qasim, M.; Zhang, Y. X.; Lee, C. K.
Vol. 25, No. 2, Apr 2024, pp 1129-1147

2024/1539
Neural network-based models versus empirical models for the prediction of axial load-carrying capacities of FRP-reinforced circular concrete columns
Ali, S.; et al.
Vol. 25, No. 2, Apr 2024, pp 1148-1164

2024/1540
Flexural strengthening of RC beams by advanced concrete canvas
Jafari, Z.; Mostofinejad, D.

Vol. 25, No. 2, Apr 2024, pp 1165-1184

2024/1541
Behavior and modeling of FRP grid-reinforced ultra-high-performance concrete under uniaxial tension
Zeng, J.; et al.
Vol. 25, No. 2, Apr 2024, pp 1185-1207

2024/1542
Flexural behavior of beams strengthened with GFRP bars and high-performance fiber-reinforced concrete
Su, Y.; et al.
Vol. 25, No. 2, Apr 2024, pp 1208-1222

2024/1543
Behavior of textile-reinforced concrete columns
Santos, F. C. A.; Campos, C. M. O.; Cardoso, D. C. T.
Vol. 25, No. 2, Apr 2024, pp 1223-1240

2024/1544
Pull-off capacity of FRP–concrete composite bonded with epoxy/geopolymer at elevated temperature
Rashid, K,; et al.
Vol. 25, No. 2, Apr 2024, pp 1241-1256

2024/1545
Modeling and probabilistic evaluation of repair strategies in the initiation phase of chloride-induced corrosion of the reinforcement of concrete structures
Hende, K. V. D.; et al.
Vol. 25, No. 2, Apr 2024, pp 1257-1274

2024/1546
Capacity assessment of uncorroded and corroded dapped-end beams by NLFE and strut-and-tie based methods
Belletti, B; et al.
Vol. 25, No. 2, Apr 2024, pp 1275-1304

2024/1547
Toward presenting an ensemble meta-model for evaluation of pozzolanic mixtures incorporating industrial by-products
Ashrafian, A.; et al.
Vol. 25, No. 2, Apr 2024, pp 1305-1323

2024/1548
Automated machine learning techniques for estimating of elastic modulus of recycled aggregate concrete
Chien-Ta, C.; Shing-Wen, T.; Liang-Hao, H.
Vol. 25, No. 2, Apr 2024, pp 1324-1342

2024/1549
Compressive strength prediction of sustainable concrete containing waste foundry sand using metaheuristic optimization-based hybrid artificial neural network
Kazemi, R.; Golafshani, E. M.; Behnood, A.
Vol. 25, No. 2, Apr 2024, pp 1343-1363

2024/1550
Estimation of elastic modulus of recycle aggregate concrete based on hybrid and ensemble-hybrid approaches
Qu, B.
Vol. 25, No. 2, Apr 2024, pp 1364-1387

2024/1551
An extended universal morphological model for concrete mode-I fracture: Formulations and preliminary verifications
Li, D.; et al.
Vol. 25, No. 2, Apr 2024, pp 1388-1403

2024/1552
Experimental investigation of punching shear behavior of flat slabs supported by rectangular columns and loaded with various load patterns
Sarvaicova, S.; Borzovic, V.; Halvonik, J.
Vol. 25, No. 2, Apr 2024, pp 1404-1417

2024/1553
Inelastic analysis of octagonal concrete-filled steel tubular short columns under eccentric loading
Ahmed, M.; et al.
Vol. 25, No. 2, Apr 2024, pp 1418-1433

2024/1554
Rehabilitation of post-heated rectangular reinforced concrete columns using different strengthening configuration
Abadel, A. A.
Vol. 25, No. 2, Apr 2024, pp 1434-1449

2024/1555
Chemical prestressing of concrete structures; state of the art review
Dhahir, M. K.; Marx, S.; Zdanowicz, K.
Vol. 25, No. 2, Apr 2024, pp 1450-1464

2024/1556
Crack monitoring on concrete structures with distributed fiber optic sensors—Toward automated data evaluation and assessment
Richter, B.; Herbers, M.; Marx, S.
Vol. 25, No. 2, Apr 2024, pp 1465-1480
Structural Engineering & Mechanics

2024/1557
Vibroacoustic analysis of stiffened functionally graded panels in thermal environments
Singh, A. K.; et al.
Vol. 89, No. 5, Mar 2024, pp 437-452

2024/1558
CO2 emission optimization of composite floor systems with cellular beams via metaheuristics algorithms
Silva, G. F.; Kripka, M.; Alves, E. C.
Vol. 89, No. 5, Mar 2024, pp 453-466

2024/1559
Design optimization of structural component (hitch bracket of tractor): A reverse engineering approach
Sahu, D. K.; et al.
Vol. 89, No. 5, Mar 2024, pp 467-477

2024/1560
Numerical simulation of infill CACB wall cracking subjected to wind loads
Li, R.; et al.
Vol. 89, No. 5, Mar 2024, pp 479-489

2024/1561
Investigation of seismic performance of a premodern RC building typology after November 26, 2019 earthquake
Leti, M.; Bilgin, H.
Vol. 89, No. 5, Mar 2024, pp 491-505

2024/1562
Numerical and experimental behavior of moment concrete frame retrofitted with TADAS metal yielding damper under lateral loading
Nazeran, R.; Hemmati, A.; Kazemi, H. H.
Vol. 89, No. 5, Mar 2024, pp 507-524

2024/1563
Evaluation of unanchorage blast-resistant modular structures subjected to blast loads and human injury response
Sari, A.; et al.
Vol. 89, No. 5, Mar 2024, pp 525-538

2024/1564
Finite element analysis of the behavior of elliptical cracks emanating from the orthopedic cement interface in total hip prostheses
Benouis, A.; et al.
Vol. 89, No. 5, Mar 2024, pp 539-547

2024/1565
Serial pendulum DVA design using Genetic Algorithm (GA) by considering the pendulum nonlinearity
Son, L.; et al.
Vol. 89, No. 6, Mar 2024, pp 549-556

2024/1566
Nonlocal bending, vibration and buckling of one-dimensional hexagonal quasicrystal layered nanoplates with imperfect interfaces
Wang, H.; Guo, J.

Vol. 89, No. 6, Mar 2024, pp 557-570

2024/1567
Electric field strength effect on bi-stability of composite thin cylindrical shell with piezoelectric layer
Wu, Y.; et al.
Vol. 89, No. 6, Mar 2024, pp 571-578

2024/1568
Curvature ductility of confined HSC beams
Haytham, B.; et al.
Vol. 89, No. 6, Mar 2024, pp 579-588

2024/1569
High-rate Single-Frequency Precise Point Positioning (SF-PPP) in the detection of structural displacements and ground motions
Bezcioglu, M.; et al.
Vol. 89, No. 6, Mar 2024, pp 589-599

2024/1570
Analysis of stiffened Al/SiC FGM plates with cutout under uniaxial and localized in-plane edge loadings
Balaraman, P.; Sreehari, V. M.
Vol. 89, No. 6, Mar 2024, pp 601-615

2024/1571
Influence of loading rate on flexural performance and acoustic emission characteristics of Ultra High-Performance Concrete
Prem, P. R.; et al.
Vol. 89, No. 6, Mar 2024, pp 617-626

2024/1572
Assessment of structural behavior of reinforced concrete slab ceiling under full load test in a residential complex project
Kadim, J. A.; et al.
Vol. 89, No. 6, Mar 2024, pp 627-634

2024/1573
An efficient numerical model for free vibration of temperature-dependent porous FG nano-scale beams using a nonlocal strain gradient theory
Merzouki, T.; Houari, S. A.
Vol. 90, No. 1, Apr 2024, pp 1 to 18

2024/1574
Apply evolved grey-prediction scheme to structural building dynamic analysis
Chen, Z. Y.; et al.
Vol. 90, No. 1, Apr 2024, pp 19-26

2024/1575
ML-based prediction method for estimating vortex-induced vibration amplitude of steel tubes in tubular transmission towers
Li, J.; Wang, T.;
Vol. 90, No. 1, Apr 2024, pp 27-40

2024/1576
Desired earthquake rail irregularity considering random pier height and random span number
Yu, J.; Jiang, L.; Zhou, W.
Vol. 90, No. 1, Apr 2024, pp 41-49

2024/1577
Influence of high axial compression ratios in RC columns on the seismic response of MRF buildings
Salinas, S. V.; et al.
Vol. 90, No. 1, Apr 2024, pp 51-70

2024/1578
Performance of headed FRP bar reinforced concrete Beam-Column Joint
Ansari, M. M.; Chourasia, A.
Vol. 90, No. 1, Apr 2024, pp 71-81

2024/1579
Warping and porosity effects on the mechanical response of FG-Beams on non-homogeneous foundations via a Quasi-3D HSDT
Nebab, M.; et al.
Vol. 90, No. 1, Apr 2024, pp 83-96

2024/1580
Exploring geometric and kinematic correspondences between gear-based crank

mechanism and standard reciprocating crankshaft engines: An analytical study
Sakhraoui, A.; et al.
Vol. 90, No. 1, Apr 2024, pp 97-106

2024/1581
Mechanical properties of coconut fiber-reinforced coral concrete
Liu, C.; et al.
Vol. 90, No. 2, Apr 2024, pp 107-116

2024/1582
Design of web-stiffened lipped channel beams experiencing distortional global interaction by direct strength method
Ahmed, H. S. S.; et al.
Vol. 90, No. 2, Apr 2024, pp 117-125

2024/1583
Pultruded GFRP box beams: State-of-the-art review on constituents and structural behavior
Dehshirixadeh, M.; et al.
Vol. 90, No. 2, Apr 2024, pp 127-142

2024/1584
An experimental and numerical study on the local buckling of cold-formed steel castellated I-Beam stiffened with oval castellation
Prabhakaran, S.; Malathy, R.; Kasiviswanathan, M.
Vol. 90, No. 2, Apr 2024, pp 143-157

2024/1585
Reasonably completed state assessment of the self-anchored hybrid cable-stayed suspension bridge: An analytical algorithm
Wang, K.; et al.
Vol. 90, No. 2, Apr 2024, pp 159-175

2024/1586
Comparative study of flexural stress estimation methods in concrete pavement considering tied concrete shoulder
Khichad, J. S.; et al.
Vol. 90, No. 2, Apr 2024, pp 177-187

2024/1587
A TSK fuzzy model optimization with meta-heuristic algorithms for seismic response prediction of nonlinear steel moment-resisting frames
Asadi, E.; et al.
Vol. 90, No. 2, Apr 2024, pp 189-208

2024/1588
Wave propagation at free surface in thermoelastic medium under modified Green-Lindsay model with non-local and two temperature
Kaushal, S.; et al.
Vol. 90, No. 2, Apr 2024, pp 209-218

Wind & Structures

2024/1589
A novel aerodynamic vibration and fuzzy numerical analysis
Chen, T.; et al.
Vol. 38, No. 3, Mar 2024, pp 161-170

2024/1590
Full-scale simulation of wind-driven rain and a case study to determine the rain mitigation effect of shutters
Vutukuru, K. S.; Erwin, J.; Chowdhury, A. G.
Vol. 38, No. 3, Mar 2024, pp 171-191

2024/1591
Wind-induced dynamic response of recessed balcony facades
Glanville, M. J.; Holmes, J. D.
Vol. 38, No. 3, Mar 2024, pp 193-202

2024/1592
Aerodynamic mitigation of wind loads on a large-span cantilevered roof: A combined wind tunnel and CFD analysis
Fubin, C.; et al.
Vol. 38, No. 3, Mar 2024, pp 203-214

2024/1593
Characterization of the wind-induced response of a 356 m high guyed mast based on field measurements

Wang, Z.; et al.
Vol. 38, No. 3, Mar 2024, pp 215-229

2024/1594
Reconstruction of wind speed fields in mountainous areas using a full convolutional neural network
Shen, R.; et al.
Vol. 38, No. 4, Apr 2024, pp 231-244

2024/1595
Deriving vertical velocity in tornadic wind field from radar-measured data and improving tornado simulation by including vertical velocity at velocity Inlet
Zhao, Y.; et al.
Vol. 38, No. 4, Apr 2024, pp 245-259

2024/1596
A compensation method for the scaling effects in the simulation of a downburst-generated wind-wave field
Haiwei, X.; et al.
Vol. 38, No. 4, Apr 2024, pp 261-275

2024/1597
Characterizing and modelling nonstationary tri-directional thunderstorm wind time histories
Liu, Y. X.; Hong, H. P.
Vol. 38, No. 4, Apr 2024, pp 277-293

2024/1598
Numerical investigation of flow structures and aerodynamic pressures around a high-speed train under tornado-like winds
Zou, S.; He, X.; Wu, T.
Vol. 38, No. 4, Apr 2024, pp 295-307

2024/1599
Probabilistic analysis of gust factors and turbulence intensities of measured tropical cyclones
Tao, T.; Jin, Z.; Wang, H.
Vol. 38, No. 4, Apr 2024, pp 309-323

2024/1600
Longitudinal reaction on conductors due to tornado wind load
Yao, D.; Damatty, A.
Vol. 38, No. 4, Apr 2024, pp 325-339

CSIR-SERC RESEARCH HIGHLIGHTS

Pages: 63-70

Engineering of large floating offshore structures and systems for renewable energy farming

Project Co-ordinators

Dr P. Harikrishna

Dr Saptarshi Sasmal

Team (WP 1)

Dr N. Anandavalli (*Leader*)
Dr P. Harikrishna
Dr M.B. Anoop
Dr Saptarshi Sasmal
Dr S. Vishnuvardhan
Dr Amar Prakash
Dr A. Subbulakshmi

Team (WP 2)

Shri G. Ramesh Babu (*Leader*)
Dr A. Abraham
Smt S. Chitra Ganapathi
Dr M. Keerthana

Significant achievement/ contributions towards technology/product/process development:

WP2: Evaluation of wind loads on different types of offshore Renewable Energy (RE) support structures

The effect of discrete wind event like gust and rapid change in wind direction during normal operation of floating 5MW RWT have been studied. Design Load Cases (DLC) 1.4 and 1.5, as per IEC 61400 standard address such events. The normal sea state has been considered for these cases as per IEC standard. For load case DLC 1.4, the effect of Extreme Coherent gust with Direction change (ECD) around rated wind speed (R) of 12 m/s for three yaw misalignment angles of -8°, 0° and +8° and four initial blade azimuth angles of 0°, 30°, 60° and 90° have been investigated. The occurrence of gust over short duration of about 10 seconds and extreme wind direction in the range of -65° to +65° influences the loads on FOWT depending on initial azimuthal position of the blade. The maximum blade root flapwise moment has been observed to be 20845 kN-m for the case of ECD-R+2.0 for yaw misalignment of -8° and blade azimuth of 90°. The maximum tower base pitching moment has been observed to be 148706 kN-m. Below rated wind speed, loads/moments are higher for rotor with yaw misalignment. Further, yaw misalignment affects the loads/ moments more than initial azimuth angle of blades.

For load case DLC 1.5, the effect of Extreme Wind Shear (EWS) in horizontal (H) and vertical (V) directions for various wind speeds in the range of 4 m/s to 24 m/s for three yaw misalignment angles of -8°, 0° and +8° and four initial blade azimuth angles of 0°, 30°, 60° and 90° have been investigated (Fig. 1). The maximum tower base pitching moment of 145044 kN-m has been observed at wind speed of 12 m/s near rated wind speed among all other wind speeds during normal operation of the turbine. The governing case is obtained as EWSH- for yaw angle of -8° and initial blade azimuth angle of 90°.

WP3: Evaluation of wave loads, hydro-dynamic loads and environmental loads on RE structures/structural components

Design of mooring configuration was performed for NREL 5 MW turbine supported on OC4 DeepCwind semisubmersible platform for a water depth of 200 m. The dynamic response of floating offshore wind turbine with three different mooring configurations namely catenary, taut and hybrid system were studied. In which the hybrid configuration was arrived with a combination of catenary and taut mooring system. Materials used for the catenary and taut system are studless steel chain and polyester, respectively. As 3-line mooring layout is non-redundant and

Team (contd...)

Team (WP 3)

Shri Nawal Kishor Banjara (*Leader*)
Dr B.S. Sindu
Dr A. Thirumalaiselvi
Shri K. Saravana Kumar
Smt N. Ramya

Team (WP 4)

Dr V. Marimuthu (*Leader*)
Dr M.B. Anoop
Dr P. Prabha
Dr M. Saravanan
Shri V. Ramesh Kumar

Team (WP 5)

Dr Amar Prakash (*Leader*)
Dr N. Anandavalli
Dr Smitha Gopinath
Dr K. Lakshmi
Dr J. Venkatesan,
Dr Srinivasa Babu Ramisetti
Dr J. Rajasankar

Team (WP 6)

Dr Mohit Verma (*Leader*)
Dr A. Subbulakshmi
Shri Manoj Kumar Nartu

Team (WP 7)

Dr S. Vishnuvardhan (*Leader*)
Dr M. Saravanan
Dr A. Kanchanadevi

large platform drifts were observed during accidental loading condition, a 6-line mooring system with 2 lines in the upwind side and 4 lines in the downwind side are considered in this study. The mooring lines were assumed to have a design life of 20 years. The numerical simulations were carried out using open-source code OpenFAST. Mooring line modelling was done using MoorDyn which uses lumped mass approach for line discretization. In this approach, the lower-bound stiffness was used to calculate extreme offset and an upper-bound stiffness was used to calculate extreme tension. Ultimate load analysis was carried out for DLCs 1.1, 1.6 and 6.1.

Numerical simulations are carried out for investigating the effect of mooring line failure on OC4 DeepCwind semisubmersible supporting NREL 5 MW wind turbine during wind wave misalignment and nacelle yaw misalignment. Numerical simulations are performed for both the intact and one of the mooring line failure conditions under operating and survival condition of the wind turbine (Fig. 2). Different load cases are considered corresponding to the below rated, around rated, around cut-out, 1-year and 50-year extreme wind speed conditions. Wind wave misalignment and nacelle yaw misalignment are also considered for the simulations. Normal turbulence, extreme turbulence, normal sea state and severe sea state models are considered for the analysis.

As part of environmental degradation studies on floating offshore wind turbine structures, investigations have been carried out to understand the influence of the high temperature, moisture and saline environment on degradation in the properties of epoxy composite adopted in FRP composites which are used for blades of wind turbines. The mechanical (elastic modulus and strength) properties of epoxy polymers when immersed in water for long duration with different degrees of salinity (0%, 2.5% and 5% salinity) are determined

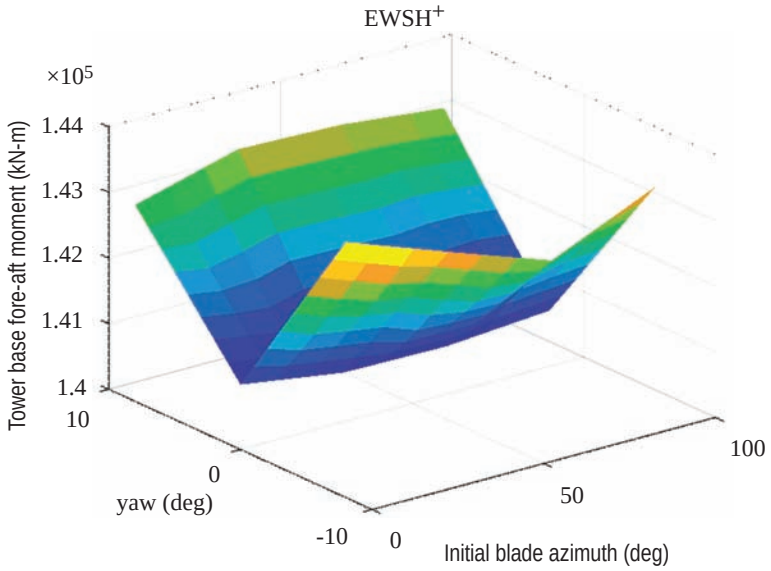

Fig. 1 *Variation of tower base fore-aft moment*

Team (contd...)

Team (WP 8)

Dr B. Arun Sundaram (*Leader*)
Dr V. Srinivas
Dr S. Parivallal
Dr J. Prawin
Dr M. Kannusamy
Shri Subhajit Das

through uniaxial tension tests. The tests are carried out in displacement control mode, extensometers are attached to the specimens to measure the strain in the gauge portion. The diffusion coefficient (a key transport property) of epoxy composite is also experimentally determined for different degrees of salinity. Attempts are also being made to engineer/tailor the epoxy composite for enhanced mechanical and transport properties when exposed to high temperature and salinity.

WP4: Computational modelling, analysis and design of identified foundation systems, platform structures and supporting structures for offshore wind turbine

The semi-submersible floating platform of NREL 5MW has been modelled in general purpose finite element software using solid elements. The plate components are modelled using 3D plate elements. The main and offset columns are interconnected through 1 sets of delta pontoons in the upper and lower level, which are 38 m and 26 m in length in length respectively. The thickness of the caps of each columns is 60 mm. The reaction forces obtained at the base of the tower is applied at the cap of the main column. The overturning moment is applied as a couple and the shear forces are applied at the base. The buoyancy force offered by the water is applied at the base of each offset columns using spring elements. Further, the hydrostatic pressure is also applied at each of the offset column and in the central column. The wave load is applied at the still water level of each column. Currently, the wave load is applied as 50% in the facing column and the remaining 50% is shared equally among the other two columns. The structure is analysed for power production plus occurrence of fault and power production load case as per IEC61400-3-2:2019. The permissible stresses for the each of the members have been obtained as per IS:800-2007, considering the imperfections and residual stress effects. The imperfection factor of 0.49 corresponding to buckling curve C is considered for all the members. While stress reduction factor for middle and offset columns obtained in the range 0.6-4.0%, it is of the range 6-45% depending on the length of pontoons. The effective length factor for the offset column as a single stepped column is obtained as 1.67 as per IS:800-2007 and the corresponding permissible axial stress is 330 MPa. The shell of each column and pontoons are verified against the shell buckling. Their critical stresses against symmetrical and asymmetrical buckling are higher than the yield strength of the chosen material. Further, the slenderness of each of the shells accounting for imperfections, residual stress and edge disturbances falls within 1.414, which represents the plastic behaviour

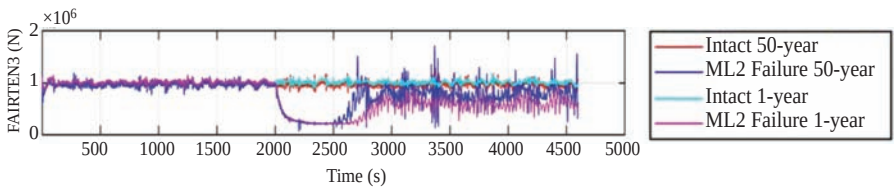

Fig. 2 *Effect of mooring line (parallel to wind and wave direction) on fair lead tensions*

of shell components. The stress values obtained from the numerical model is less than the permissible stress. However, the design of the semi-submersible platform is governed by buoyancy requirements. Design checking for other load distributions and the connection design are also carried out.

WP5: Computational modelling, analysis and design of identified platform with mooring and panel supporting structures for offshore solar farms

In the previous studies, a taut mooring configuration for floating solar farm unit structure has shown to experience low axial forces in mooring cables. So, the same configuration is analyzed in the present study further under extreme load conditions. A similar AQWA computational model has been adopted with the mooring cable unstretched length of 128.5 m. The wave inputs corresponding to irregular wave representing extreme conditions are considered. An irregular wave of 6.98 m amplitude and 11.70 s period is chosen. The unit structure 6-DOFs such as displacement and rotation, and mooring cable tension force, and forces on the unit structure are extracted. The maximum surge and sway are ±12 m and ±8 m respectively. The heave of the unit structure does not follow the wave elevation. This is due to the larger taut mooring length, which should be adjusted to make the heave follow the wave elevation. Likewise, the rotations in the 3 directions are extracted. All four mooring cables are experiencing the maximum axial force above 100 kN. However, as the unit structure with the taut mooring subjected to extreme wave conditions is causing huge rotations in pitch and yaw directions, the unit structure mooring design is being revised to make it suitable for all design load cases as per IEC 64400-1 design guidelines for floating structures.

WP6: Development of strategies for the stabilization and control of Floating Offshore Wind Turbines (FOWT)

Under a mooring line breakage condition, the floating offshore wind turbine (FOWT) is subjected to sudden loads. The response control of FOWT during such an event is of immense importance to avoid the catastrophic failure. Although TMD is usually designed for vibration reduction in the steady state, it can also be used for the transient response reduction. The investigations are carried out for a case where TMD is installed in the nacelle of FOWT. A reduced order model is used for the design of TMD. An optimum TMD is obtained by minimizing the infinity norm of the system response when subjected to mooring line failure. The performance of the designed TMD is assessed by carrying out the coupled nonlinear dynamic analysis using aero-hydro-servo-elastic code, OpenFAST (Fig. 3). Three different environmental conditions (corresponding to below rated, nearer to rated and nearer to cut-out wind speed) are considered for the analysis. The effectiveness of the TMD is also assessed for the scenario of multiple mooring lines failure. The cases corresponding to both concurrent and non-concurrent mooring line failures are considered. Various performance indices, defined in terms of peak, root mean square and standard deviation of the response parameter are evaluated for each of the cases. The designed TMD is found to be advantageous for reducing the transient response of FOWT based on the performance

indices. Thus, TMD can be effectively used for transient response reduction of FOWT thereby enhancing its safety in the event of accidental mooring line failure.

A prototype, representative of the tower-nacelle assembly, is fabricated for the experimental evaluation of the TMD design methodology. A resonance search test is carried out for the dynamic characterization of the tower-nacelle assembly. The next step involves the evaluation of the primary structure properties for which the optimal TMD will be designed. The performance of the TMD is evaluated using hybrid testing.

WP7: Identification of fatigue critical components of different offshore RE structures, and fatigue resistant design

With an objective of developing S-N curve, fatigue life evaluation of IS 2062 Grade E 350 steel identified for floating offshore support structures has been carried out. ASTM E 466 - 21 has been followed in preparing the test specimens. In continuation to the previously conducted tests, further fatigue tests were carried out at a maximum stress value equal to 75% of the yield strength of the material (Fig. 4). The stress ratio was kept as 0.10 and the stress range was 228.15 MPa. Earlier, fatigue tests at maximum stress value equal to 95%, 90%, 85% and 80% of the yield strength of the material were carried out. S-N data obtained from the tests were compared with the S-N curves for Detail Categories 103 and 92 given in IS 800 : 2007.

Fatigue life evaluation of welded specimens made of IS 2062 Grade E350 steel have been taken up. ASTM E 466 was followed in preparing the test specimens. The overall size of the specimens is considered as 500 mm × 32 mm × 16 mm. The transverse butt welded specimens are fabricated from 16 mm thick plate by Manual Metal Arc (MMA) welding using weld run-off tabs, which were subsequently removed and ends ground flush in the direction of stress. Welds are made from both sides by making V grooves of 45º. Fatigue tests are also conducted under constant amplitude sinusoidal cyclic loading at various values of maximum stress decided as a percentage of yield strength of the material.

Further, numerical analysis of the joint between one of the side upper columns, delta pontoons, Y pontoon and cross bracing of floating offshore support system of 5 MW NREL FOWT has been carried out. The side upper column, delta pontoons, Y-pontoon

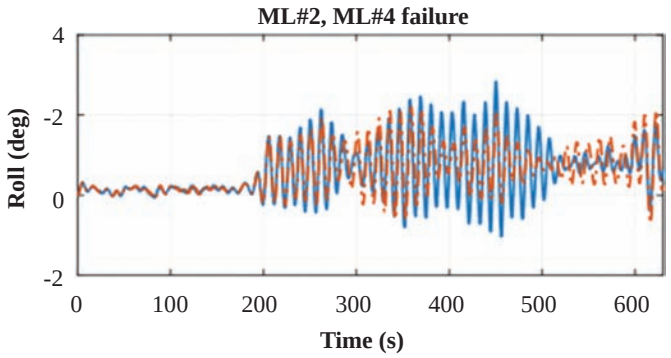

Fig. 3 *Effect of TMD on response of floating platform under mooring failure*

and cross bracings are designated as UC2, DU1, DU2, YU2 and CB2 respectively. In order to evaluate stress concentration factor (SCF) values, a pressure of 0.10 MPa was applied initially to one of the braces, namely DU1, DU2, YU2 and CB2 at one instance. Then the pressure was applied to both braces YU2 and CB2 simultaneously. Furthermore, the pressure was applied simultaneously to all the braces. The SCF values are obtained for all the cases. The maximum principal stress values obtained for braces DU1 (Fig. 5), DU2, YU2 and CB2 were 0.450 MPa, 0.448 MPa, 0.439 MPa and 0.422 MPa respectively. The corresponding SCFs for braces DU1, DU2, YU2 and CB2 were 4.51, 4.48, 4.39 and 4.20 respectively. When the braces were loaded individually, the SCF values were almost the same in all the braces. The maximum SCFs are observed at the crown point of the joint in all the cases. When the braces YU2 and CB2 are loaded simultaneously with a pressure of 0.10 MPa, the stresses between the braces YU2 and CB2, i.e., at the crown toe was found to be 0.771 MPa. Thus, when the braces are loaded simultaneously, there was increase in the magnitude of stress. When all the braces are loaded simultaneously, the stress values of the individual braces were almost the same. The maximum principal stress at crown point between YU2 and CB2 was 0.68 MPa. Numerical studies are being continued on the joint between main column, Y pontoon and cross bracing of the NREL FOWT.

WP8: Development of robust health monitoring strategies for floating offshore RE structures

In continuation of the studies carried out on localization of multiple damage in the thin plate structures, further studies are carried out to localization of the multiple damages present in the plate-like structures using Lamb wave virtual time reversal (VTR) technique. A modified VTR algorithm was proposed in which the physical generation and sensing of Lamb waves are performed using broadband Gaussian excitations instead of the conventional narrowband modulated

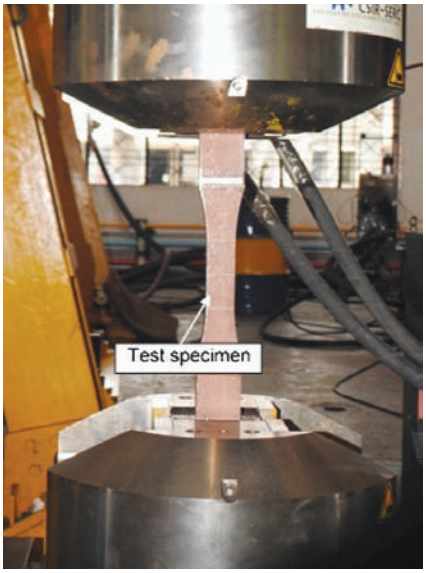

Fig. 4 *Fatigue testing of E350 grade steel*

tone burst excitation. It eliminates the numerical error arising in the transfer function due to zero or close to zero amplitude at several frequencies present in the narrowband signal. Combining the modified VTR algorithm with refined time reversal method, probing the structure at the best reconstruction frequency. It leads to accurate localization of dual damage locations in plates with single pitch catch measurement per sensing path without requiring any baseline signal to compare.

Further, damage identification of wind turbine support tower structures using modal data has been carried out. A new metaheuristic algorithm has been developed for damage identification using vibration data. The damage identification of wind turbine tower and mooring structures using deep learning techniques and acceleration data is in progress. In this regard, a joint damage detection study has been performed by using the Qatar University Grandstand Simulator (QUGS) experimental data for joint damage detection. Further, binary classification has been used for damage classification. The structure was utilized to generate vibration data under severa structural damage cases. A total of 31 scenarios are considered: in 30 scenarios, damage was introduced by loosening the bolts at the joints 1 to 30, respectively, and one scenario was undamaged case where all bolts of all 30 joints are tightened. 1D CNN, LSTM, and Bi-LSTM are used to identify the damage location. Once the models are trained using optimal hyperparameter values, they are used to assess the condition of the structure. The model for a joint is used to compute an index that reflects the likelihood of damage at that joint, given by probability of damage (POD). It is inferred from the results that 1D CNN has given considerably better results than both LSTM and Bi-LSTM. Also, Bi-LSTM has performed better than LSTM (Fig. 6). Further, this study was extended for damage identification of mooring and tower structures using the acceleration data.

Investigations have also been carried out on a numerically simulated faulty bearing signal and KAU bearing fault dataset to verify and validate the developed enhanced

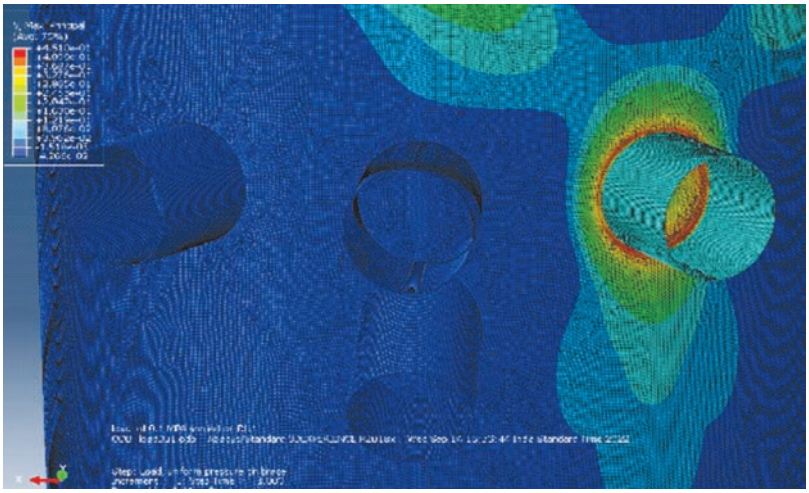

Fig. 5 *Principal Stress Contour for OC4 platform at joint with member DU1*

envelope analysis technique for bearing fault diagnosis. The results of the investigations conclude that the isolation of transient impulse features caused by rolling bearing faults from corrupted discrete frequency components of gear and shaft is possible by AR model and spectral kurtosis provides reliable identification of the region of resonance frequencies when fault occurs otherwise the fault signal is modulated. Finally, the envelope signal obtained through the Hilbert Transform of band pass filtered response gives fault information by peak amplitudes related to bearing fault frequencies in the Fourier spectrum.

Scope / Objectives

- Identification of the suitable renewable energy structural configurations for Indian offshore
- Evaluation of wind, wave, hydro-dynamic and environmental loads for offshore Renewable Energy (RE) structures
- Analysis and design of the identified types of substructures for the floating wind turbines and floating solar farms
- Analysis and design of the appropriate support structures for the floating wind turbines and floating solar farms
- Development of methods for stability and control of offshore RE structures
- Fatigue resistant design of structural components of offshore RE structures
- Development of robust strategy for health monitoring of floating offshore structures

Pages: 71-78

MIT CSHub proposes concrete carbon uptake accounting framework

July 9, 2024

Sources: Concrete Sustainability Hub at Massachusetts Institute of Technology, Cambridge; CP staff

https://concreteproducts.com/index.php/2024/07/09/mit-cshub-proposes-concrete-carbon-uptake-accounting-framework/

A new report from the MIT-hosted Concrete Sustainability Hub probes statistical and scientific methods for measuring carbon dioxide uptake in hardened concrete and other cement-based products (CBP). It proposes a framework to account for carbon uptake in Product Category Rules (PCRs), documents key to creating verifiable environmental product declarations (EPD). Credible uptake calculations will contribute to EPDs offering a more comprehensive view of life-cycle carbon dioxide emissions metrics than current declarations for CBPs. The focus on uptake, where carbon dioxide in the atmosphere reacts with calcium-rich cement hydration products and is permanently sequestered in CBPs, aligns with Carbonation, the fifth of five Portland Cement Association Roadmap to Carbon Neutrality pillars, and the UN Intergovernmental Panel on Climate Change's recognition of the process as a carbon sink.

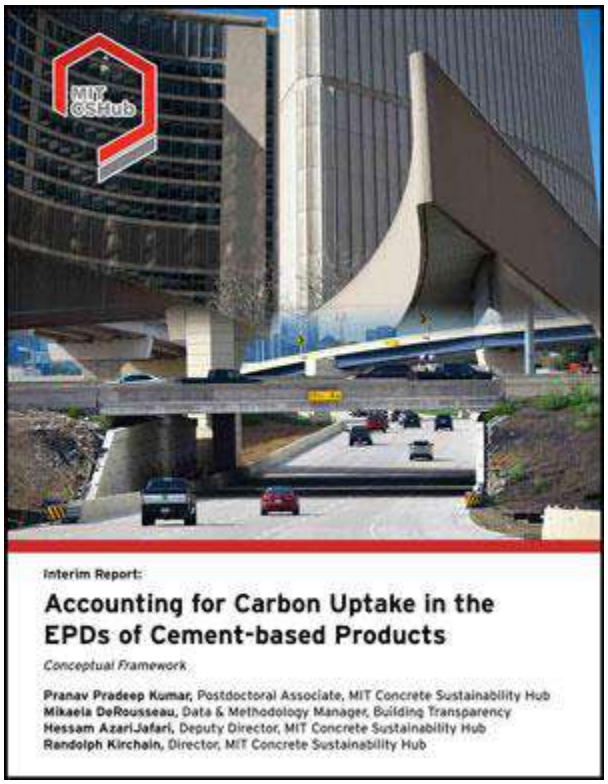

"Accounting for Carbon Uptake in the EPDs of Cement-based Products" authors weigh four major factors behind the intensity and extent of CO_2 sequestration in hardened elements or structures:

- **Climate and exposure conditions**, including local CO_2 concentration, proximity to industrial sources; ventilation; plus, temperature, humidity, exposure to moisture. Higher temperatures generally accelerate carbon uptake; moderate moisture facilitates CO_2 transportation within CBP pores.
- **CBP types and properties**, the latter including permeability and porosity properties.
- **Binder system**. Portland cement (clinker only) and blended cements have varying impacts on carbon uptake rates and volume.
- **Geometry**. Uptake primarily occurs at the CBP surface, where coatings, sealers or other treatment can reduce CO_2 sequestration.

"A uniform methodology for computing the carbon uptake potential using equations for different levels is proposed to be used to provide consistent guidelines for the EPD development process such that there is flexibility for input variables at different levels," authors note. "The consistency of this methodology would facilitate its use over a wider range of climatically diverse regions and applications. These advantages may help a PCR committee standardize the introduction of carbon uptake data in EPDs."

Authoring "Accounting for Carbon Uptake" are CSHub's Randall Kirchain, director, and Hessam Azari Jafari, deputy director, and Pranav Pradeep Kumar, postdoctoral associate; and, Mikaela DeRousseau, Data & Methodology manager for Building Transparency, Embodied Carbon Calculator (EC3) administrator. Assisting them are Carbonation Working Group members, including representatives of Heidelberg Materials, Salt River Materials Group, Cement Association of Canada, Canadian Precast/Prestressed Concrete Institute, Concrete Masonry & Hardscapes Association and Portland Cement Association. Findings in their interim report are primarily applicable to ready mixed concrete and cast-in-place surfaces or structures, but will inform forthcoming work on carbon uptake in manufactured concrete, wet or dry cast.

New contaminant-tolerant catalyst could help capture carbon directly from smokestacks

*By **Tyler Irving,*** JULY 4, 2024

Source: https://news.engineering.utoronto.ca/new-contaminant-tolerant-catalyst-could-help-capture-carbon-directly-from-smokestacks/

A newly designed catalyst created by U of T Engineering researchers efficiently converts captured carbon into valuable products — even in the presence of a contaminant that degrades the performance of current versions.

The discovery is an important step toward more economically favourable techniques for carbon capture and storage that could be added on to existing industrial processes.

"Today, we have more and better options for low-carbon electricity generation than ever before," says Professor David Sinton (MIE), senior author on a paper published in *Nature Energy* that describes the new catalyst.

"But there are other sectors of the economy that will be harder to decarbonize: for example, steel and cement manufacturing. To help those industries, we need to invent cost-effective ways to capture and upgrade the carbon in their waste streams."

Sinton and his team use devices known as electrolyzers to convert CO2 and electricity into products such as ethylene and ethanol. These carbon-based molecules can be sold as fuels or used as chemical feedstocks for making everyday items such as plastic.

Inside the electrolyzer, the conversion reaction happens when three elements — CO2 gas, electrons and a water-based liquid electrolyte — come together on the surface of a solid catalyst. The catalyst is often made of copper but may also contain other metals or organic compounds that can further improve the system. Its function is to speed up the reaction and minimize the creation of undesirable side products, such as hydrogen gas, which reduce the efficiency of the overall process.

While many teams around the world have produced high-performing catalysts, nearly all of them are designed to operate with a pure CO2 feed. But if the carbon in question comes from smokestacks, the feed is likely to be anything but pure.

"Catalyst designers generally don't like dealing with impurities, and for good reason," says Panos Papangelakis, a PhD student in mechanical engineering and one of five co-lead authors on the new paper. "Sulphur oxides, such as SO2, poison the catalyst by binding to the surface. This leaves fewer sites for CO2 to react, and it also causes the formation of chemicals you don't want.

"It happens really fast: whereas some catalysts can last hundreds of hours on a pure feed, if you introduce these impurities, within minutes they can be down to 5% efficiency."

Though there are well-established methods to remove impurities from CO2-rich exhaust gases before feeding them into the electrolyzer, they take time, require energy and raise the cost of carbon capture and upgrading. Furthermore, in the case of SO2, even a little bit can be a big problem.

"Even if you bring your exhaust gas down to less than 10 parts per million, or 0.001% of the feed, the catalyst can still be poisoned in under 2 hours," says Papangelakis.

In the paper, the team describes how they went about designing a more resilient catalyst that could stand up to SO2 by making two key changes to a typical copper-based catalyst.

On one side, they added a thin layer of polyteterafluoroethylene, also known as Teflon. This non-stick material changes the chemistry at the catalyst surface, impeding the reactions that enable SO2 poisoning to take place.

On the other side, they added a layer of Nafion, an electrically-conductive polymer often used in fuel cells. This complex, porous material contains some areas that are hydrophilic, meaning they attract water, as well as other areas that are hydrophobic, meaning they repel water. This structure makes it difficult for SO2 to reach the catalyst surface.

The team then fed this catalyst with a mix of CO2 and SO2, with the latter at a concentration of about 400 parts per million, typical of an industrial waste stream. Even under these tough conditions, the new catalyst performed well.

“In the paper, we report a Faraday efficiency — a measure of how many of the electrons ended up in the desired products — of 50%, which we were able to maintain for 150 hours,” says Papangelakis.

“There are some catalysts out there that might start at a higher efficiency, maybe 75% or 80%. But again, if you expose them to SO2, within minutes or at most a couple of hours, that drops down to almost nothing. We were able to resist that.”

Papangelakis says that because his team’s approach doesn’t affect the composition of the catalyst itself, it should be widely applicable. In other words, teams that have already perfected high-performing catalysts should be able to use similar coatings to confer resistance to sulphur oxide poisoning.

Although sulphur oxides are the most challenging impurity in typical waste streams, they are not the only ones, and it’s the full set of chemical contaminants that the team is turning to next.

“There are lots of other impurities to consider, such as nitrogen oxides, oxygen, etc.,” says Papangelakis.

“But the fact that this approach works so well for sulphur oxides is very promising. Before this work, it was just taken for granted that you’d have to remove the impurities before upgrading CO2. What we’ve shown is that there might be a different way to deal with them, which opens up a lot of new possibilities.”

Energy Efficient and Carbon Sequestering Lightweight CMU Walls

June 27, 2024 Kevin Cavanaugh

Source: *https://concreteproducts.com/index.php/2024/06/27/energy-efficient-and-carbon-sequestering-lightweight-cmu-walls/*

Two of today's major focus areas in the design community are reducing the amount of energy (usually in the form of fossil fuel to heat, cool and operate buildings) and reducing the embodied carbon in building materials. To help meet the moment, the concrete products industry has two readily available and affordable solutions that can be used to address both priorities:

1. Lightweight concrete masonry units (CMU), when made with lightweight aggregate like expanded shale, clay or slate, is the concrete world's high-efficiency, energy-saving deliverable. Some will even say it qualifies as the concrete world's version of insulation.

2. Dry-cast CMU are excellent at sequestering carbon dioxide (CO2). They readily absorb and convert atmospheric CO2 into limestone.

Foam-insulated Next-Generation CMUs yield R-value 2-3 times higher than normal for such an assembly. PHOTO: Kevin Cavanaugh for ESCSI

HIGH-EFFICIENCY LIGHTWEIGHT CMU

For many years, using insulation in ever-increasing quantities was the key to achieving energy efficiency in buildings. In today's energy efficiency world, the name of the game, as far as buildings go, is "high efficiency." Many believe that more energy savings are only to

be found by using automated, high-efficiency lighting systems, hot water heaters, furnaces, air-conditioners and heat pumps. And while insulation specifications in walls, ceilings and floors still get a lot of attention, the Law of Diminishing Returns indicates that very little extra energy savings are found when adding more insulation.

A reliable solution—the concrete in a lightweight CMU—has roughly three times more resistance to heat flow than the regular concrete in a "normalweight" CMU. When combined with today's "Next Generation" CMU (with thinner and fewer webs) insulated with injection foam, which completely fills all the hollow cores in a CMU wall and the tiny nooks and crannies between units, the net effect is a wall assembly with two to three times higher R-values than possible if the CMU were made with regular, normalweight concrete. (See Table 1)

When the entire lifespan of a building is considered, lightweight CMUs' higher R-value saves significant amounts of heating and cooling energy. So much energy is saved that even though a normalweight CMU's environmental product declaration (EPD) is better than a lightweight CMU's EPD, the cumulative energy saved with insulated lightweight CMU, thanks to its higher R-value, creates a net positive impact for a building.

Table 1. Comparison of 12-inch Concrete Masonry Assembly R-Values (hr-ft^2-°F/Btu)

Unit Density	Conventional Three-Web, Two-Core Unit [1,2]	Minimum One-Web Permitted by ASTM C90-11b [2]
85 lb/ft^3	11.9	30.9
95 lb/ft^3	9.9	28.0
105 lb/ft^3	8.2	25.1
115 lb/ft^3	6.8	22.3
125 lb/ft^3	5.7	19.7
135 lb/ft^3	4.7	17.3

Source: Jason Thompson, Masonry Edge/Story Pole Magazine, Vol. 7, No. 2
[1] See Reference 3, Thermal Catalog of Concrete Masonry Assemblies, for modeling procedure and design assumptions.
[2] Values assume all ungrouted cells contain foam-in-place insulation and moisture-corrected values for thermal conductivity.

CMU SEQUESTER CARBON

Receiving equal attention, if not more, is the design community's goal of reducing the amount of a) embodied carbon contained in building materials, and b) energy required to operate buildings built with today's materials. The Concrete Masonry & Hardscapes Association (CMHA) is studying how much CO2 typical CMU can sequester. Results so far are very encouraging. Due to the thinness of CMU face shells and cross webs and the more porous structure of the dry-cast concrete, atmospheric CO2 can easily penetrate the CMU matrix, differentiating it from wet-cast concrete. This results in significantly higher natural carbonation rates.

While the concrete industry continues advocating that today's 'cradle to gate' EPDs do not fully capture a material's impact on energy savings or on its larger carbon footprint, it is important for the design community to know that these two solutions offered by the concrete industry are readily available and inexpensive to implement. As Chair of American Concrete Institute/The Masonry Society Joint Committee 122 on Energy Efficiency of Concrete and Masonry Systems and two other CMU-related committees, I have learned that these are two of the few timely solutions that our industry offers. Another very important one is to use the "trade-off" compliance path and accompanying COMCheck software program to meet energy code requirements. However, we need more solutions. For which, we need to come together as an industry and support creating and sharing these solutions with our design community partners. If you are interested in becoming an ACI/TMS 122 member or discussing more about these or other solutions, please contact me directly.

Pages: 79-83

CREATE IMPRESSISSIVE BIM STRUCTURES WITH STAAD & RAM

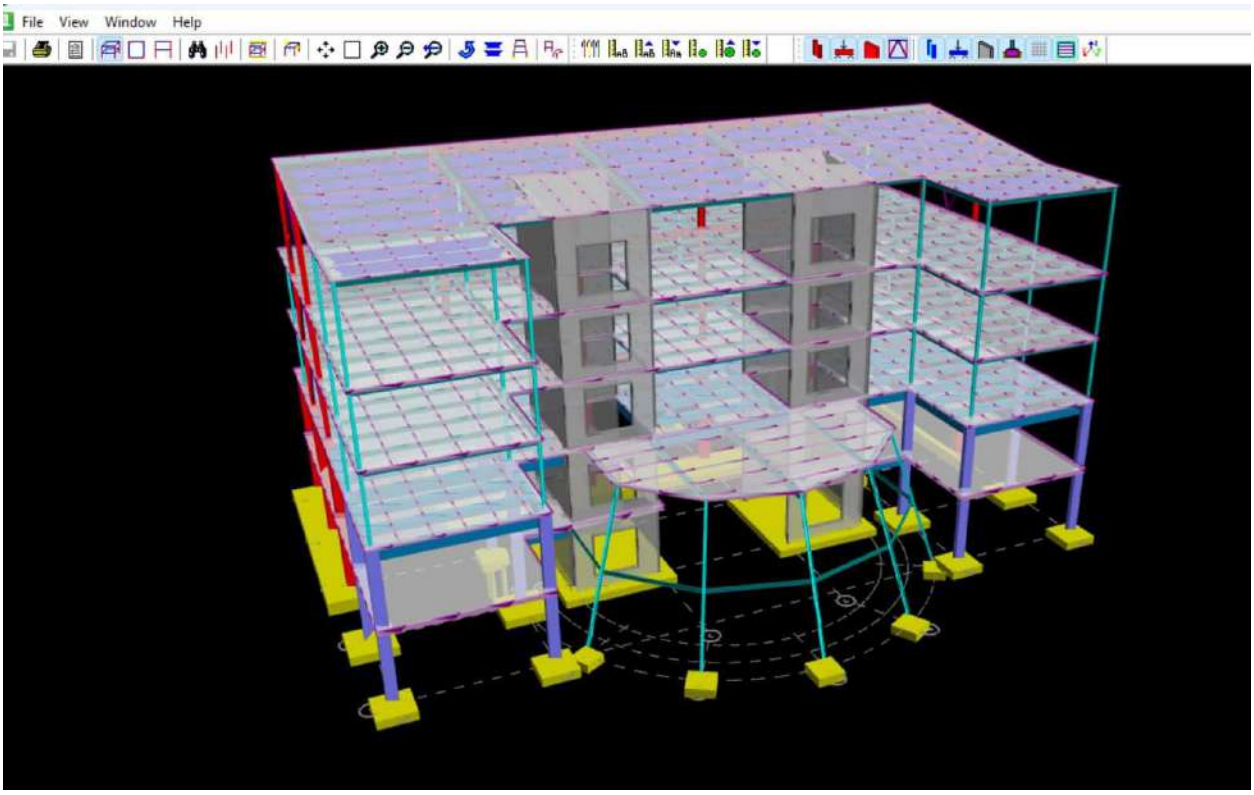

As engineers in the architecture, engineering, and construction (AEC) sector, we have observed the widespread adoption of building information modeling (BIM). Over the past five years, the term “infrastructure digital twin” has taken center stage. What is the difference between BIM and an infrastructure digital twin? As structural engineers, we use software to create 3D models for analysis and design—so are we creating BIMs or infrastructure digital twins?

BIM is a static visualization capability employed during the design and construction phases of a building. BIM integrates all disciplines into a CAD-based model. The purpose of BIM is to enable collaboration between disciplines and visualize spatial constraints. BIM serves as foundational data used to create an infrastructure digital twin.

For example, your 3D structural analysis model can be exported and translated into a CAD format for use in BIM.

An infrastructure digital twin is a virtual representation of a real-world entity, synchronized at a specified frequency and fidelity. Real-time data from sensors and the Internet of Things (IoT) are linked to the accurate as-built digital model. The infrastructure digital twin serves as the smart building hub for owners and operators to schedule maintenance and ensure that the building is operating optimally.

Level of development

The International BIM Forum authors the Level of Development (LOD) specification. The LOD definitions provide a method to classify the level of detail and accuracy of information required in your digital model throughout the project's lifecycle. We can align these levels with our project workflows and the software that we utilize.

LOD 100 and 200 take your model from mass models to more specific design. The design professional will use CAD-based applications to create these models.

In LOD 300, the BIM model is refined by adding accurate sizes and locations. The engineers will import their analysis models into the BIM model.

LOD 400 adds specific fabrication and installation information. Software that creates fabrication drawings is utilized in this step. The BIM model integrates with construction phasing software.

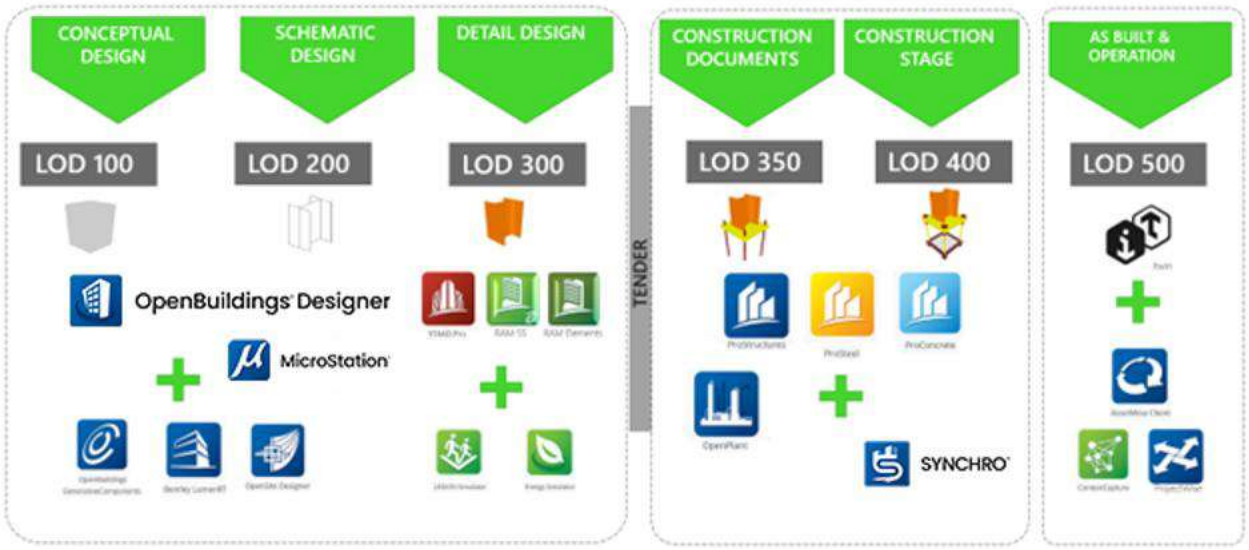

LOD 500 is the point when the BIM model is transitioned to an infrastructure digital twin. The model reflects the as-built condition, and the team uses asset management systems and digital models that read sensor data.

BIM toward the infrastructure digital twin

We are aware of the importance of BIM adoption around the world, considering that there are already very strong regulatory bodies. At the same time, there have been recent efforts in countries that include Chile, Colombia, Mexico, Brazil, and Argentina toward adoption.

BIM is a crucial part of the infrastructure digital twin. It takes the dimensions and levels of development of the BIM model to complete the rest of the audited information with an additional step of incorporating real-time sensors. A BIM file with a high level of development could have a robust model with lifecycle and operation included. On the other hand, the infrastructure digital twin incorporates audited information in real time, as it represents a complete virtual representation of all data, positive or not, and all relevant information, which almost completely replicates the multidiscipline system. It not only includes the model itself, but also external factors that include pressure measurements, earthquakes, winds, variable loads, and changes in the resistance of elements, as well as the impact of the environment in general.

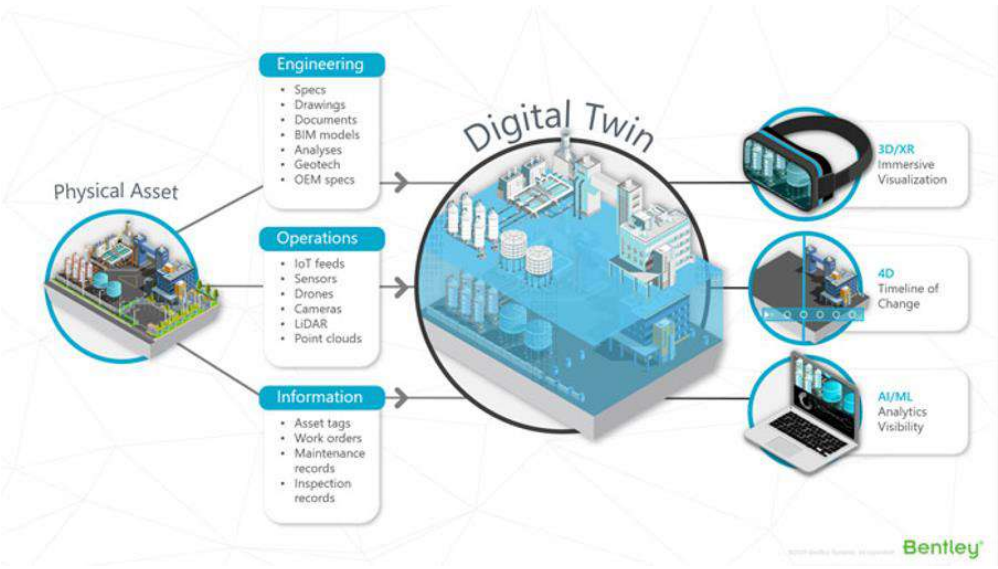

Bentley's structural portfolio

Bentley's structural analysis software portfolio is comprised of STAAD.Pro, RAM Elements, RAM Structural System, RAM Concept, RAM Connection, STAAD.Foundation Advanced, and STAAD Advanced Concrete.

Each application has specific capabilities that correspond to analytical and physical modeling programs at the same time. Physical modeling is responsible for BIM interoperability and includes STAAD, RAM Structural System, and RAM Elements.

Modeling or analytical interpretation is focused on the process of analysis and design:

- **STAAD.Pro:** Powerful structural analysis and design software that can model any type of structure with any material.
- **RAM Structural System:** Structural design software for buildings.
- **RAM Elements:** 3D structural analysis and design software for performing 3D finite element analysis of almost any type of structure or structural component.

Bentley BIM portfolio

Bentley's BIM portfolio is diverse and covers all software that have BIM information associated with them, including:

ProStructures: Allows you to model structural systems, including fabrication elements, as well as the generation of drawings. It is subdivided into ProSteel and ProConcrete to direct attention towards steel or concrete structures.

OpenPlant: The main software for plant modeling. It works as an ideal link with ProStructures for multidiscipline projects of this type.

OpenBuildings: Building design software that enables BIM workflows for the design, analysis, simulation, and documentation of buildings.

Each software provides specialized solutions within the BIM environment, facilitating multidiscipline collaboration and efficient model creation for a wide range of projects in engineering and architecture.

Source:https://www.thestructuralengineer.info/news/create-impressissive-bim-structures-with-staad-ram

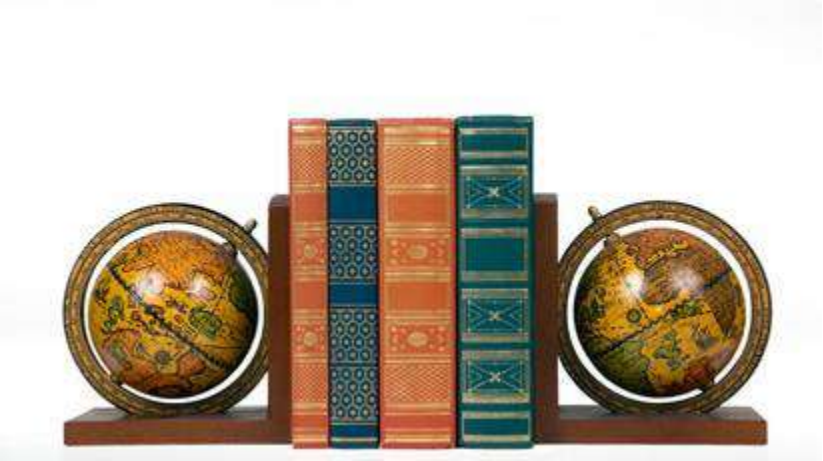

Book Shelf

Pages: 84-87

Performance-Based Seismic Design of Structures

Satyabrata Choudhury

ISBN 9781032444826 CRC Press July 2024 426 Pages

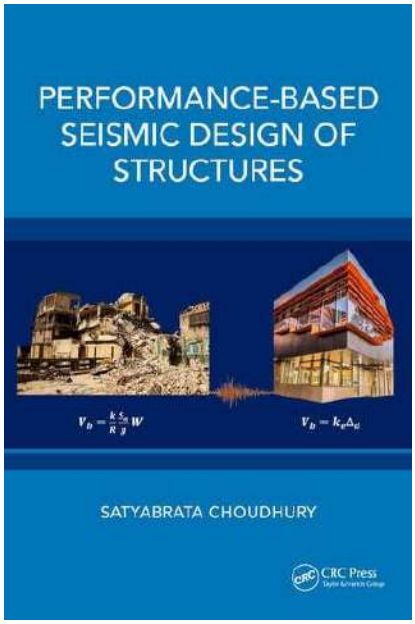

DESCRIPTION

Seismic design of structures is fast turning to performance-based design (PBD) from old codal force-based design (FBD) method. The aim of the book is to expose readers to the meaning and need of PBD, the evolution of PBD to date, its various forms and applications. Various design philosophies and procedures have been described including modelling aspects and hazard considerations backed by examples. Direct displacement-based design (DDBD) and Unified PBD (UPBD) of reinforced concrete (RC) frame buildings, RC dual systems, steel frame buildings and bridge piers have also been explained.

The main features of this book are as follows:

- Illustrates performance-based seismic design to achieve the design target by performance objective-oriented design procedure
- Covers modern design philosophies, modelling aspects, concepts in nonlinearities and use of supplemental damping devices
- Contains a chapter on seismic safety of nonstructural components
- Describes UPBD design procedure and examples of different structural systems
- Includes application and examples with reference to SAP2000 software

This book is aimed at graduate students, researchers and professionals in civil engineering, earthquake engineering and structural design.

1st Edition

Vibration Engineering Modeling, Simulation, Experimentation, and Applications

Edited By Nitesh P. Yelve, Susmita Naskar

ISBN 9781032515281 CRC Press May 2024 108 Pages

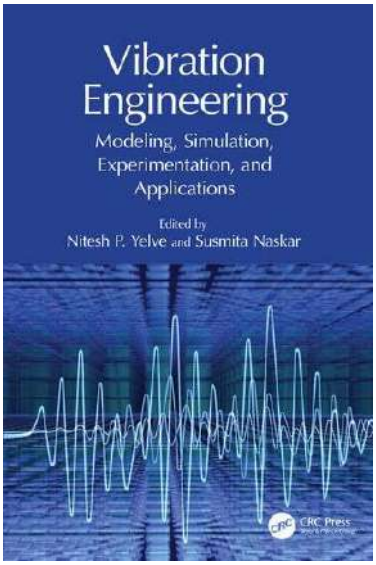

DESCRIPTION

Vibration Engineering presents recent developments in the field of engineering, encompassing industrial norms, applications within the finite element method, infrastructure safety assessment, and active vibration control strategies. It offers a study in seismic vibration control and analysis for building structures and liquid storage tanks.

Spanning across the multiple domains of vibration engineering, the book highlights machinery diagnostics, modal analysis, energy harvesting, balancing, vibration isolation, and human-vibration interaction. It discusses experimental fault identification in journal bearings using vibration-based methods. This book also considers advances in vibration-based structural health monitoring of civil infrastructures.

This book will be a useful reference for industry professionals and engineers facing challenges while dealing with the vibrations in the fields of mechanical, aerospace, structural, and civil engineering.

1st Edition

Shotcrete Materials, Performance and Use

By Dudley Robert Morgan, Marc Jolin

ISBN 9781032039718 CRC Press May 2024 510 Pages

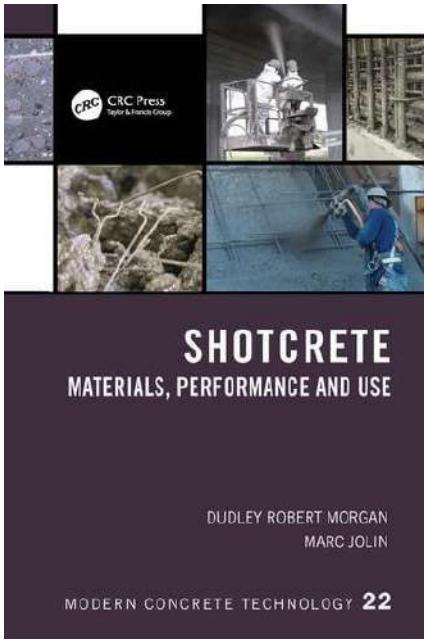

DESCRIPTION

Shotcrete: Materials, Performance and Use is a comprehensive textbook covering the current state-of-the-art shotcrete technology. It provides an overview of the many and various uses of shotcrete. Shotcrete is well suited for construction of curvilinear structures (domes, shells, bobsleigh/luge tracks, etc.) and overhead shotcrete applications (seismic retrofit, repairs, ground support, etc.) that could not be constructed technically and/or economically using conventional formed, cast-in-place concrete construction methods.

It contains chapters on history, shotcrete materials and mixture proportioning, performance, shotcrete research, equipment and shotcrete application. It is also comprised of shotcrete case history examples including buildings and structures, infrastructure repair and rehabilitation, ground support and shoring, underground support in tunnels and mines, swimming pools and spas, and, finally, architectural shotcrete.

This text should be of interest to design engineers and architects considering the use of the technology, as well as academics. It serves as a useful guide to contractors using shotcrete in one or more of its many and various applications.

READ. RESEARCH. WRITE. REPEAT.

FOR MORE DETAILS CONTACT:

KNOWLEDGE RESOURCE DIVISION
CSIR-STRUCTURAL ENGINEERING RESEARCH CENTRE
CSIR CAMPUS, TARAMANI, CHENNAI 600113
PHONE : 044 22549131 / 132 / 133
EMAIL LIBA@SERC.RES.IN